AD-773 758

FUEL SLOSH ENERGY DISSIPATION ON
A SPINNING BODY

J. T. Neer, et al

Hughes Aircraft Company
El Segundo, California

February 1972

FUEL SLOSH ENERGY DISSIPATION

ON A SPINNING BODY

HUGHES

HUGHES AIRCRAFT COMPANY
SPACE AND COMMUNICATIONS GROUP

FEBRUARY 1972

AUTHORS:

J. T. Neer

J. O. Salvatore

SCG 20047R

ACKNOWLEDGMENTS

ABSTRACT

This report presents the results of a series of tests conducted by
Hughes Aircraft Company to experimentally establish the energy dissipated
in Intelsat IV (HS-312) and HS-318 conispherical propellant tanks when sub-
jected to nutational excitations similar to those experienced by the
respective spacecraft in orbit. To date three test series have been conducted:
Phase I tests on an Intelsat IV type vehicle were run at the Culver City facility
during the fall of 1970; Phase II tests on a scaled version of a HS-318 vehicle
were run at the El Segundo site during the winter of 1970; and during Phase III,
a repeat and an extended test on both the HS-318 and Intelsat IV configurations
were conducted in late summer 1971.

The purpose of this report is to serve as an interim documentation of
the fuel slosh investigation program to date. Additional testing at inertia
ratios near 0.6 and 1.1 is presently scheduled for early 1972. This testing,
together with the testing already completed, is intended to establish an
empirical energy dissipation ($\dot{E}$) equation that will permit scaling test and
flight data for arbitrary roll-to-pitch ratios. Such scaling is critical for
determining spacecraft stability margins for vehicle configurations inertially
dissimilar to the Intelsat IV and HS-318 designs.

CONTENTS

Preceding page blank

1. SUMMARY

State-of-the-art reaction control systems for both spin stabilized and three axis stabilized satellites utilize liquid propellant (e.g., hydrazine) which is catalytically decomposed to generate the desired control thrust. A common problem to any satellite using such a propulsion system is to what extent fuel sloshing affects its dynamical behavior and thus influences either hardware design or operational procedures.

At Hughes the development of the Gyrostat stabilization technique focused attention on this problem. In particular, the Intelsat IV and HS-318 satellites stored a large amount of hydrazine (as much as 300 pounds in the former vehicle) in conispherical tanks. In view of the analytical difficulties associated with determining the rate of energy dissipation due to fuel slosh on a spinning body, it was realized that no estimate would be credible unless experimentally verified. To that end, a series of fuel slosh tests were initiated to especially address the problem of Intelsat IV and HS-318.

The fuel slosh test program at Hughes is now 2 years old. During this time, the test procedures, hardware, data reduction method, and physical insight into the problem have been refined to a point where testing is more a science than an art. This report is intended to update and give insight into the work already completed.

Initially, the most significant fact obtained from the test program was that the Intelsat IV spacecraft was potentially in danger of being unstable in synchronous orbit as a result of fuel slosh dissipation. This knowledge led to an engineering change in the nutation damper performance to cope with the new dedamper predictions. Moreover, active nutation control was implemented on the spacecraft in order to handle any large nutational transients that might occur and to provide automatic control in the event propellant dumping became necessary. The awareness of nutation stability stimulated by the test program and reflected in these spacecraft modifications proved valuable in the successful launch of the first three Intelsat IV spacecraft. But, more important, this awareness also stimulated the fuel slosh test program in anticipation that a more general empirical structure could be found from which an analytical theory could evolve. This would help ensure nominal nutational behavior for a wide class of future satellites, from Gyrostat-stabilized to unstable spinners in the transfer orbit.

As the test program matured through several phases of development, emphasis was placed on dimensional analysis as the primary empirical method by which all data would be evaluated. This had the advantages of providing an efficient graphical representation of all the data for general interpretation as well as a straightforward approach of extrapolating earth-based results to the 0 g environment. Specifically, this led to an unambiguous correlation of the test results with the Intelsat IV in orbit dedamping time constant. By means of a special test conducted on F-3 shortly after reaching synchronous orbit, the dedamper was determined to be about 170 seconds. This value agreed within the test accuracy with the 0 g extrapolated data for a 75 percent fraction propellant fill.

This result is encouraging as it confirms the general validity of the various empirical curves pertaining to different fraction fills, tank geometry, and roll-to-pitch moment of inertia ratios. While there are insufficient test data to extend the present test and flight results to all new designs, it is expected that the next test series will significantly add to the knowledge upon which an empirical model will be based.

Experience at Hughes shows that determination of energy dissipation rates in spinning nutating tanks can only be established to the required engineering accuracy through experimental testing. Until empirical and analytical theories are structured consistent with all available data, caution must be exercised in estimating dissipation rates for new designs. Of particular concern are new designs that are Gyrostatically stabilized with inertia ratios greater than Intelsat IV and three axis satellites that are spin stabilized in the transfer orbit. There is optimism at this time of obtaining a fuel slosh model consistent with the empirical results to date as a result of the analytical efforts of Dr. R. H. Edwards.

2. STATEMENT OF PROBLEM AND HISTORY OF INVESTIGATION TO DATE

2.1 PROBLEM REVIEW

The problem of estimating energy dissipation in rotating nutating propellant tanks has existed since the first spin stabilized satellites. Those in the Syncom, Intelsat I (Early Bird), and Intelsat II class were passively stable by design, i.e., fuel sloshing effected nutation in a positive or stabilizing manner. In 1965, D. D. Williams attempted to estimate the effect of sloshing in a spherical tank by making several simplifying assumptions (Reference 1). The sloshing motion was assumed analogous to a spherical segment free to move as a spherical pendulum inside the container. The energy dissipation was calculated at the boundary layer formed by the container and the fluid. Following Lamb (Reference 2), Williams calculated the energy dissipated due to shearing stress set up at the boundary layer by the sinusoidal nutation acceleration.

Supporting evidence of the validity of the Williams model came from sloshing tests and measurements conducted at NASA and the Southwest Research Institute (References 3, 4, and 5). A major shortcoming of these sloshing tests is the nonspinning environment in which the measurements were made. In space, the fluid experiences a steady centripetal acceleration due to the spacecraft spin. It was assumed that this impressed acceleration field was analogous to the static gravitational field on earth. However, the obvious omission of the coriolis acceleration leads to a greatly simplified fluid dynamical motion. Notwithstanding the shortcomings of the model and the lack of good test confirmation, the fuel sloshing problem was dealt with in terms of order of magnitude accuracies. For the spacecraft designs of interest, such accuracies were acceptable.

Meanwhile, a new stabilization concept was being developed and incorporated in new satellite designs which renewed the interest in the fuel slosh problem. Referred to as the Gyrostat spacecraft (Reference 6), the vehicle is no longer passively stable in the same sense as Syncom. The vehicle is spin stabilized about the configuration axis of minimum moment of inertia, and nutation stability is achieved by energy dissipation on a despun platform overcoming the dissipation on the rotor. Thus, to size the despun nutation damper, it is necessary to accurately estimate, or reasonably bound, the rotor dissipation rates. The peroxide or hydrazine reaction control propellant is, perhaps, one of the most nonrigid elements of the rotor.

TACSAT I, the first Gyrostat spacecraft, carried peroxide in six 11 inch diameter spherical tanks. At the time of the vehicle design, the Williams model was used to bound the fuel slosh dissipation rates. While TACSAT did experience a nutation anomaly (Reference 7), the cause of the anomaly was attributed to excessive dissipation in the bearing assembly. The estimated fuel slosh dissipation would have to be a hundred times greater than the estimated value to have caused the observed phenomenon. While such inaccuracy is possible in the fuel slosh estimate, the cause of the problem has been isolated in the bearing assembly.

Following the TACSAT I launch in February 1969, ATS V was launched in August 1969. In the case of ATS V, excessive energy dissipation in 16 heat pipes led to a catastrophic flat spin condition. Subsequent to this launch, laboratory tests were conducted at Hughes on an air bearing fixture that confirmed quantitatively that the heat pipes were the source of the ATS V problem. The tests conducted at the time are described in Reference 8. An important consequence of this test program was the accuracy with which energy dissipated in a rotating nutating vehicle could be measured in the laboratory and shown to agree with the flight conditions.

At the end of the heat pipe tests, a short fuel slosh experiment was conducted on ATS (TACSAT) spherical tanks. The results of those tests, reported in Reference 9, were inconclusive. The experimental accuracy could not detect dedamping greater than 1000 seconds. However, the data suggested that the fuel sloshing effects were greater than expected and indicated substantial discrepancies with Williams' model. This test, while crude in accuracy, evoked growing concern that the rotating fluid dynamical motion was substantially different from the nonrotating pendulous motion described by Williams.

Work on Intelsat IV and I'   ' '   generated further concern in this area. Both were Gyrostat spacecraft   .   ' ' !, but each carried newly designed propellant tanks. Conceived   nt over the spherical tank, the new conispherical configurat   plete fuel drainage, both in the static 1g field on earth and   g centrifugal field of space. The advantage of the tank then   one additional manifold port over the spherical shape previously used.

An early attempt to analytically modify the Williams model to the conispherical geometry was made by Edwards (Reference 10). The conclusions of Reference 10 were applied to Intelsat IV (Reference 11). However, in light of the ATS V and TACSAT I experience, concern mounted over the validity and accuracy of the above analyses.

Discussions with experts in the field of fluid dynamics, viz., Dr. P. G. Saffman of Caltech and Dr. H. Norman Abramson of the Southwest Research Institute (Reference 12), led to the conclusion that an experimental approach was the only meaningful way energy dissipation rates could be accurately determined under the conditions of interest.

A new test vehicle was configured based on the ATS experience, but designed to simulate an Intelsat IV spacecraft. This vehicle carried two full-size conispherical tanks located at the same radial and axial positions relative to the cg as in the flight configuration. Instrumentation techniques were improved to resolve energy dissipation rates on the order of milliwatts. An error analysis (Reference 13) indicated that the test vehicle was consistent with measuring the desired quantities. The Hughes test program began in spring 1970.

A similar fuel slosh test program at the Comsat Laboratories was occurring at the same time under the direction of E. R. Martin. To simplify the test program, the objectives were limited to qualitative verification of the Williams model motion. The 312 tank was positioned on an air slide, which in turn was attached to a single degree of freedom spin table. After reaching flight spin speed (nominally 50 rpm), the tank was subjected to a linear oscillatory excitation at the appropriate amplitudes and frequencies to simulate a nutating spacecraft.

After removing the forced input, the potential energy stored in the fluid was observed to dissipate. The amplitude of the free surface was monitored and recorded. Such data permitted calculating the logarithmic decrement of the motion, thus allowing calculation of the Q of the oscillatory motion. It should be noted that fluid motion observed was the fundamental, or first, sloshing mode. After the forced input was removed, all the higher order modes of oscillation were rapidly damped, and therefore only dissipation in the fundamental mode was measured. The results of these tests tended to corroborate more than refute Williams' model. Summaries of the Comsat Phase I test program are given in References 14 through 17.

One especially useful test result obtained during this Comsat program was measurement of the fundamental sloshing frequency for the conispherical tank. The results of the test are summarized in Reference 18. It was shown that the nonspinning natural frequencies versus fluid fraction fill agreed very well with the spherical frequencies for an equivalent sized tank. These frequencies were all above 1 Hz. It was also established that, when spinning, the fundamental mode is split into two modes — one above and the other below the nominal mode. This splitting is due to a coriolis coupling between the axial and tangential oscillatory modes. As the spin rate increases and the effect of gravity is reduced, the coriolis coupling subsequently reduces. The result, being the lower mode, converges to the uncoupled modal frequency. This result had been predicted by R. H. Edwards. The implications were favorable relative to 0 g scaling and for ensuring that the fundamental sloshing mode was always above the driving nutation frequency. As it turned out, the dissipation due to the fundamental mode was small relative to the total dissipation occurring in the tank.

While the Comsat test program was entering a second phase designed to more accurately simulate the inertial tank motion, the Hughes spinning tests were beginning in September. The initial test conditions of 66 percent fraction fill and spin speeds of 40 to 60 rpm simulated the Intelsat IV flight

conditions. The observed vehicle nutation diverging time constant of 73 seconds exceeded by nearly two orders of magnitude the value estimated via the Williams model approach.

The first few months of the test program constituted a learning period for both the test operation crew and the data interpretation group. The early thrust of the analysis was directed toward understanding the implications of testing in the 1g field. Concern over some form of parametric excitation of the fluid and/or dynamic instability of the spinning, precessing, nutating, nonrigid top prompted several computer simulations. Studies at Hughes (References 19, 20, and 21) and at Aerospace (Reference 22), addressed the 0 g versus 1 g question from an analytical viewpoint. It was anticipated that the increased energy dissipation rates recorded in the test could be attributed to the laboratory test environment; and, in fact, in space the energy dissipation rate would more closely approximate the preconceived estimates. Unfortunately, both of these efforts suffered from the same shortcoming of assuming a penduluous fluid model with modified damping to account from the increased dissipation observed in the laboratory.

While much was learned about the test vehicle dynamics, e.g., effect of spin speed on static stability and effect of pendulosity on the time constant, the conclusions were limited by the rigid body (Williams model) assumption for the fluid motion in the simulation. Thus, while the studies indicated some reduction in $\dot{E}$ in a 0 g environment, quantitative estimates of the actual reduction were difficult to justify.

Numerous modified Williams models were formulated in an attempt to find agreement with the test data and thus permit scaling to flight. One model, constructed by J. V. Harrington and H. O. Curtis of Harrington, Davenport and Curtis, Inc. (consultants to Comsat), arrived at a reasonable fit with all the Phase I data. This work is summarized in References 23 and 24. However, in light of the tests completed to date, the model constructed fits only the Intelsat IV test configuration and, more specifically, operating conditions where gravity effects are significant.

All attempts to formulate a "simple" mechanical model for the fluid motion were thwarted by visual observation of nonlinearity of the motion. Movies taken during the actual testing phase clearly showed through the aid of surface and submerged particles that the fluid was undergoing multiple modes of excitation. While the fundamental forced oscillation of a pendulum could indeed be observed, the realization of surface swirl and high velocity boundary layer shearing near the cone apex essentially terminated the modeling analysis.

The investigation proceeded from a purely empirical viewpoint. The major effort became one of interpreting the data relative to their implication on the flight spacecraft. With the first Intelsat IV scheduled for a January 1971 launch, the question of nutation stability margin became acute. If the test data could not be legitimately extrapolated to space conditions based on sound technical reasoning, then the data must be interpreted at face value.

To accommodate the maximum energy dissipation rates observed in tests, the Intelsat IV nutation damper performance was improved. In addition, active nutation control was implemented as a backup for the transfer orbit. Thus, while Intelsat IV was ready for launch with a stability margin substantially smaller than initially intended, the vehicle's flight readiness could be attributed to the opinion of the study team that the energy dissipation in space would be less than on earth.

Subsequent to the first Intelsat IV launch and demonstration of successful nutational performance, additional fuel slosh testing and in-orbit tests on the second flight vehicle have shown the above assumption relative to the gravity effect to be wrong.

The only data available prior to the Intelsat IV launch were from the Phase I series. In reviewing that data, it appeared as if the fuel sloshing approached some kind of "resonance" as the operating spin speed limit of 100 rpm was approached. The data indicated at the nominal operating speed of 50 to 60 rpm that the dissipation rate was substantially below the resonance value. While it was recognized that gravity was an inseparable part of the data, it was expected (based on the work not only at Hughes but at Comsat and Aerospace as well) that in the absence of the earth's field the dissipation rate would be less than the value measured in the laboratory. However, the increased dissipation at the high spin speeds could not be ignored. It was decided that the most conservative way in which to utilize the test data was to assume that the satellite would operate at this resonant point. Therefore, the data were interpreted in a conservative or worst case sense to reevaluate the system stability margin.

It is now clear that the worst case estimates of the dedamper time constant turned out to be the best estimate of the 0 g interpolated results of that data. What was confusing was that, contrary to the widely held belief at the time, gravity was concealing the dissipation rate due to nutation. And at a high enough spin speed, namely, 100 to 120 rpm, gravity effects became negligible, and the test data represented a 0 g condition in the laboratory. The above conclusion is discussed in more detail in Section 5.

Extending the test results to vehicles of different configurations, specifically ones with a roll-to-pitch ratio other than that of Intelsat IV, was extremely risky in the absence of a fuel slosh model. To deal with the HS-318 spacecraft and its inertia ratio (σ) of 0.1, a new test vehicle was build following an accident on 29 October 1970 which severely damaged the original test vehicle (inertia ratio of typically 0.35).

In addition to accommodating both Intelsat IV and HS-318 inertia ratios, the new vehicle, scaled to 5/8 of the original vehicle's dimensions, had one new significant capability. The spin speed could exceed 200 rpm. The old vehicle could not exceed roughly 100 rpm. At these lower spin speeds, the ratio of centrifugal-to-gravitational acceleration (referred to as the Froude number) was on the order of unity. In the Phase I tests, the much sought after condition where gravitational effects became negligible was never achieved.

The new vehicle afforded the possibility of reaching a 0 g test condition, thus increasing the accuracy of flight extrapolation.

Time constant predictions for the new vehicle were made prior to testing by scaling the results from the old vehicle (References 25 and 26). The first testing with the small vehicle occurred around the end of January 1971. Operating in the $\sigma = 0.35$ configuration, the test data essentially confirmed the dimensional scaling law used to relate the full-size test machine to the 5/8 scale version. Following this dimensional check, the testing at $\sigma = 0.1$ was begun.

Results of the HS-318 test program are summarized in Reference 27. The test data when applied to HS-318 resulted in longer time constants than had existed for Intelsat IV. In addition, the data clearly indicated that at the maximum operating spin speeds of >200 rpm, the energy dissipation rate was substantially less than at the operating speed of 60 rpm. Thus, while it was not evident that a 0 g test condition had been reached nor was it clear how gravity corrupted the test, the quantitative implications were encouraging. Contrary to the $\sigma = 0.35$ case, at $\sigma = 0.1$, gravity effects tend to dominate the nutational effects, making the data look worse than it would be in a 0 g environment. Therefore, the data were used to compute a lower bound on the flight time constant.

By the end of March, the fuel slosh test program entered a period of inactivity. Comsat had completed its Phase II test program and reported its findings (Reference 28). No work at Hughes was expended on this problem until midsummer. At that time, what may be referred to as Phase III of the investigation began. The renewed interest in the problem developed from the following concern.

While the fuel slosh test program had been successful in determining the flight readiness of both vehicles, the test data had been compromised to arrive at the desired ends. In reviewing the data, the test matrices were incomplete. Some data did not appear repeatable. In summary, the data were not in a form that could be used in formulating an empirical equation for $\dot{E}$. A number of important questions remained unanswered. Inasmuch as future vehicle designs may differ from HS-318 and Intelsat IV configurations in certain critical areas, an attempt to unify and generalize the test data was undertaken. Some of the specific unanswered questions were the following:

1) Can a 0 g test be conducted in the laboratory?

2) Can the data be scaled to flight with reasonably accuracy, say within a factor of 2?

3) How does the energy dissipation rate vary with roll-to-pitch ratio?

4) How dependent is the $\dot{E}$ on Reynolds number?

5)   Are spherical tanks preferred to conispherical?

6)   Is it preferable to have a few large tanks or a lot of small
     tanks?

7)   Should the tanks be mounted close to the spin axis or as far
     from it as possible?

8)   Should the tanks be mounted near the cg plane?

The Phase III test program began late in August 1971 and was completed in early October. By means of the test program and corroborative flight data on Intelsat IV, several of the above questions have been satisfactorily answered but others remain unanswered. The conclusions of the entire program constitutes the body of this report. The data are presented and reviewed in light of current knowledge relative to this problem. Therefore, this document serves as an interim report on the fuel slosh problem and also serves as a prelude to additional testing scheduled for early 1972. The next series of tests, conducted with NASA participation, are intended to investigate fuel sloshing at inertia ratios near 0.6 and 1.1.

# 3. TEST FIXTURES, INSTRUMENTATION, AND TEST PROCEDURES

3.1 TEST METHOD

The method of measuring energy dissipation in spinning nutating tanks is severely compounded by a signal-to-noise problem. Typically, the power dissipated varies from milliwatts to microwatts. Because of instrumentation sensitivities and structural nonrigidities, it is difficult to separate the fluid dissipation from other parasitic dissipators. However, due to the success of measuring the energy dissipation in the ATS V heat pipes, the test method developed for that test was refined for the fuel slosh test.

Instead of measuring directly the quadrature component of the forced motion and then computing the resulting damping torque, the indirect effect of the fluid $\dot{E}$ on the nutational stability of a nonrigid freely spinning body was monitored, i.e., the divergence of the nutation angle was observed.

3.2 PHASE I TEST SETUP

The Phase I test vehicle is shown in Figure 3-1. The vehicle consists of a spinning rotor which is attached to the ball segment of a 3 degree of freedom air bearing. The full-sized Intelsat IV conispherical tanks are mounted to the rotor at the appropriate radial and axial location with respect to the vehicle cg to properly simulate the flight configuration. The vehicle is spun up by a rotor-mounted motor and then lifted from the cup by applying air to the bearing. By locating the vehicle cg coincident with the center of curvature of the air bearing when pressure is applied radially through the point of rotation, the force of gravity is countered and the vehicle is free to exhibit nearly frictionless rotational freedom about its cg. To minimize air damping and drag effects, the vehicle is located in a high altitude chamber during the tests. The air bearing leakage rate produced no problem in maintaining the desired altitude (typically 100,000 feet).

When spinning on the air, the vehicle motion is analogous to a top. The spin axis exhibits a coning motion at nutation frequency about the angular momentum vector which, in turn, cones about the local vertical at precession frequency.
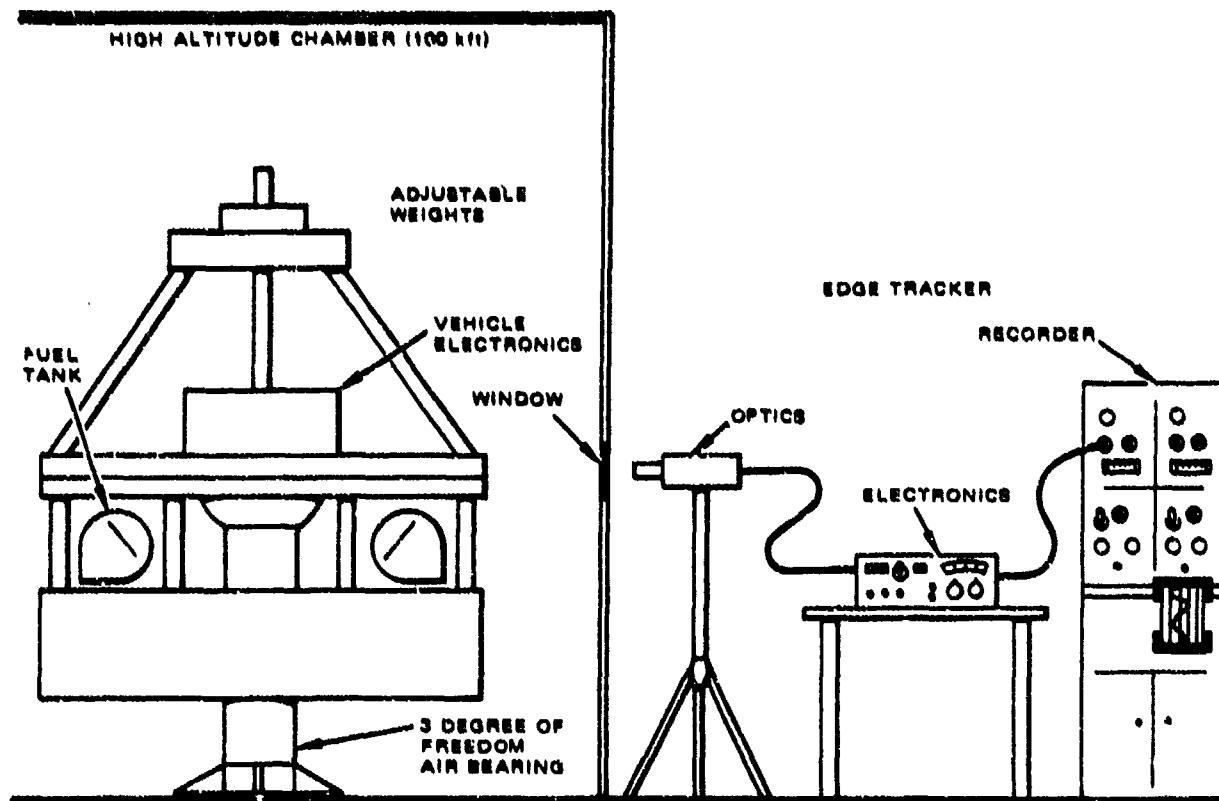
Figure 3-1. Test Fixture and Instrumentation

To minimize the gravity precession motion, the vehicle is statically balanced on the air bearing by moving the cg axially until the precession component is essentially nulled. For long runs >15 minutes duration, the precessional motion is biased to essentially null the earth's rotational rate. Thus, the angular momentum vector remains inertially fixed over the duration of the run. The vehicle is also dynamically balanced prior to testing to minimize coning at spin frequency due to noncollinearity of the geometric spin axis and the vehicle's principal axis.

The vehicle is spin stabilized about its minimum moment of inertia (MOI). In this configuration, any nonrigidities in the vehicle will give rise to energy dissipation when cyclically excited by nutational motion. As spin energy is dissipated as heat, spin momentum is transferred to the transverse (maximum MOI) axis. The spin axis then increasingly deviates from the angular momentum vector as time progresses. If not stopped, the vehicle would tumble off the air bearings. Therefore, nutational motion is mechanically limited to about 10 degrees half-angle amplitude.

Since the rate of change of the nutation angle is related to the amount of energy being dissipated in the system, this parameter is recorded. It can be shown (see Section 4) that the nutation angle history can be described as an exponential with a time constant which is inversely proportional to $\dot{E}$. On the test vehicle, the nutation angle is measured in a vertical by an optical edge tracker which tracks the terminator of a light and dark band that circles the periphery of the test vehicle. The tracker, mounted external to the vehicle, observes the nutation motion as an inertially fixed observer. Therefore, the recording made from this instrument includes the combined motion of nutation, precession, and wobble (coning due to dynamic imbalances). The edge tracker, an instrument manufactured by Physitech, converts the amount of reflected light into a voltage which is then proportional to the displacement of the edge within the instruments optical field of view. The analog output from the electronics is then recorded on a strip chart recorder. (Appendix D contains an edge tracker trace showing precession impressed on the exponentially diverging nutation angle.)

A second means of recording the nutation angle history is by a rotor-mounted accelerometer. This device has a single sensitive axis which is aligned parallel to the spin axis and located near the periphery of the vehicle. As a rotor-mounted observer, the accelerometer senses the cyclic nutational acceleration at a frequency different from the inertially fixed observer. The accelerometer senses the difference between the inertial nutation frequency and the rotor spin frequency. The nutational acceleration being proportional to the nutation angle gives a direct indication of the amplitude of the nutation. The information from the accelerometer transmitted across the air bearing interface is received, demodulated, and recorded on a strip chart. The accelerometer data have the attractive feature of sensing only nutational acceleration — wobble and precession are sensed in rotor coordinates as dc terms.

Since any nonrigid device on the rotor will give rise to energy dissipation, it is necessary to calibrate the system before loading in the fluid. To measure the parasitic dissipation of the vehicle due to actions such as slippage of the structure at its joints or flexing of wires or nonrigid structural elements, dummy weights replaced the loaded propellant tanks and the vehicle was then operated and a time constant recorded. By repeating the test with the fluid, the reciprocal difference in time constants is then attributed to the fuel slosh mechanism.

In the Phase I test program, the fluid fraction fill was varied from 10 to 100 percent. As a result of the varying mass of fluid, the vehicle inertia properties varied. Table 3-1 gives the critical inertia parameters of this vehicle.

3.3 PHASE II AND III TEST SETUP

The second-generation test vehicle was generically the same type of vehicle as the original one; however, several changes and improvements were incorporated in the design. The following vehicle and operation description is taken from Reference 27.

To achieve the 0.1 inertia ratio, the test tanks were scaled to 5/8 of the flight tank dimensions. This also required scaling the radial offset distance from the spin axis by the same amount. As the fraction fill was varied, the inertia ratio was maintained at a constant value. Furthermore, the transverse inertias were held equal. (This axisymmetric configuration is typical of spacecraft designs.) The structure was of an all-welded construction except where ballast weights were attached. This construction results in a more rigid structure than that of the Phase I test vehicle.

TABLE 3-1. PHASE I TEST VEHICLE INERTIA PARAMETERS

Fraction Fill	Transverse Inertias			Spin Inertia	Inertia Ratio	Weight, pounds
	X Axis	Z Axis	Mean			
0.1	95.8	88.4	92.0	26.7	0.29	655
0.3	109.3	95.5	100.0	32.6	0.326	707
0.5	120.9	101.9	111.0	38.8	0.35	760
0.66	129.0	106.5	117.0	41.0	0.36	797
1.00	143.0	114.0	129.0	49.0	0.38	877

Figure 3-2 indicates the various parts of the second test vehicle. When configured in the HS-318 test condition, the vehicle weighs about 1300 pounds. When configured in the Intelsat IV test condition, the vehicle weighs about 470 pounds. The vehicle parameters are listed in Table 3-2.

Four erectors (pneumatically driven) are mounted 90 degrees apart under the air bearing ball to provide a means of orienting the vehicle to any desired attitude, as well as exciting nutation if required.

An indication of the vehicle spin speed is provided by strips of reflective tape attached to the lower cylinder. A photo cell arrangement senses the reflected light from the strips of tape and sends a chain of pulses to an electronic package which converts these pulses into a measure of the vehicle rpm.

The technique utilized to maintain a constant, nonchanging, vehicle configuration for different fluid fraction fills is illustrated in Figure 3-3. The total weight of the mounted elements within the vicinity of a tank is maintained essentially constant. As can be noted from Figure 3-4, the tanks are mounted between the support structures provided. The orientation of the tank is fixed by the placement of the position set screws. Fluid compensating weights are mounted outside each support structure. For a 100 percent fraction fill (tanks full) no weights are attached to the outside of the support structures. When a lesser fraction fill is required, the weight of removed fluid is equally distributed on either side of the support structures via appropriate circular plates. It should be noted that the new tanks were of plexiglass construction. In view of the Phase I experience, the wall thickness and support mounts were substantially strengthened to eliminate the tank as a source of parasitic dissipation.

TABLE 3-2. PHASE II AND III TEST VEHICLE PARAMETERS

Test Vehicle	I_s, slug-ft^2	I_T, slug-ft^2	σ	Weight, pounds
HS-318	25.3	254	0.10	1300
Intelsat IV	14.4	43	0.335	470
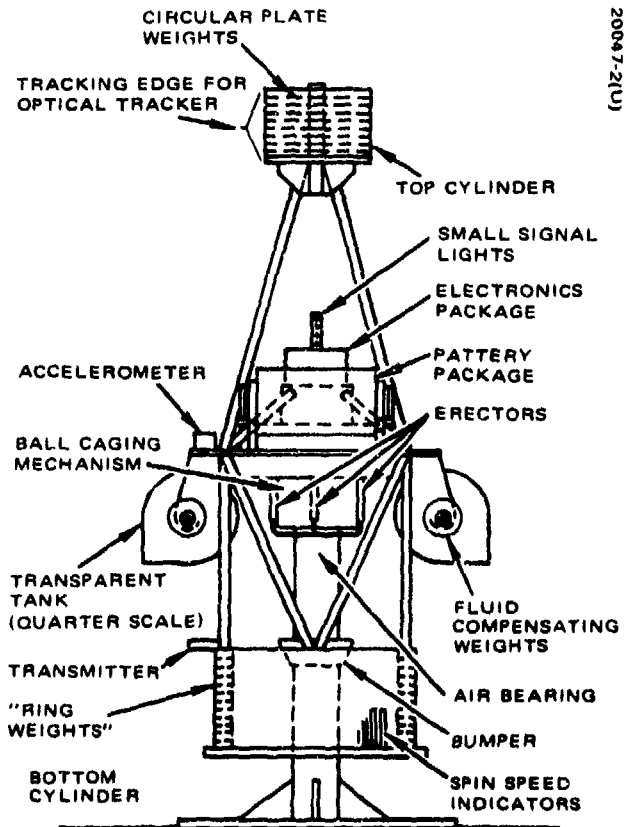
Figure 3-2. Phase II and III Fuel
Slosh Test Vehicle
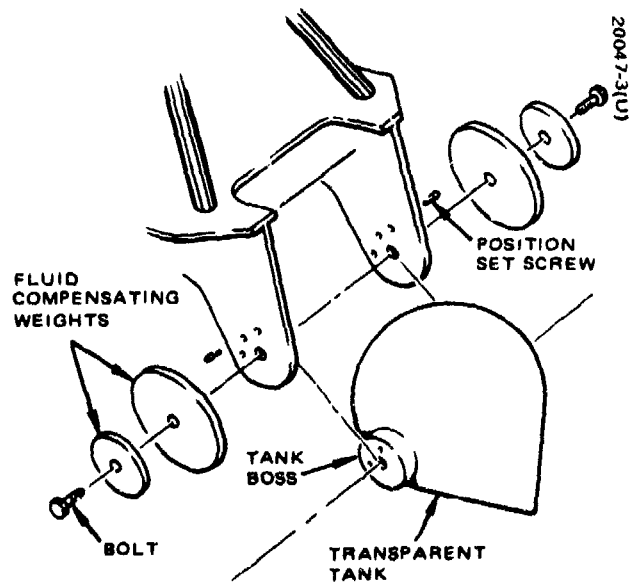
Figure 3-3. Fuel Tank and Fluid
Compensating Weights for Phase
II Vehicle

3-6

SPIN AXIS

$\vec{\omega}_S$

CG

MOUNT

VOLUME = 2848 in.³

CONE
INTERNAL
RADIUS
6.4 in.

SPHERE
INTERNAL
RADIUS
8.86 in.

Z

R

85°

MOUNT

FLIGHT CONISPHERICAL TANK IN
FLIGHT ORIENTATION

1G

CONISPHERICAL TANK INVERTED FOR
SPHERICAL TANK TEST

Figure 3-4. Shape, Size, and Location of Conispherical and Spherical
Propellant Tanks for Fuel Slosh Tests (Note: The above dimensions
pertain to a full-size tank as used in Phase I.)

3.4 TEST OPERATION

The following sequence is typical of a normal test run:

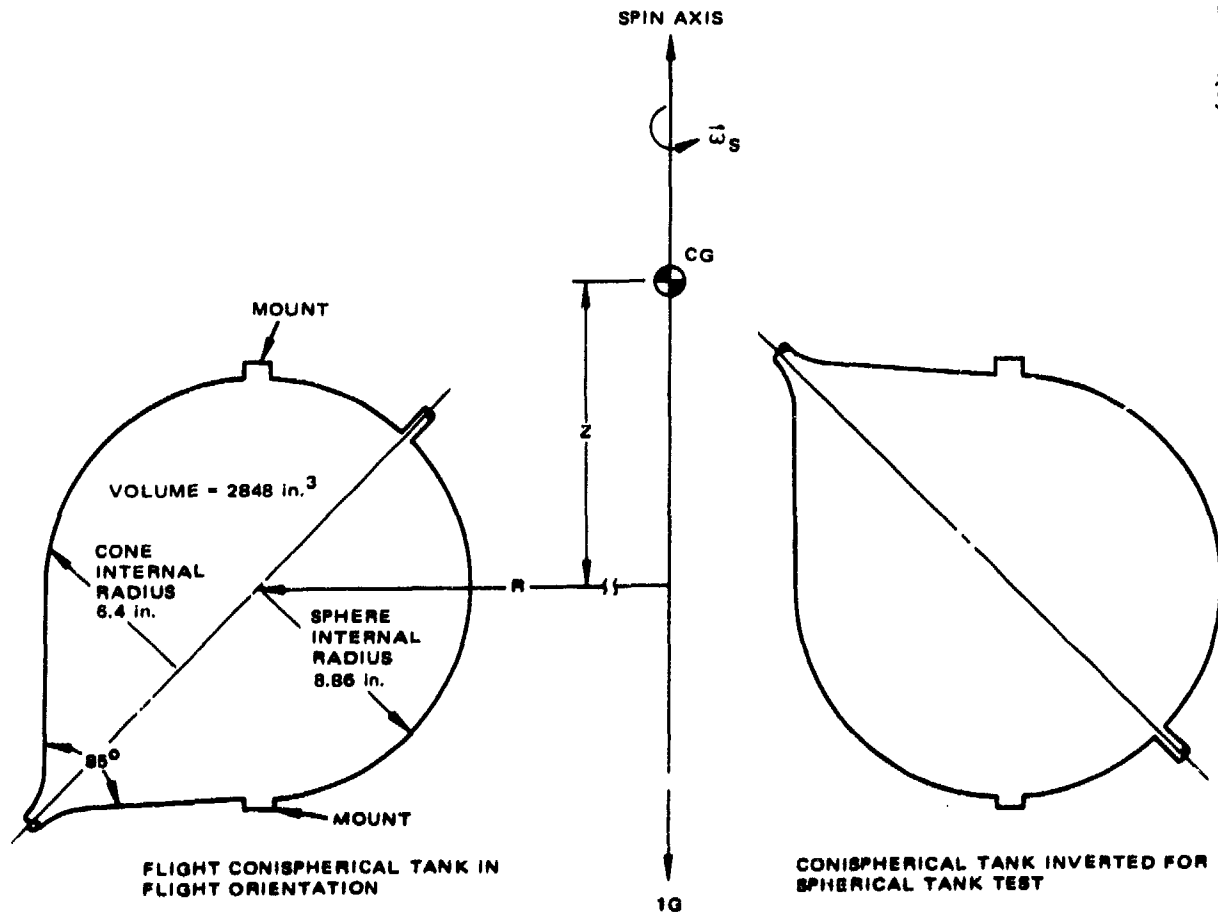1) All bolts restraining the ballast weights are torqued prior to each day's testing.

2) The vehicle is configured for the desired inertia ratio and number of tanks.

3) The tank(s) are filled to the required fraction fill with fluid giving the desired properties (viscosity, density, etc.)

4) Weights are added to the tank supports in order to compensate for fraction fills less than 100 percent.

5) Vehicle gravity precession is checked and minimized if necessary, via vertical shifting of vehicle cg.

6) The vehicle is tilted in preparation for motor rim drive spinup.

7) The altitude chamber is closed and programmed for a simulated altitude of ~140,000 feet.

8) The appropriate accelerometer range and recorder settings, based on run pa imeters, are selected.

9) The spinup motor pneumatic piston is actuated, causing the small wheel on the motor shaft to contact the lower rim of the vehicle.

10) The spinup motor is turned on. An attempt is made to time this operation such that the vehicle is up to the desired spin speed at the time the chamber achieves maximum altitude. Occasionally, the motor must be run through an on-off cycle.

11) The motor is turned off when the desired speed and altitude have been attained.

12) The erectors and air bearing are energized (in that order) to erect (bring to a nominal upright position) the vehicle. The erectors alone cannot support the vehicle weight.

13) Once the vehicle is erect, the air bearing and the erectors are deenergized (in that order).

14) The recorder is turned on.

15) The air bearing is then energized, and one of the erectors is used as a kicker to initiate nutation.

16) Data are now recorded. The termination of a run is dictated by one of the following: a) nutation angle approaching ±10 degree limits, b) one to two time constants worth of data, and c) too much spin speed decay.

17) At the end of a run, the air bearing is deenergized. Nutation is immediately damped out, and the vehicle winds up tilted at some arbitrary angle.

18) The erectors and air bearing are, in turn, energized and the vehicle erected.

19) The air bearing and erectors are, in turn, deenergized.

20) The next run is prepared by increasing the spin speed (tilting the vehicle, etc.) or allowing a coasting decrease, whichever is necessary.

21) After completion of a run sequence, the vehicle is allowed to coast (air bearing deenergized) and the chamber environment is returned to sea level.

22) The chamber is opened and preparation for the next series of runs started.

4. DIMENSIONAL ANALYSIS AND DATA INTERPRETATION

Energy dissipation resulting from fuel slosh on a nutating body manifests itself through the diverging or converging character of the coning or nutation angle. The prevalent method for describing the latter behavior is the time constant approximation, the basic assumption being that the rate of nutation angle change is proportional to nutation angle ($\dot{\theta} = k\theta$). This implies an exponential buildup or decay of nutation angle with time constant $\tau = 1/k$. This model is an excellent one, corroborated by in-orbit observations of Syncom, ATS, and Intelsat IV; moreover, as will be discussed later, the same model aptly characterizes the laboratory observations of the test vehicle.

It is essential to relate the time constant, τ, to the energy dissipation rate, $\dot{E}$, in order to extract from the observations information about the specific properties of the dissipation. A simple derivation of this relationship is formulated as follows: For a vehicle symmetric about the spin axis, the rotational kinetic energy, E, can be expressed in terms of the rotational angular momentum, h, by

$$E = \frac{1}{2} I_T \omega_T^2 \left(\frac{\sigma - 1}{\sigma} \right) + \frac{h^2}{2 I_S} \tag{1}$$

where

I_T = transverse moment of inertia

I_S = spin moment of inertia

$\sigma = \dfrac{I_S}{I_T}$ = roll to pitch ratio

ω_T = transverse angular velocity magnitude (positive)

ω_S = spin speed

Constraining the angular momentum to be constant (torque-free vehicle) and noting that moments of inertia remain nearly constant for small internal motions (fuel slosh), Equation 1 is differentiated to obtain

$$\dot{E} = I_T \, \omega_T \dot{\omega}_T \left(\frac{\sigma-1}{\sigma}\right) \tag{2}$$

If rotational energy is being dissipated, $\dot{E}$ is always negative. Thus if $\sigma < 1$, the transverse angular velocity and, hence, the nutation angle must increase. For small angles, the nutation angle is related to the transverse rate by the equation

$$\omega_T \approx {}^\sigma \omega_S \theta \tag{3}$$

Differentiating, with ω_S approximately constant (ω_S varies as $\cos \theta$ at small θ), and substituting into Equation 2 yields

$$\frac{\dot{\theta}}{\theta} = \frac{\dot{E}}{\theta^2} \frac{1}{\sigma(\sigma-1)\, I_T \omega_S^2} \tag{4}$$

In order for the nutation angle to exhibit an exponential behavior in time, the time constant must be identified as

$$\tau = \frac{\sigma(\sigma-1)\, I_T \omega_S^2}{\dfrac{\dot{E}}{\theta^2}} \tag{5}$$

and the function $\dot{E}/\theta^2$ must be independent of θ, or equivalently, $\dot{E} \, \alpha \, \theta^2$. Note that for n identical dissipators, an exponential behavior requires that the composite time constant is $1/n$ times the individual time constant, implying that the energy dissipation rate is additive.

Thus, exponential growth or decay of nutation requires the existence of one or more dissipators whose rate of energy dissipation is proportional to the square of the nutation angle. The $\dot{E}/\theta^2$ function can be related to the test vehicle time constant (the fundamental output of the tests) by Equation 5.

4.1 DIMENSIONAL ANALYSIS

To evaluate the convergent or divergent nutation angle composite time constant for a specific spacecraft, it is necessary to identify the various dissipators onboard and to determine their individual $\dot{E}/\theta^2$ functions. The latter

assignment is not easy and, for example, in the case of fuel slosh, not yet amenable to analytic solution. It is possible to conduct experimental tests according to the procedures described in Section 3 and determine representative time constants for "point" configurations (specific sets of spin speed and moments of inertia). In view of the difficulty of analyzing energy dissipators and the apparent success in simulating the effects of energy dissipators in the laboratory, it is natural to ask whether some appropriate model for dissipators can be extracted from experimental data. The basic technique required to extract such a model is known as dimensional analysis.

The essential utility of dimensional analysis is derived from the fact that while the relationship between a set of variables associated with a physical phenomenon is not known, the variables themselves are usually known. With dimensional analysis, the phenomenon may be formulated as a relation between a set of dimensionless groups of the variables, the groups numbering less than the variables. This approach requires considerably less experimentation to establish a relationship between the variables over a given range, results in the most efficient graphical presentation of the data for general interpretation, and provides an effective way of extrapolating earth-based results to the 0 g environment. The procedure will now be illustrated by applying it to that energy dissipation phenomenon known as fuel slosh.

It is first assumed that the energy dissipation rate per unit nutation angle squared, $\dot{E}/\theta^2$, is a function of spin speed, ω_S; body nutation (excitation) frequency, $\lambda = (1-\sigma)\omega_S$; mass of fluid, m; density of fluid, ρ; viscosity of fluid, μ; radial distance of tank center from spin axis, R; axial offset of tank center from vehicle center of mass, z; diameter of tank, d; number of tanks, n; special tank geometry denoted by a shape factor, S; and, for earth-based results, gravitational acceleration, g. Functionally, this dependence is expressed as

$$\frac{\dot{E}}{n\theta^2} = f(\omega_S, \lambda, m, \rho, \mu, R, z, d, S, g) \tag{6}$$

where the additive property of the energy dissipation rate has been used to define f as the $\dot{E}/\theta^2$ per tank (n identical tanks). It is further assumed that f may be expressed as an infinite series in its arguments, i.e.,

$$\frac{\dot{E}}{n\theta^2} = \sum_i K_i \left(\omega_S^{e_{1i}} \lambda^{e_{2i}} m^{e_{3i}} \rho^{e_{4i}} \mu^{e_{5i}} R^{e_{6i}} z^{e_{7i}} d^{e_{8i}} S^{e_{9i}} g^{e_{10i}} \right) \tag{7}$$

where the K_i are dimensionless coefficients and e_{1i}, e_{2i} ... are exponents required by the series. Each term in the series must have the same dimension by the law of dimensional homogeneity. Denoting the dimensions of mass,

4-3

length, and time by M, L, and T, respectively, one obtains for each term of the series:

$$\frac{ML^2}{T^3} = \left(\frac{1}{T}\right)^{e_1}\left(\frac{1}{T}\right)^{e_2}(M)^{e_3}\left(\frac{M}{L^3}\right)^{e_4}\left(\frac{M}{LT}\right)^{e_5}(L)^{e_6}(L)^{e_7}(L)^{e_8}\left(\frac{L}{T^2}\right)^{e_{10}} \quad (8)$$

Equation 8 leads to the following three constraints between exponents:

$$e_1 = 3 - e_2 - e_5 - 2e_{10}$$

$$e_3 = 1 - e_4 - e_5 \quad (9)$$

$$e_6 = +2 + 3e_4 + e_5 - e_7 - e_8 - e_{10}$$

Substituting Equation 9 into Equation 7 yields

$$\frac{\dot{E}}{n\theta^2 m R^2 \omega_S^3} = \sum_i K_i \left(\frac{\lambda}{\omega_S}\right)^{e_{2i}}\left(\frac{\rho R^3}{m}\right)^{e_{4i}}\left(\frac{\mu R}{m\omega_S}\right)^{e_{5i}}\left(\frac{Z}{R}\right)^{e_{7i}}\left(\frac{d}{R}\right)^{e_{8i}}(S)^{e_{9i}}\left(\frac{g}{R\omega_S^2}\right)^{e_{10i}} \quad (10)$$

Returning to the functional representation of the series,

$$\frac{\dot{E}}{nm\theta^2 R^2 \omega_S^3} = f\left(\frac{\lambda}{\omega_S}, \frac{\rho R^3}{m}, \frac{\mu R}{m\omega_S}, \frac{Z}{R}, \frac{d}{R}, S, \frac{g}{R\omega_S^2}\right) \quad (11)$$

Note that the original functional relationship between 11 variables has been simplified to one between eight independent dimensionless groups. Several of these groups will now be manipulated to express them in a more recognizable form. Since $\lambda/\omega_S = 1 - \sigma$, the first argument of the function f is taken to be σ, the roll-to-pitch ratio. Now $\rho R^3/m \propto 1/FF \cdot (d/R)^3$, where FF is the fraction fill of the tank; since FF is independent of d/R, FF can be chosen to be the second argument. Noting also that $\mu R/m\omega_S \propto (\mu/\rho d^2 \lambda)(\lambda/\omega)/FF \cdot (d/R)$ and $\rho d^2 \lambda/\mu = \lambda d^2/\nu = R_e$ ($\nu = \mu/\rho$ = kinematic viscosity of fluid), the third argument of f will be taken to be the Reynolds number.

The last dimensionless argument is the reciprocal of the Froude number, $FR \sim R\omega_S^2/g$, and can be identified as this number directly. Finally,

$$\dot{E}/nm\theta^2 R^2 \omega_S^3 = \left(\dot{E}/n\rho d^5 \omega_S^3 \theta^2\right)(d/R)^2/FF,$$

and the dimensionless energy group will be identified as $\dot{E}/n\rho d^5 \omega_S^3 \theta^2$. In summary, then, Equation 11 can be expressed in the following more desirable form:

$$\boxed{\frac{\dot{E}}{n\rho d^5 \omega_S^3 \theta^2} = \text{function}\left(\frac{\lambda d^2}{\nu}, \; \frac{R\omega_S^2}{g}, \; FF, \; S, \; \sigma, \; \frac{d}{R}, \; \frac{Z}{R}\right)} \qquad (12)$$

Equation 5 can be used to define the dual to the energy group; namely, the time constant group:

$$\boxed{\frac{n\tau\rho d^5 \omega_S}{I_T} = \frac{\sigma(\sigma-1)}{\dfrac{\dot{E}}{n\rho d^5 \omega_S^3 \theta^2}}} \qquad (13)$$

While the energy group is more appropriate to study the characteristics of fuel slosh dissipation, the time constant group is more useful in assessing the effect of such dissipation on the nutation angle behavior of a spinning vehicle.

4.2 APPLICATION OF DIMENSIONAL ANALYSIS TO CONDUCT AND INTERPRETATION OF FUEL SLOSH TESTS

If the original assumptions of the functional dependence of $\dot{E}/\theta^2$ are correct, dimensional analysis implies that some functional relationship between the dimensionless groups of Equation 12 exists. Experiments can be made to determine how $\dot{E}/\theta^2$ and τ, implicit in the energy and time constant groups, respectively, vary as a function of each of the groups. If a sufficient number of experiments are performed, an empirical model can be constructed for the function described by Equation 12.

Most important, however, is the construction of such a model for the limiting condition, $R\omega_S^2/g \to \infty$, since the effect of fuel slosh on the nutation angle behavior of a spinning vehicle is of primary importance in the 0 g environment. Intuitively, it is suspected that for a sufficiently high spin speed the effect of gravity on the data is negligible. Dimensional analysis

points out a specific way to test this hypothesis. The energy group versus Reynolds number behavior is experimentally determined at different Froude numbers by varying the spin speed of the test vehicle (a parameter common to all three groups). This results in a set of points in the energy group/Reynolds number plane, each of which is identified by Froude number and all of which pertain to a specific fluid, fraction fill, tank shape, σ, d/R, and Z/R. By changing the fluid (kinematic viscosity) only and repeating the test, another set of points, different from the first, is generated in the plane. This allows a family of straight lines defining energy group versus Reynolds number with Froude number as a parameter to be constructed. A family of higher order polynomials can be obtained by repeating the test on additional fluids. Now, if the effect of gravity on the data is negligible for spin speeds greater than a critical value, ω_{S_*}, members of the family corresponding to Froude numbers greater than $R\omega_{S_*}^2/g$ should all converge to the 0 g curve. If the spin speed achievable on the test vehicle is not sufficiently large to obtain convergence for a special configuration, all is not lost since a useful bound on the 0 g curve will be available. The end product, then, of such a sequence of tests is a 0 g approximation of energy group (and time constant group) versus Reynolds number for a specific set of constants defining the other "geometrical" groups. Symbolically, one obtains

$$\frac{\dot{E}}{n\rho d^5 \omega_S^3 \theta^2} = f\left(\frac{\lambda d^2}{\nu}\right), \ \frac{R\omega_S^2}{g} \to \infty, \ FF = C_1, \ \sigma = C_2, \frac{d}{R} = C_3, \frac{Z}{R} = C_4, S \quad (14)$$

The next step is to systematically accumulate 0 g curves from which an empirical model can be extracted. The basic technique is to determine a family of 0 g curves, energy group versus Reynolds number with one of the geometrical groups as a parameter; the remaining groups are maintained constant. Similar families of 0 g curves are then generated with each of the latter groups as sole parameter. For example, during the Phase III test series, a family of limiting energy group versus Reynolds number curves was determined for fraction fills of 30, 50, 60, 66, 75, and 100 percent. The other groups were constant during the test series with $\sigma = 0.335$, d/R = 0.77, Z/R = 0.49, and conispherical tank geometry. The corresponding curves for fraction fills of 66 and 100 percent were also obtained for $\sigma = 0.1$, d/R = 0.77, Z/R = 0.49, and conispherical tank geometry. These two series of tests help define how the energy group versus Reynolds number curves vary with fraction fill and roll-to-pitch ratio (measure of excitation frequency) for conispherical tanks mounted on spacecraft such as Intelsat IV and HS-318.

The Phase IV series of tests discussed later will define the corresponding curves for roll-to-pitch ratios associated with other spacecraft like SMS ($\sigma \approx 0.6$ after apogee motor burn) and the Canadian Domestic Satellite ($\sigma \approx 1.1$); this will aid in developing a much needed model of how the roll-to-pitch ratio affects fuel slosh energy dissipation.

The Phase III tests also included the same intensive testing on the
spherical tank geometry so that a model for energy dissipation in a spherical
tank can also be extracted when the test program is complete. Although the
other two geometrical groups, d/R and Z/R, were constant during all Phase I,
II, and III tests (values correspond to both Intelsat IV and HS-318), it is
presently hoped that some limited variation of d/R during tests in Phase IV
will be accomplished.

All the data from the Phase I, II, and III series of tests have been
illustrated and compared in the same basic graphical format. The energy
group is plotted versus Reynolds number on log-log paper with Froude num-
ber as a parameter, and the constants defining the three principal geometri-
cal groups (i.e., fraction fill, roll-to-pitch ratio, and tank geometry) are
clearly labeled. A companion plot where the time constant replaces the
energy group with all the other groups as before is also presented. These
two plots represent the empirical data bit from which the 0 g curve or its
bound can be readily extracted. Where several 0 g curves are available for
a geometric group (as is currently the case for the fraction fill group), a
special plot illustrating a family of energy group versus Reynolds number
curves with that group as a parameter is presented. Other plots associated
with repeatability, superposition, and test series comparison will be explained
in the appropriate context.

5. PRESENTATION AND DISCUSSION RESULTS

The test data are presented and discussed in this section. The Intelsat IV results are reviewed first since they constitute the bulk of the data to date. The method of plotting was discussed in Section 4.2. For convenience, the critical plotting and test parameters are listed in Table 5-1.

The physical properties of the fluids used in the test program are summarized in Table 5-2. For the sake of graphical uniformity, the data symbols have been standardized and represent the fluids shown in the table. Any reuse of these symbols is noted in the appropriate graphs.

Table 5-3 is a summary test matrix of the entire test program to date. The table is designed to provide the reader with all critical parameters for any specific test run. The best way to read the matrix is down a given column. The table first identifies the test phase, then identifies the tank geometry, and then gives the test inertia ratio followed by the physical parameters of the test machine. The fraction fill is next followed by the dimensional characteristics of the tank location. The number of tanks, n, is next. The test fluids are then listed. Here, one or more fluids are listed. When dual or triple fluids are noted, it means that all other parameters in the column are held constant, i. e. , the test is simply rerun with the new fluid. The fluid weight is given for reference. In Appendix C a curve relates fluid weight and fraction fill. The last parameter, spin speed, is actually a range of values. With all the other test parameters constant, the test is operated at various spin speeds in the cited range. The rate is incrementally varied to map this range. In Phase II and III testing, the spin speed increments were 30 rpm. In Phase I, steps of 10 rpm were used.

5.1 TANK SUPERPOSITION DEMONSTRATION

In the early phase of the test program, it was not clear if indeed the principle of superposition of tanks would apply to the test vehicle. One would assume this principle to hold if the energy sink concept is valid. The analysis in Section 4 discusses this in more detail. While it was felt that in flight this principle would hold, it was not clear that it would in the small test vehicle. The central concern was over the mass fraction represented by the fluid with respect to the total mass of the vehicle. It was possible to have a nonlinear coupling between the vehicle mass and the large

TABLE 5-1. PARAMETER DEFINITION

Symbol	Definition	Unit
I_T	Transverse moment of inertia	$Slug\text{-}ft^2$
σ	Roll-to-pitch ratio, $\dfrac{\text{spin MOI}}{\text{transverse MOI}}$	—
n	Number of tanks	—
d	Tank diameter	Feet
R	Radial offset of tank center and spin axis	Feet
Z	Axial offset of tank center and space-craft cg	Feet
ρ	Density of fluid	$Slug/ft^3$
μ	Viscosity of fluid	$Lb\text{-}sec/ft^2$
υ	Kinematic viscosity, μ/ρ	ft^2/sec
ω_s	Spin speed	Rad/sec
λ	Rotor nutation frequency, $(1-\sigma)\omega_s$	Rad/sec
Fr.	Froude number $(R\omega_s^2/g)$	—
Re.	Reynolds number $(\lambda d^2/\nu)$	—
FF	Fraction fill by volume	Percent
τ	Time constant	Seconds
$\dot{E}$	Energy dissipation rate	Ft-lb/sec
$\theta *$	Nutation angle	Degree
$\dfrac{n\tau\rho d^5}{I_T}\omega_s$	Time constant group	—
$\dot{E}/\theta_n^2\rho d^5\omega_s^3$	Energy group	—

*Note: Data have been plotted as a function of nutation angle according to the following standardized format:

1) If the data best fit a single exponential curve, a solid line denotes the best τ over the full range of θ, typically 1 to 8 degrees.

2) If two time constants more accurately fit the data, a dashed curve is used for $\theta < 2$ degree (typically) and a solid line is used for $2 < \theta < 8$ degrees.

5-2

TABLE 5-2. TEST FLUID PARAMETER TABLE

Test Fluid	Notation	ρ, slug/ft^3	μ, lb-sec/ft^2 x10^{-5}	ν ft^2/sec x10^{-5}	Data Symbol*
Water	A	1.94	2	1.0	⊡
Glycerine and water	B	2.14	8.35	3.9	⊙
Freon	C	1.94	1	0.51	△
Glycerine and water	D	2.04	3.1	1.54	⊙
Glycerine and water	E	2.02	2.92	1.44	⊙
Glycerine and water	F	2	3.32	1.66	⊙
Freon	G	1.96	0.98	0.5	△

*Three data symbols have been used throughout. Unless otherwise noted on the particular graph, the symbols above have the respective connotation given here.

moving fuel mass. As it turned out, neither test vehicle was plagued by a "tail wagging the dog" effect. The exponential behavior of the nutation envelope itself gave credibility to the conclusion that the energy dissipation rates per tank must add in series.

However, to experimentally verify the tank superposition principle, tests were run on both the Phase I and II test vehicles. The results of the tests are shown in Figure 5-1. The upper half of the figure gives the Phase I test results. Here, only a limited spin speed range was tested. The results showed that the reciprocal addition of the titanium and plexiglass tanks gave the expected resultant value. The test also pointed out the fact that the plexiglass tank had additional losses beyond those just due to fuel sloshing. After this test, the plexiglass tank was removed and all subsequent Phase I testing was with the single titanium flight tank.

The Phase II test for superposition was conducted at 66 percent fraction fill and at $\sigma = 0.1$. The test consisted of first running both tanks and then removing one and repeating the test. The results of the single tank test were simply doubled since the tanks were identical. The resultant overlapping of the curves gives proof that the superposition principle is valid for this test vehicle as well.
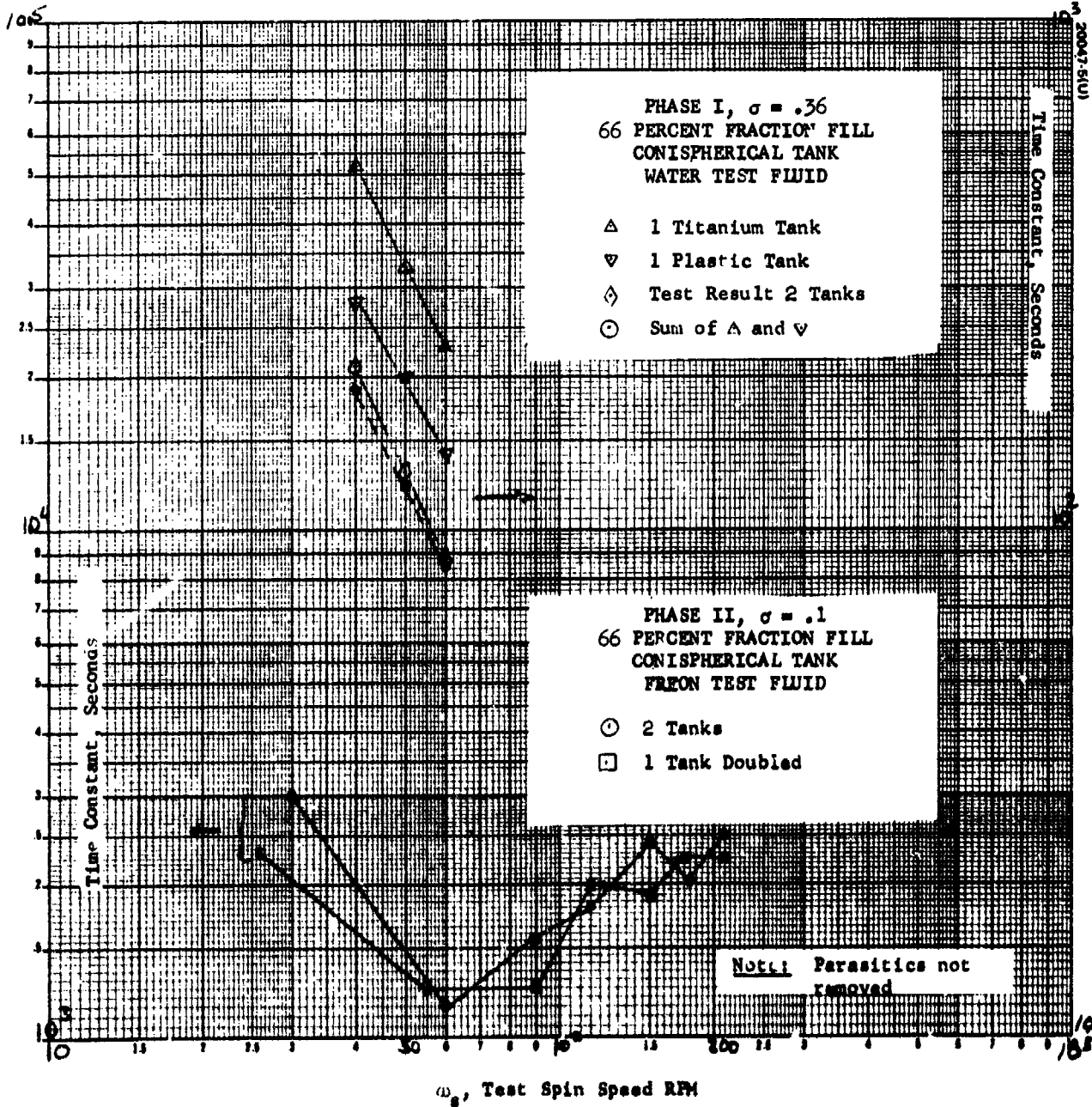
Figure 5-1. Test Demonstrations of Superposition of Number of Tanks —
Phases I and II

TABLE 5-3. FUEL SLOSH TEST MATRIX

Parameter	Phase I Test Conispherical Tank						Spherical	
σ	0.29	0.326	0.35	0.36	0.38	0.36	0.1	0.1
l_T	92	100	111	117	129	117	254	254
Test vehicle weight, pounds	655	707	760	797	877	797	1318	1318
FF	10	30	50	66	100	66	30	50
d	1.44	1.44	1.44	1.44	1.44	0.92	0.92	0.92
R	1.90	1.90	1.90	1.90	1.90	1.90	1.2	1.2
z	1.17	1.17	1.17	1.17	1.17	1.17	0.59	0.59
n	1[1]	1	1	$1, 2$[2]	1	1	2[5]	$2, 1$[6]
Test fluid	A, B	A, B	A, B[3]	A, B[3]	A, B	A	C, D	C
Test fluid weight, pounds	10	30	50	$66, 132$[2]	100	66	16.4	27.4
Spin speed range, rpm	$30-110$[4]	30-110	30-110	30-110	30-110	40-60	$30-210$[8]	30-210

NOTES:

[1] Flight titanium tank mounted in flight orientation (all single tank tests).

[2] Special 1 and 2 (second tank was plastic) tank comparative test was made at 66 percent ff. A fluid only; the results are plotted in Figure.

[3] Glycerine and water solution (B) tests were run in both Culver City and El Segundo.

[4] Spin speed incrementally varied in steps of 10 rpm in all tests.

[5] Plexiglass conispherical tanks mounted in flight orientation.

[6] Comparative 1 and 2 tank test was made with C fluid only.

[7] C fluid tests run to compare with Phase I 10 and 66 percent A fluid tests (i.e., d^2/ν = constant)

[8] Spin speed incrementally varied in steps of 30

[9] Test fluids F and G intended to be the same as C and D.

[10] "Spherical" tank configuration achieved by inverting conispherical tank.

Conispherical Tank							Conispherical Tank					
0.1	0.1	0.1	0.1	0.1	0.335	0.335	0.1	0.1	0.335	0.335	0.335	0.335
254	254	254	254	254	43	43	254	254	43	43	43	43
1318	1318	1318	1318	1318	463	463	1318	1318	463	463	463	463
30	50	66	80	0.00	10	66	66	100	30	50	60	66
0.92	0.92	0.92	0.92	0.92	0.92	0.92	0.92	0.92	0.92	0.92	0.92	0.92
1.2	1.2	1.2	1.2	1.2	1.2	1.2	1.2	1.2	1.2	1.2	1.2	1.2
0.59	0.59	0.59	0.59	0.59	0.59	0.59	0.59	0.59	0.59	0.59	0.59	0.59
2[5]	2,1[6]	2	2	2	2	2	2	2	2	2	2	2
C,D	C	C,D	C	C,E	C[7]	C[7]	F,G[9]	F,G	A,F,G	A,F,G	F,G	A,F,G
16.4	27.4	36,18[6]	44	54.5	5.4	36	36	54.5	16.4	27.4	32.8	36
30-210[8]	30-210	30-210	30-210	30-210	30-150	30-150	60-210	60-210	60-210	60-210	60-210	60-210

compare with Phase I 10 and
tests (i.e., d^2/ν = constant)

entally varied in steps of 30 rpm.

G intended to be the same as

onfiguration achieved by
rical tank.

Phase III Test											
Conispherical Tank						Spherical Tank[10]					
0.335	0.335	0.335	0.335	0.335	0.335	0.1	0.335	0.335	0.335	0.335	0.335
43	43	43	43	43	43	43	43	43	43	43	43
463	463	463	463	463	463	1318	463	463	463	463	463
30	50	60	66	75	100	66	30	50	60	66	75
0.92	0.92	0.92	0.92	0.92	0.92	0.92	0.92	0.92	0.92	0.92	0.92
1.2	1.2	1.2	1.2	1.2	1.2	1.2	1.2	1.2	1.2	1.2	1.2
0.59	0.59	0.59	0.59	0.59	0.59	0.59	0.59	0.59	0.59	0.59	0.59
2	2	2	2	2	2	2	2	2	2	2	2
A,F,G	A,F,G	F,G	A,F,G	A,F,G	A,F,G	F,G	A,F,G	A,F,G	F,G	A,F,G	A,F,G
16.4	27.4	32.8	36	40.5	54.5	36	16.4	27.4	32.8	36	40.5
60-210	60-210	60-210	60-210	60-210	60-210	60-210	60-210	60-210	60-210	60-210	60-210

5.2 DATA REPEATABILITY

The ability to repeat a test and achieve essentially the same result is central to any empirical test program. Repeatability should not be taken for granted and must be experimentally established. However, it is obviously unreasonable to repeat the entire test matrix just for the sake of completeness. Several positive demonstrations of data repeatability should be sufficient to validate the entire complement of test data. These special tests, together with an error analysis (see Appendix B), give credibility to the entire test program.

The following tests constitute the basic proof of repeatability in the test program. It should be noted that no data exist for the Phase I test series. This is perhaps unfortunate since it is shown later that the data are suspect to a secondary source of dissipation which was not removed from the data.

Perhaps the most demonstrative piece of data related to repeatability is indicated in Figure 5-2, which shows the test results taken on the Phase II vehicle at the 0.335 inertia first in January 1971 and again in September 1971. Between the two sets of data was a major vehicle modification to the 0.1 inertia ratio and back again to the 0.335 condition. The close agreement between the two sets of data indicates that not only the fuel sloshing is repeatable but, equally significant, that the vehicle can be modified, reassembled, and retested and still preserve the critical information. When it is realized that the energy dissipation rates being observed are on the order of milliwatts, it is impressive that a quarter ton piece of machinery can be characterized as a truly rigid body. At least on a comparative scale the residual nonrigidities of the vehicle are at least an order of magnitude below the fuel slosh effects.

Other tests of repeatability are shown in Figure 5-3. In Figure 5-3a, the 66 percent fraction fill 0.1 inertia ratio data show good agreement between Phase II and Phase III tests. Likewise, the 100 percent fraction fill data in Figure 5-3b show good agreement for the glycerine solution while, the freon data look a little discrepant at the low spin speed. It is noted that the Phase II data have some questionable value due to uncertainties in the parasitic dissipation in the vehicle.

5.3 CONISPHERICAL TESTS, $\sigma = 0.335$ (INTELSAT IV) DATA

This section presents the Phase III data collected on the conispherical tank configuration for the Intelsat IV inertia condition. The discussion progresses through the data starting at 100 percent fraction fill down to 30 percent fraction fill. Then, the data are summarized and Phase I and III data are compared.
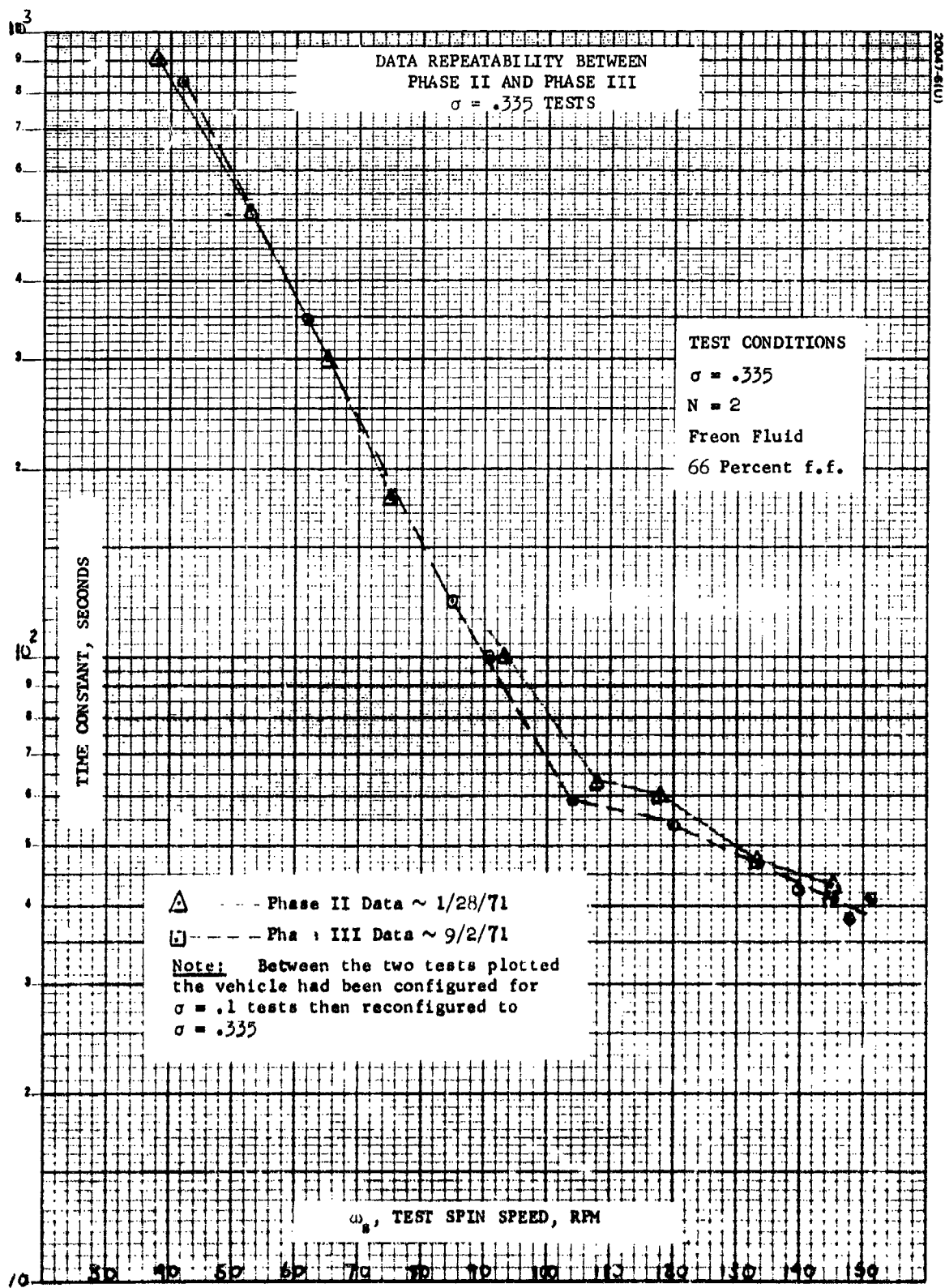
Figure 5-2. Data Repeatability Between Phase II and III
Where σ = 0.335

Glycerine/H$_2$O Fluid

[·]— Phase II
○— Phase III

Freon Fluid

⊡—Phase II Corrected for Parasitics
○—Phase III August 20, 1971
△—Phase III August 25, 1971
▽—Phase III August 26, 1971

ω_s, Spin Speed, RPM
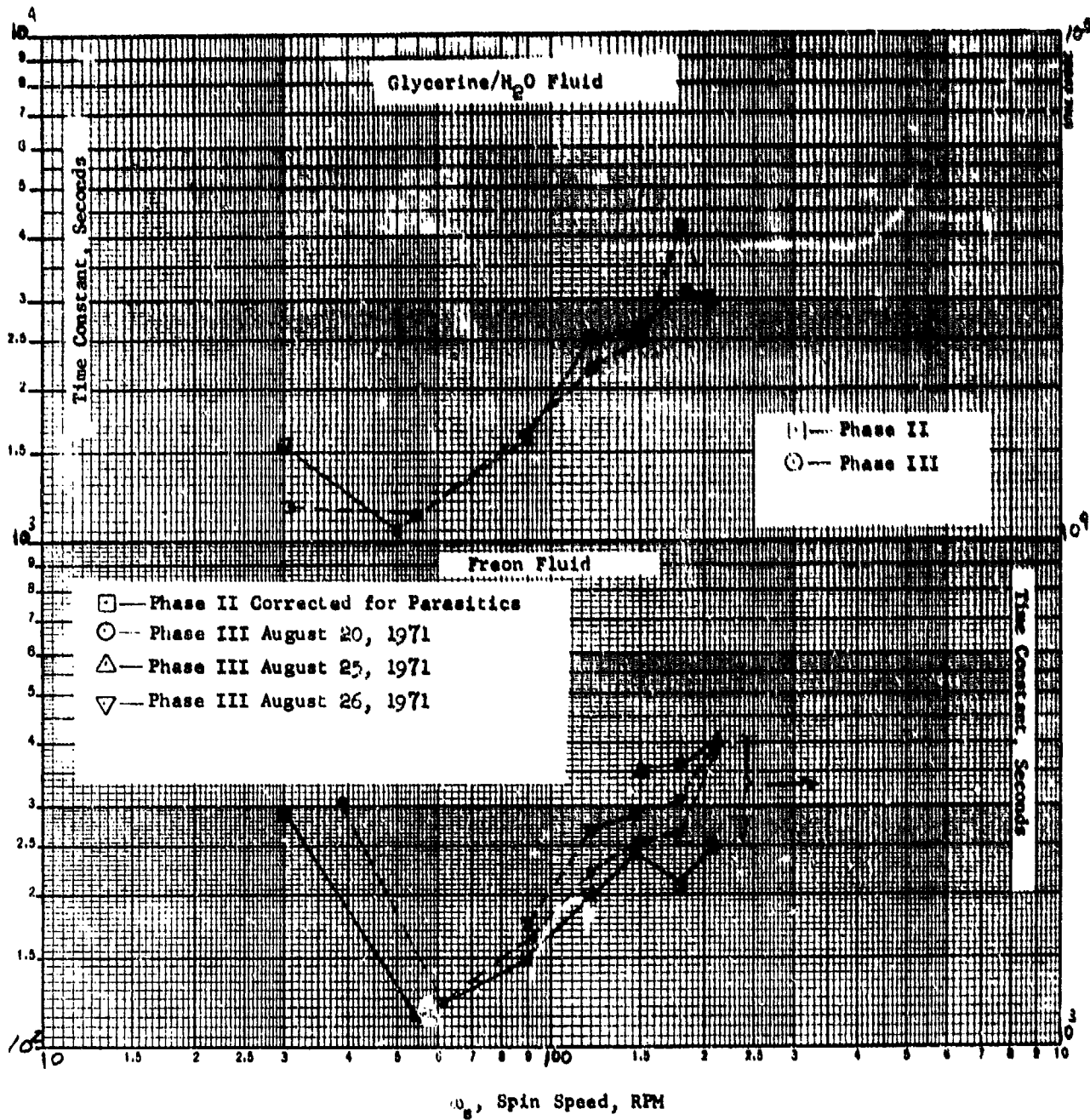
a) 66 Percent Fraction Fill

Figure 5-3.   Data Repeatability Between Phase II and III
Where $\sigma = 0.1$

5-9

ω_s, Test Spin Speed, RPM
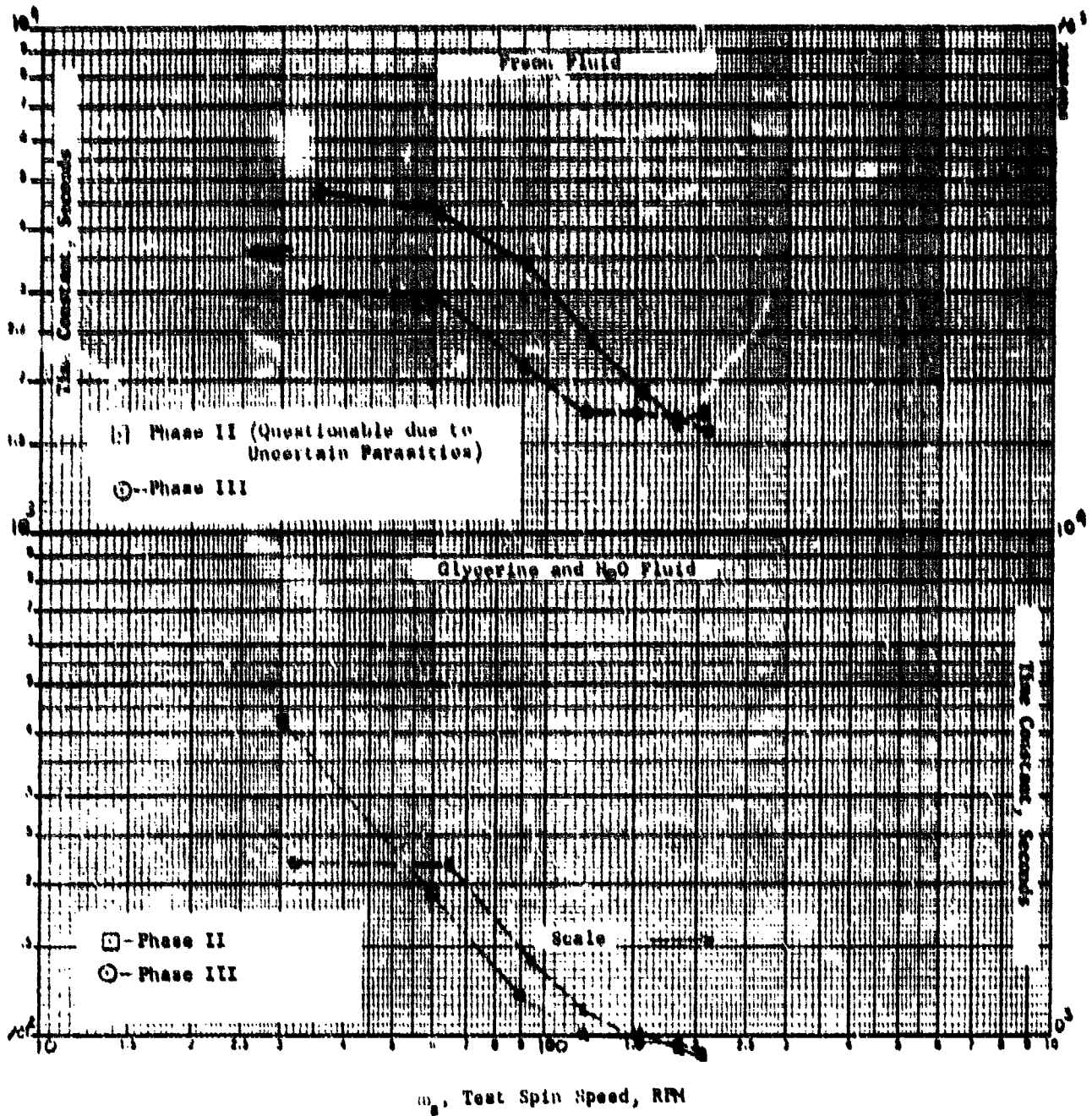
b) 100 Percent Fraction Fill

Figure 5-3 (continued). Data Repeatability Between Phase II and III
Where $\sigma = 0.1$

5.3.1 100 Percent Fraction Fill

Figure 5-4a indicates the fuel sloshing behavior at 100 percent fraction fill. While this case is not of engineering significance, it is important from a fluid dynamics viewpoint. It, therefore, serves as a reference point which will hopefully shed some light on the behavior of the fuel sloshing at partial fraction fills.

The two most important facts contained in Figure 5-4 are that the time constant group is a function of Reynold's number and that gravity does not affect the results. This latter point is significant since fluid dynamically the 1 g field can be absorbed as a pressure gradient in the fluid and would therefore be expected to have no influence on the energy dissipation rate. Thus, Figure 5-4 contains experimental confirmation of an intuitive fluid dynamical behavior expected to be observed in the test.

The other key point that the energy dissipation rate is some function of Reynolds number is also consistent with previous analysis of this problem. Experimentally, it appears that the energy dissipation rate is roughly inversely proportional to the square root of the Reynolds number, i.e.,

$$\dot{E} \alpha \frac{1}{(\text{Reynolds number})^{1/2}}$$

Or, stated differently, the energy dissipation rate is proportional to the square root of the fluid viscosity. This functional relationship is the one originally used by D. D. Williams and characteristic of a laminar boundary layer.

In summary, the 100 percent case appears somewhat consistent with existing knowledge of the expected fluid behavior.

As a point of reference when looking at Figures 5-4 and the others to follow, the Intelsat IV flight Reynolds number is about 7.2×10^5. Also, to project the time constant group numbers to a flight time constant value, simply multiply the group constant at the highest Froude number and at the above Reynolds number by 2; the value obtained is the flight dedamping time constant in seconds for the synchronous orbit condition. For example, in Figure 5-4, the group number is about 500; so multiply by 2, and the resultant 1000 seconds is the expected flight time constant. (Section 6 describes in more detail the flight extrapolation method summarized here.)

5.3.2 75 Percent Fraction Fill

The fluid behavior at 75 percent fraction fill is considerably different than the 100 percent case. Figure 5-5 gives the respective time constant and energy group data. Several facts are apparent when looking at these curves.
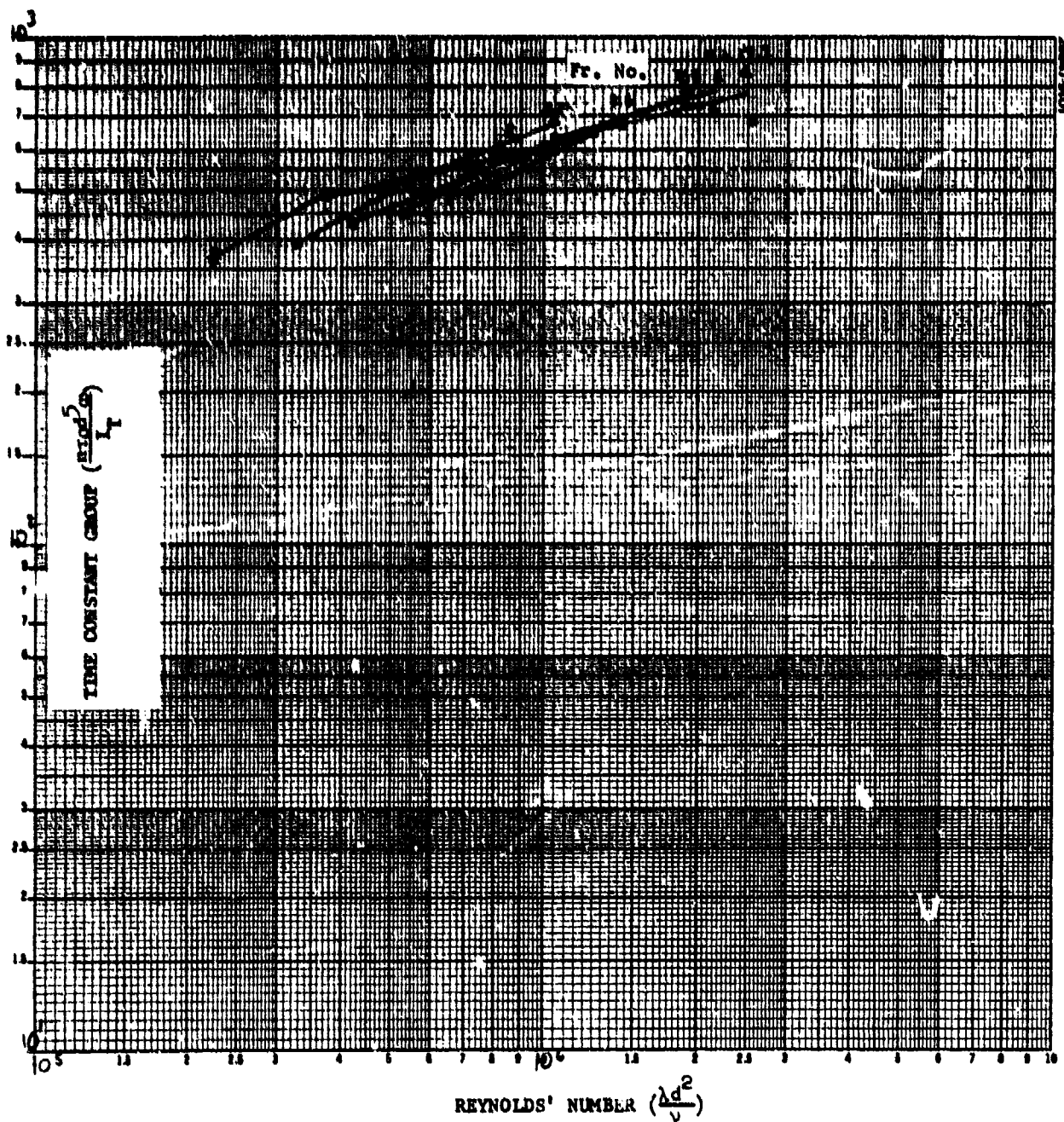
a) Time Constant Group Versus Reynolds Number

Figure 5-4. Phase III Conispherical Tank Fuel Sloshing at 100 Percent Fraction Fill ($\sigma = 0.335$)
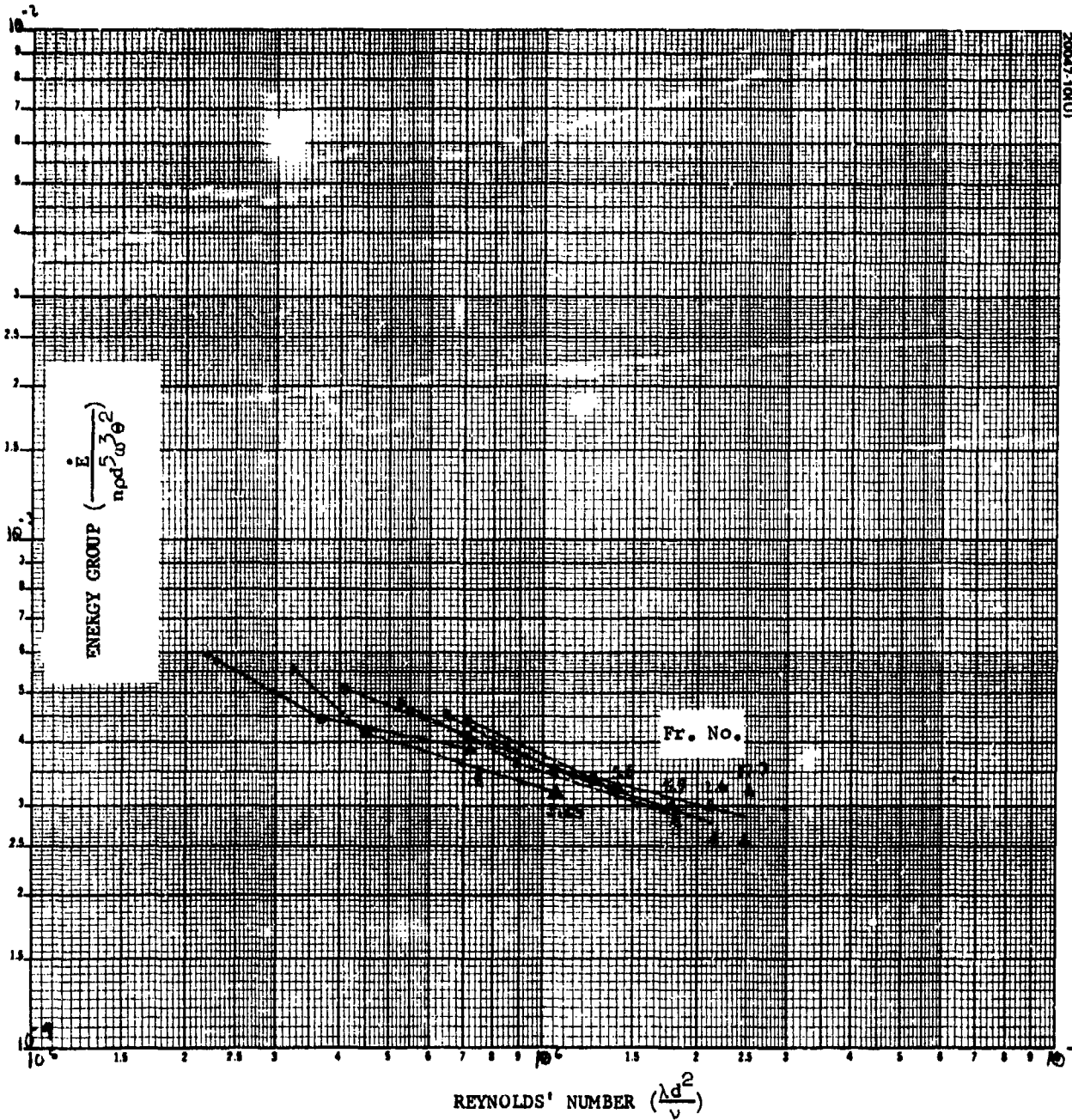
b) Energy Group Versus Reynolds Number

Figure 5-4 (continued). Phase III Conispherical Tank Fuel Sloshing at
100 Percent Fraction Fill (σ = 0.335)
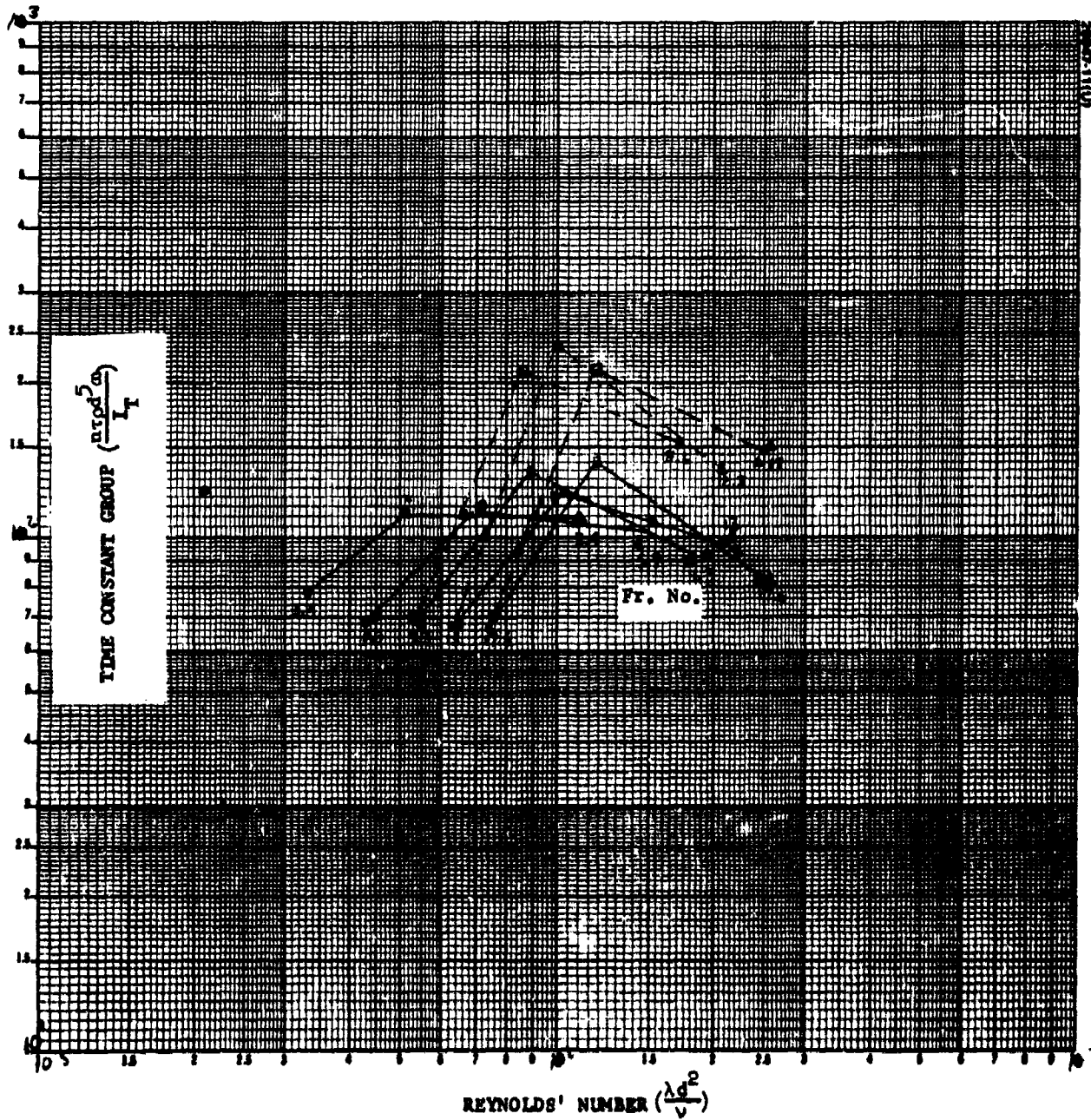
a) Time Constant Group Versus Reynolds Number

Figure 5-5. Phase III Conispherical Tank Fuel Sloshing at 75 Percent
Fraction Fill (σ = 0.335)

Y-axis label: ENERGY GROUP $\left(\dfrac{\dot{E}}{n\rho d^5\omega^3\theta^2}\right)$

X-axis label: REYNOLDS' NUMBER $\left(\dfrac{\lambda d^2}{\nu}\right)$

Fr. No.

Fr. No.
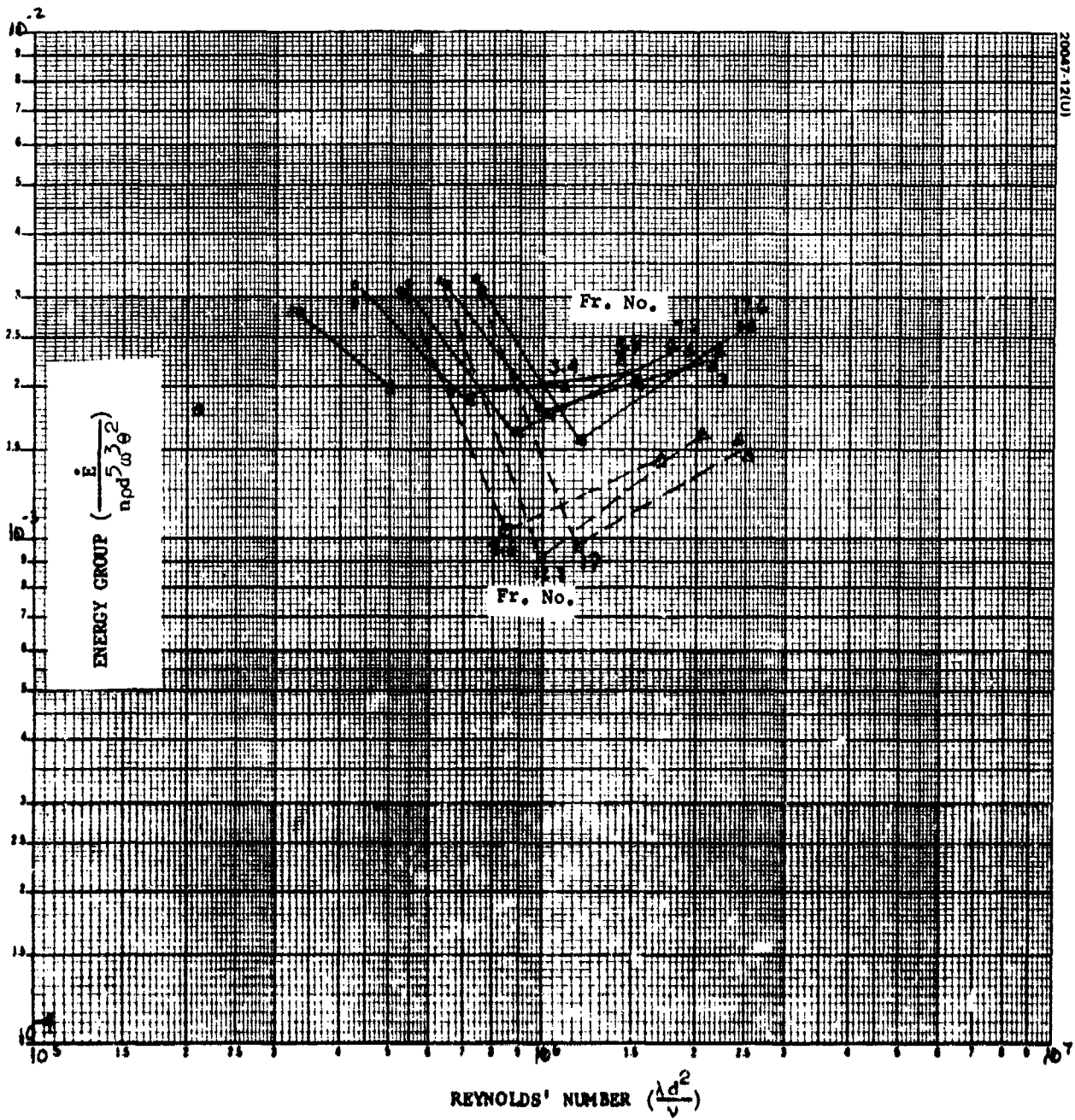
b) Energy Group Versus Reynolds Number

Figure 5-5 (continued).   Phase III Conispherical Tank Fuel Sloshing at 75 Percent Fraction Fill (σ = 0.335)

5-15

Gravity effects are minimal since the group constants are insensitive to nearly an order of magnitude change in the Froude number. There is a definite Reynolds number behavior which is substantially different from the 100 percent case. The data suggests that the tests are being conducted near a sensitive Reynolds number region. This may be the reason for the time constant change evidenced by the nutation angle behavior. The data show that at small nutation angles ($\theta < 2$ degrees) the time constant is longer than that at the larger angles (2 degrees $< \theta < 8$ degrees). This result suggests the excitation of a secondary, more lossy, mode of dissipation at the higher amplitudes.

Obtaining a flight time constant from this curve is difficult. At best, a bound can be placed on the value and it could run between 140 and 220 seconds.

5.3.3 66 Percent Fraction Fill

The 66 percent fraction fill case, shown in Figure 5-6, contains some interesting results. The most significant characteristic of Figure 5-6a is the Froude number convergence. Starting at a value less than 1, where gravity acceleration exceeds the centrifugal acceleration, the time constant group levels incrementally decrease for each change in Froude number. At a value of about 5.5 convergence is achieved and the data beyond this point can be interpreted as a 0 g simulation. Obviously though, when interpolating the results to space, it would be desirable to select the highest Froude number obtained, thereby minimizing gravity effects. It is interesting to note how rapidly the convergence occurs once the critical spin speed, ω_s^*, is reached. In this case, ω_s^* is around 120 rpm. Thus, above this spin speed, all of the data are applicable to flight interpolation. Once this convergence had been demonstrated, the tests at lower spin speed were terminated. For that reason, much of the data subsequently plotted lack Froude number results below roughly 5.

The explanation for why or how gravity acts to suppress the fluid motion is not known. When viewed in light of all the other test data available, it is clear that the gravitational effects are both subtle and significant. They can vary with fraction fill and, more significantly, with inertia ratio. It is therefore important to any empirical model of this fluid dissipation to be careful of the data used and ensure that the effects of gravity are not present.

On this point, the extensive analysis and modelings attempts of Curtis and Harrington (References 23 and 24) unfortunately suffered from the lack of insight presently at hand. In retrospect, the Phase I data, as will be noted later, came tantalizingly close to the desired Froude number of 5. However, test vehicle limitations prevented higher speed runs required to ensure that 0 g convergence had been reached. Had that occurred, the conclusions of the Phase I tests would have been different.
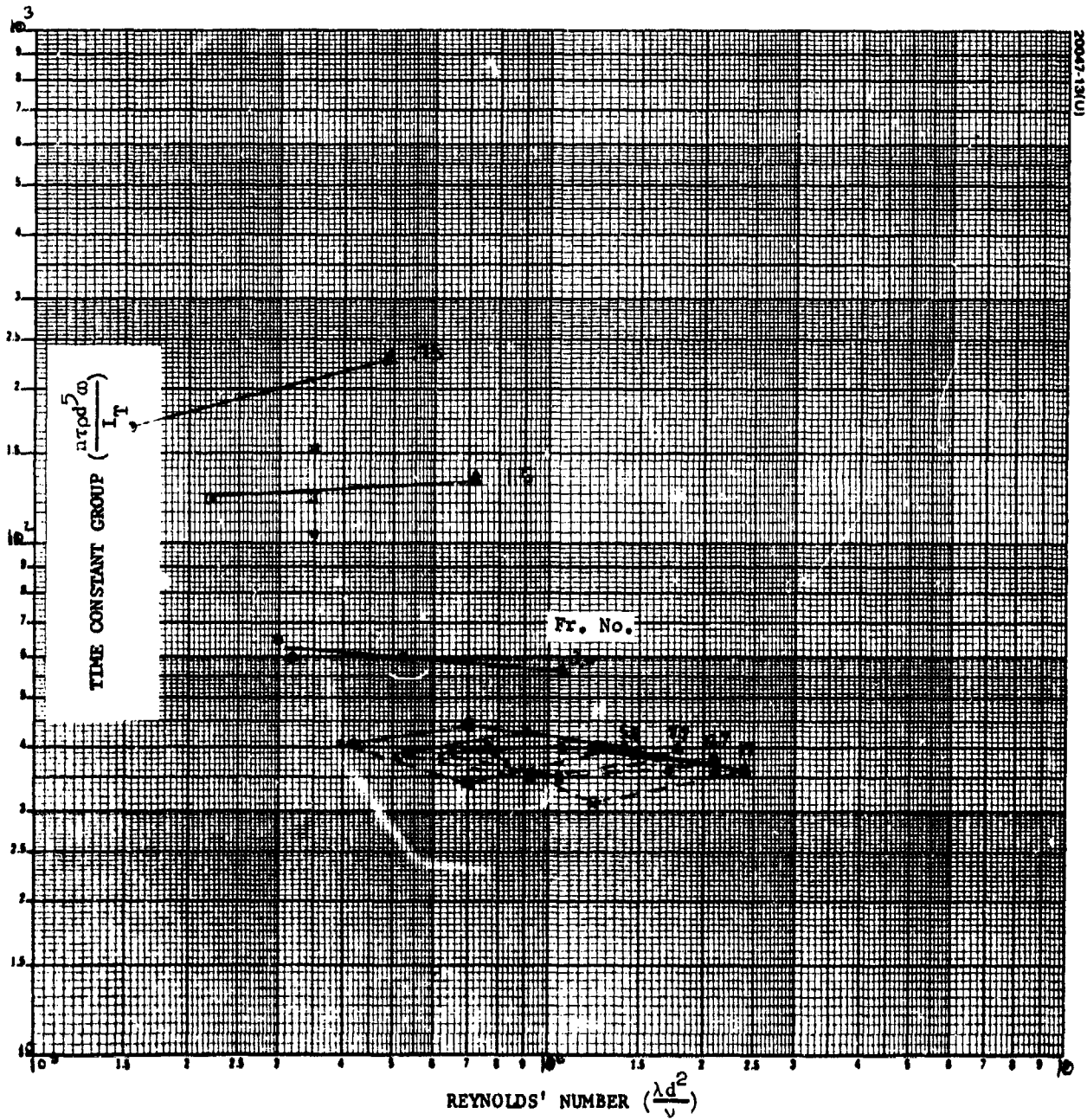
a) Time Constant Group Versus Reynolds Number
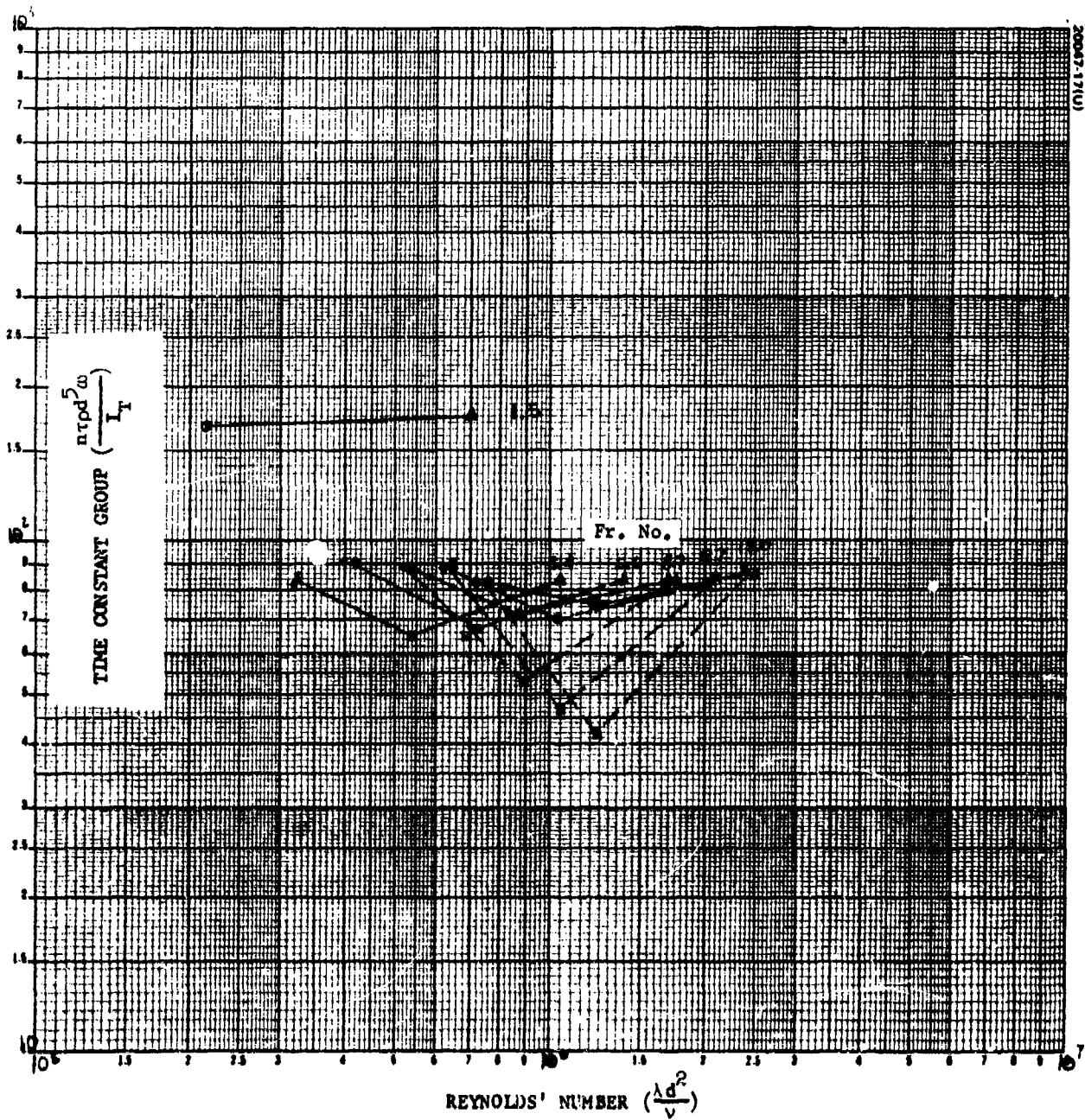
Figure 5-6. Phase III Conispherical Tank Fuel Sloshing at 66 Percent
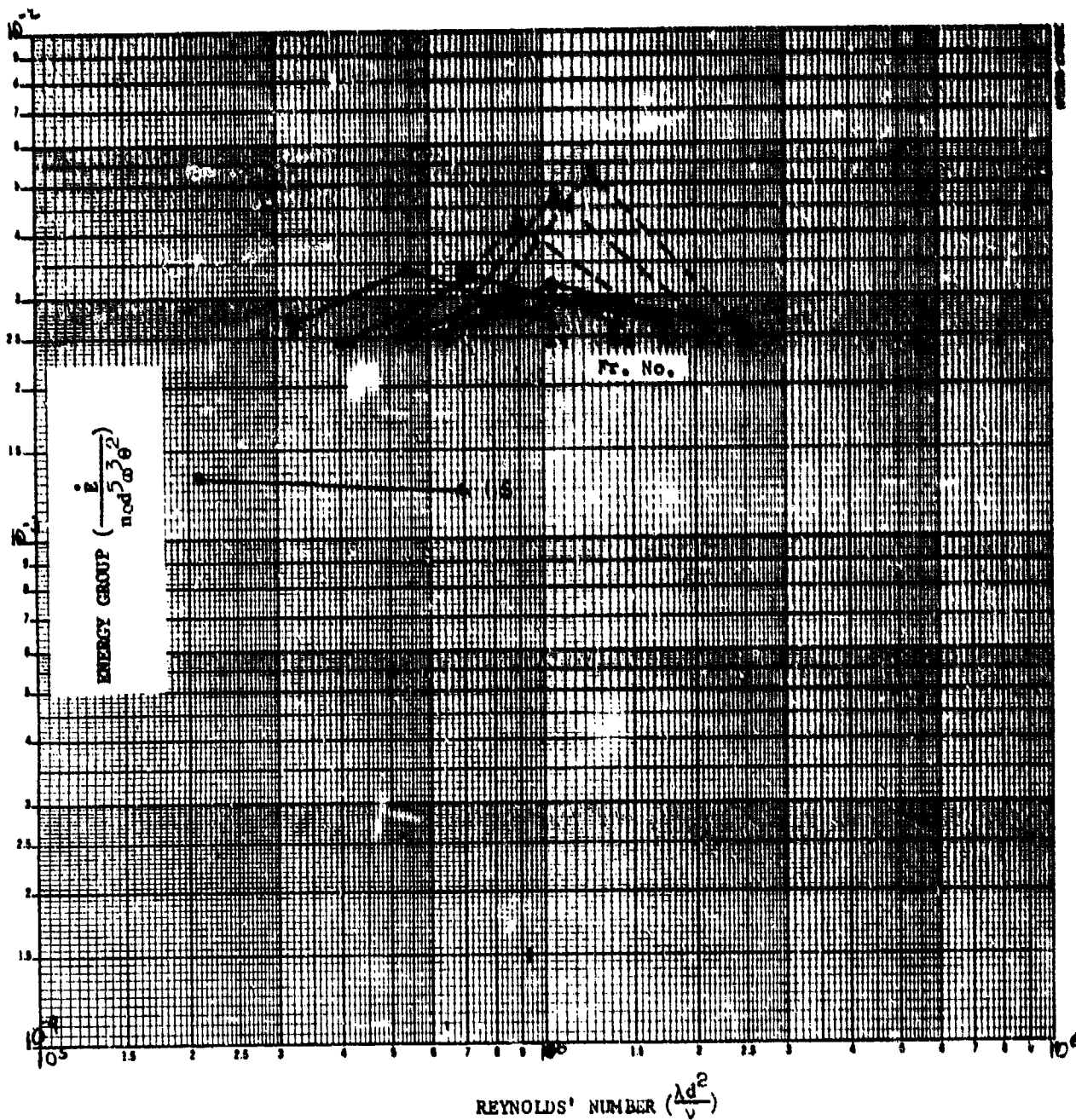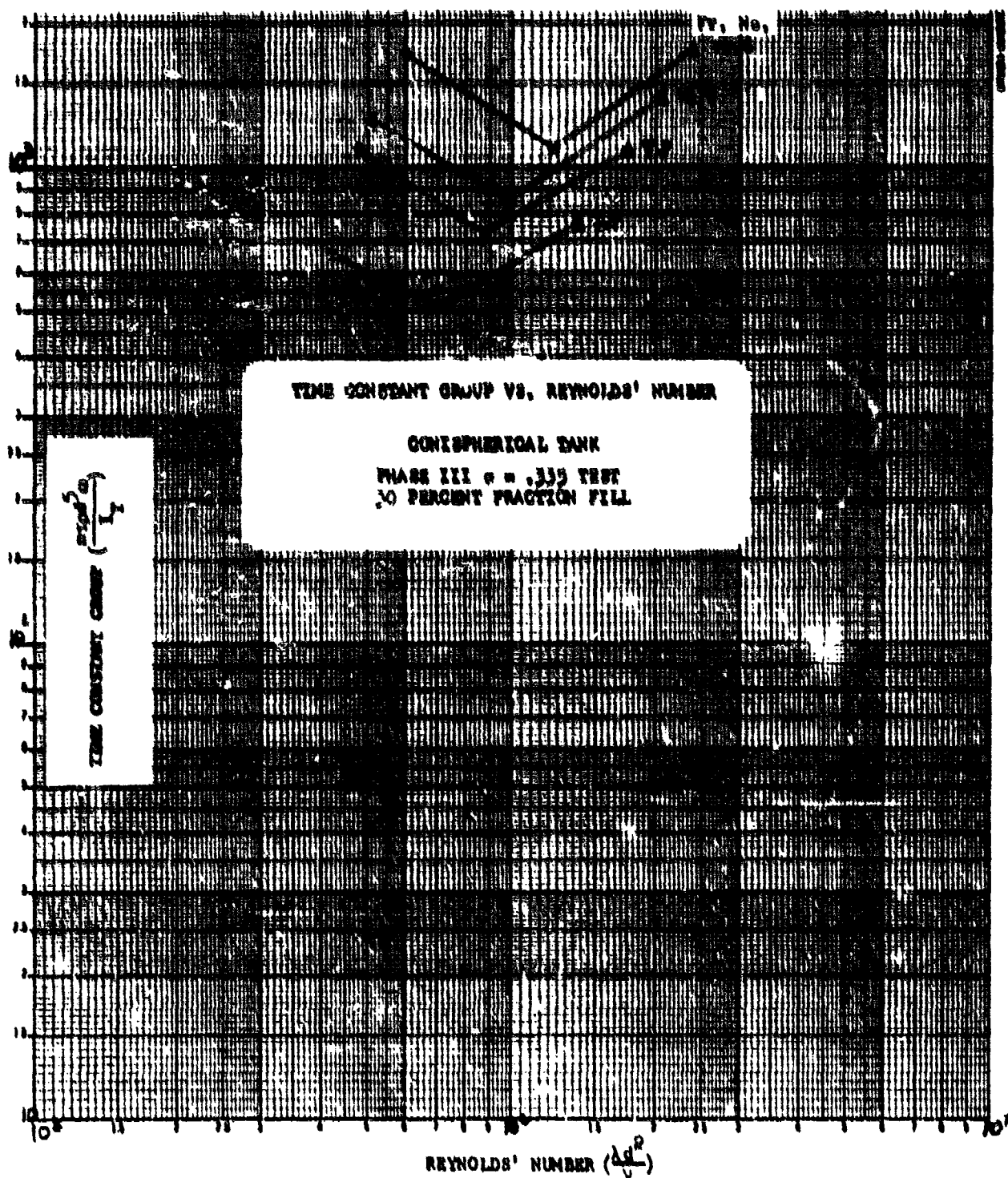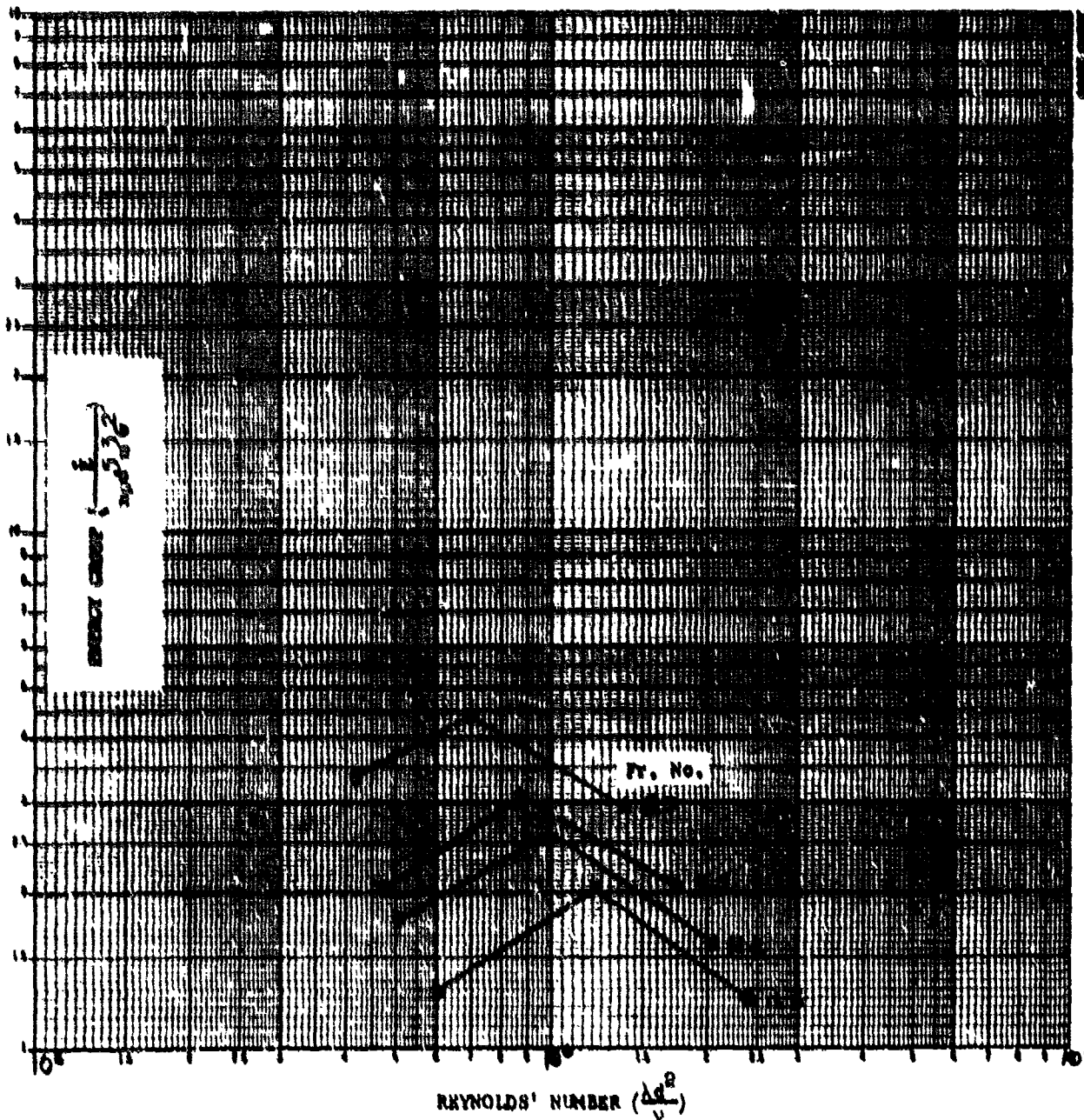Fraction Fill ($\sigma = 0.335$)
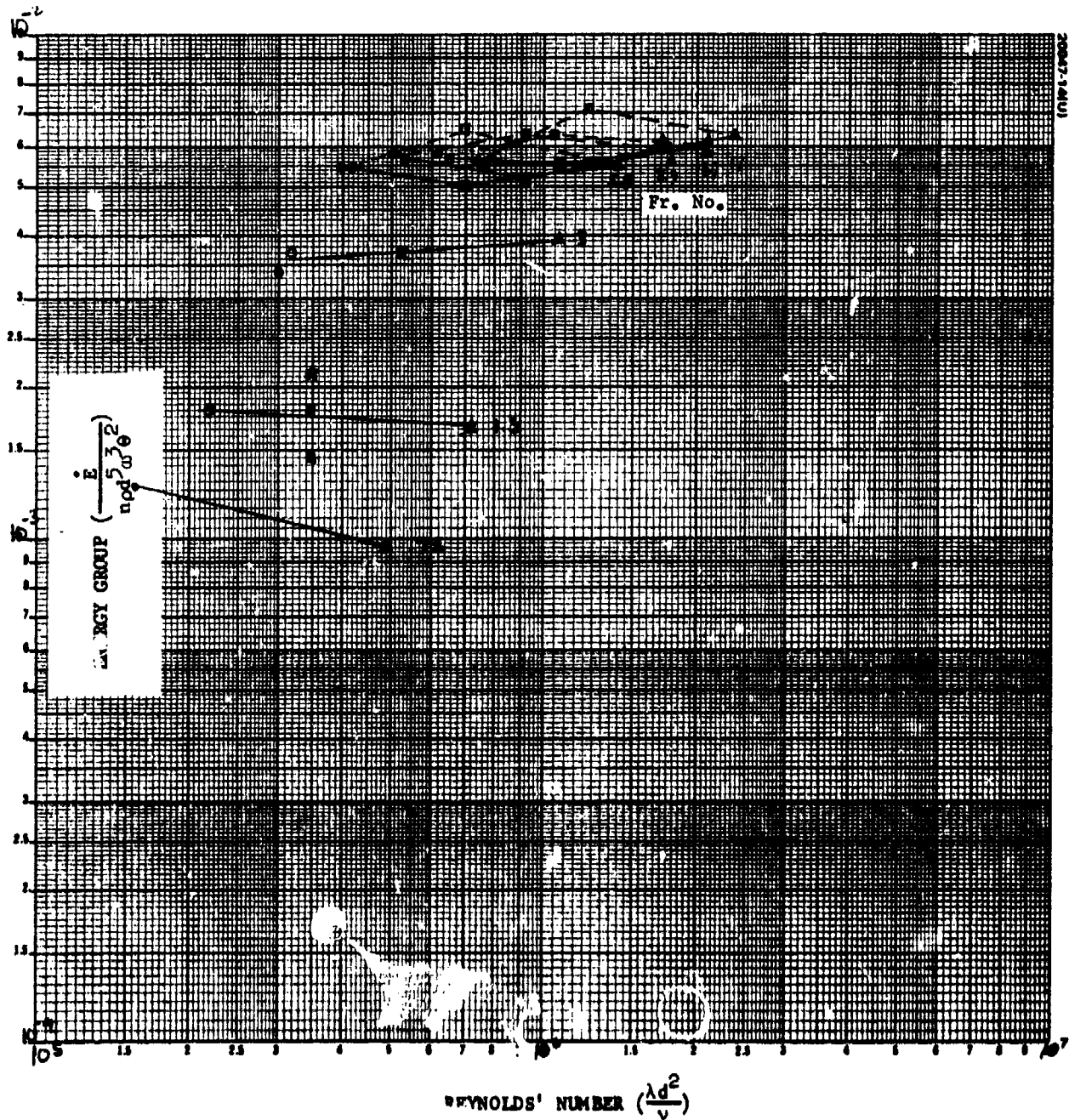
b) Energy Group Versus Reynolds Number

Figure 5-6 (continued). Phase III Conispherical Tank Fuel Sloshing at
66 Percent Fraction Fill ($\sigma = 0.335$)

Another observation from Figure 5-6 is the weak Reynolds number dependence. The energy dissipation rate is virtually independent of this parameter. It is perhaps more than coincidence that this fraction, showing weak Reynolds number behavior, also corresponds to the peak dissipation of all fraction fills tested.

The divergence rate also indicated a slight time constant change this time; however, the dissipation is more lossy at the small amplitudes than at the large amplitudes.

5.3.4 60 Percent Fraction Fill

The 60 percent fraction fill data lack the water solution as a third test fluid. This is unfortunate in that this fraction has an unusual characteristic. Figure 5-7 summarizes the available test data. The data appear to contain convergence as in the case of 66 percent. Further, it appears that the dissipation follows a well behaved function of Reynolds number. The dependence appears weak as in the case of 66 percent.

The unusual time constant change is the worst observed in all the data. The curves suggest that a secondary mode of dissipation is being excited at the larger amplitudes. The energy dissipation rate increases a factor of two when the nutation angle exceeds 2 degrees.

5.3.5 50 Percent Fraction Fill

The 50 percent fraction fill shows more interesting behavior. Figure 5-8 summarizes the 50 percent data.

First, the data show convergence with Froude number, which is important. The energy dissipation rate is dependent both on Reynolds number and nutation angle. The data suggest, just as in the 75 percent case, that the dissipation mechanism is sensitive to Reynolds number within the region being investigated. However, at 50 percent fill, the functional dependence of $\dot{E}$ on Reynolds number has reversed as the dissipation went through resonance. This behavior is continued at 30 percent and more profoundly seen in the spherical data (Section 5.4). It appears quite reasonable that the Reynolds number dependence is coupled to the fluid resonance phenomena.

Again at 50 percent, the time constant is seen to be sensitive to nutation angle. In this case, however, the time constant is smaller at the smaller amplitudes. This is the same behavior as observed at 66 percent but is in opposition to the 60 percent results.

5.3.6 30 Percent Fraction Fill

The 30 percent fraction fill tests show some different characteristics than previous fills. Figure 5-9 gives the test data.
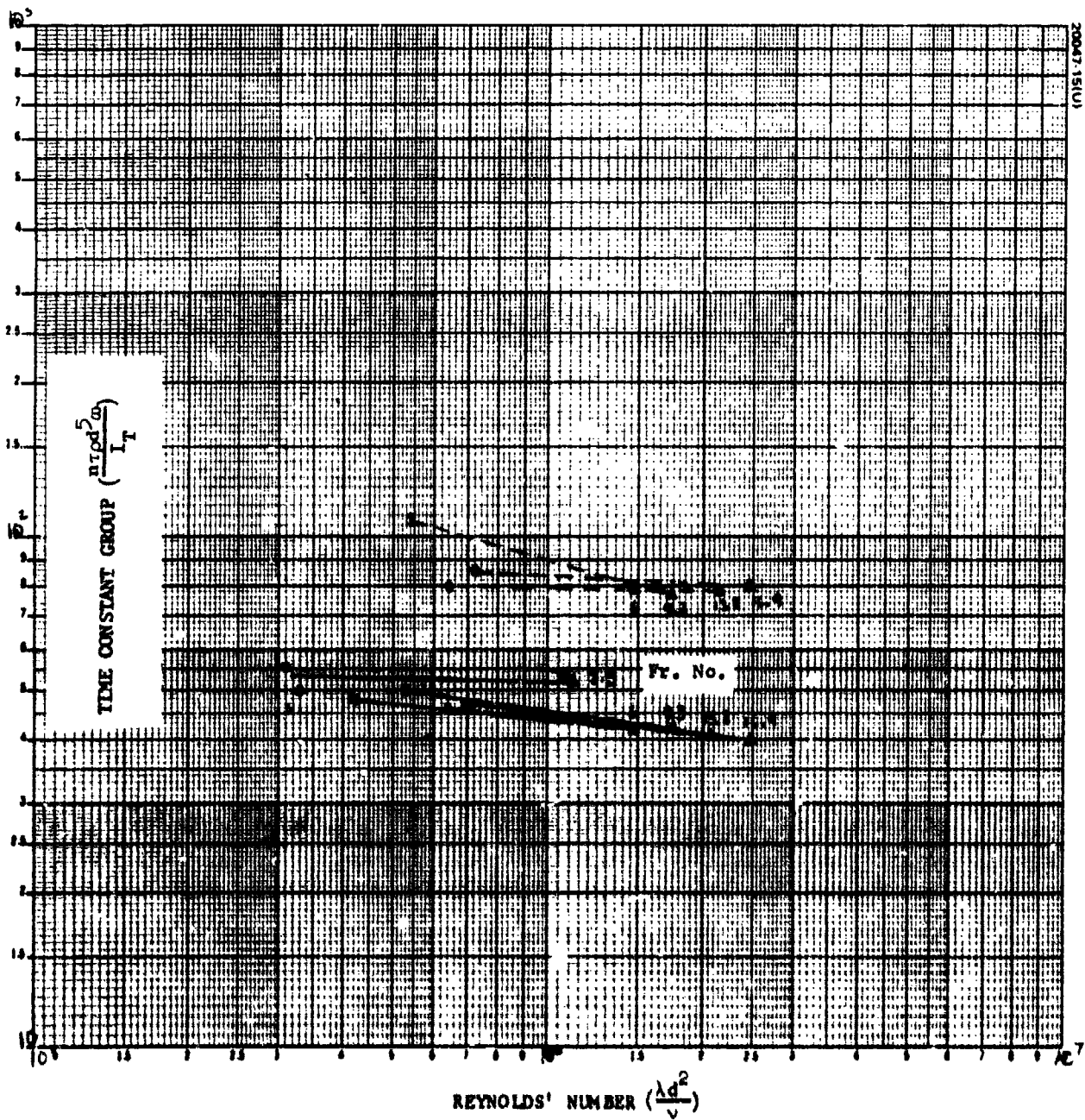
a) Time Constant Group Versus Reynolds Number

Figure 5-7. Phase III Conispherical Tank Fuel Sloshing at 60 Percent Fraction Fill ($\sigma = 0.335$)
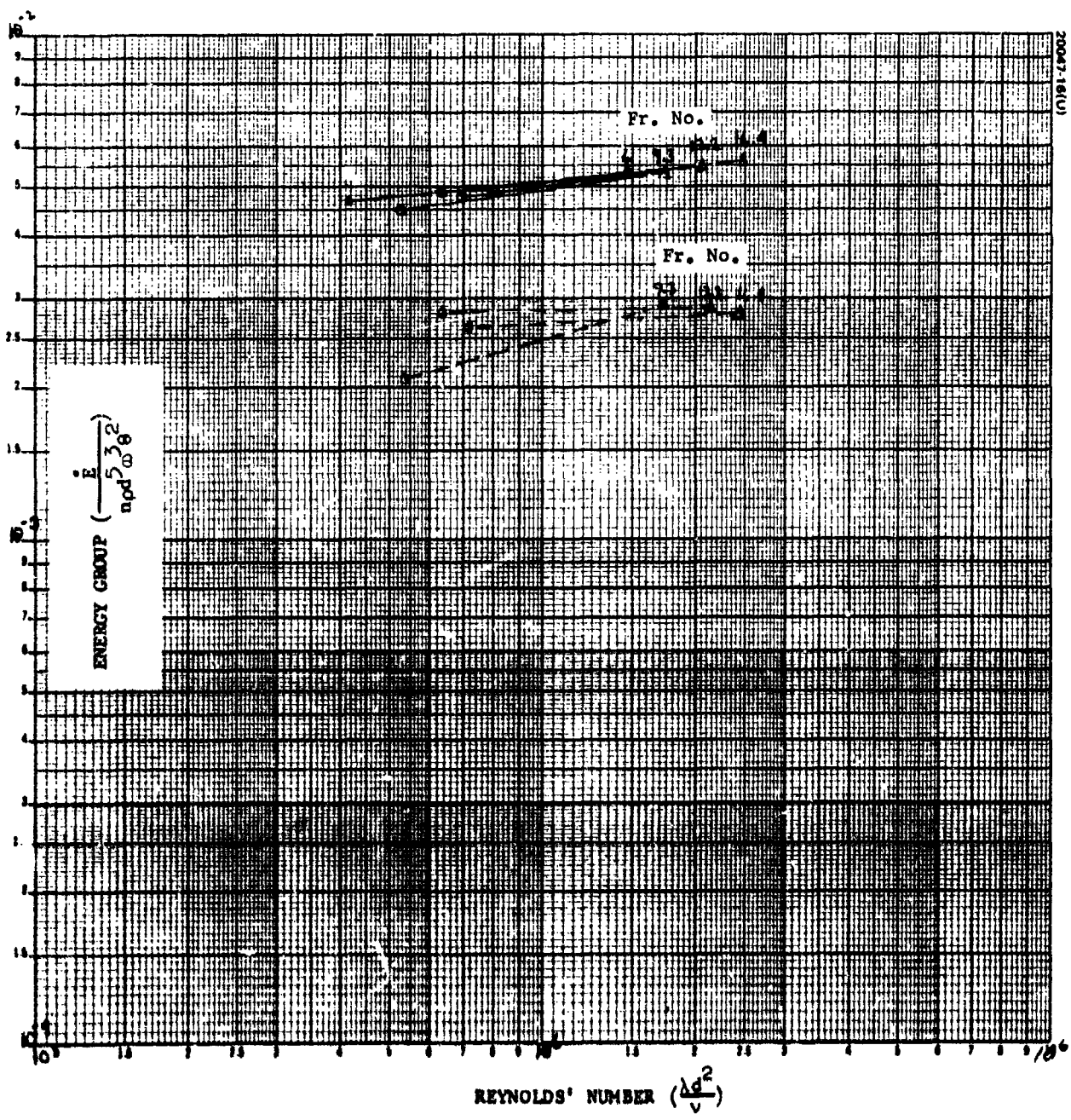
b) Energy Group Versus Reynolds Number

Figure 5-7 (continued). Phase III Conispherical Tank Fuel Sloshing at 60 Percent Fraction Fill ($\sigma = 0.335$)

5-21

a) Time Constant Group Versus Reynolds Number

Figure 5-8. Phase III Conispherical Tank Fuel Sloshing at 50 Percent Fraction Fill ($\sigma = 0.335$)

ENERGY GROUP $\left(\dfrac{\dot{E}}{\rho\omega d^5 3\overline{\omega}^2}\right)$

Fr. No.

REYNOLDS' NUMBER $\left(\dfrac{\Delta d^2}{\nu}\right)$

b) Energy Group Versus Reynolds Number

Figure 5-8 (continued). Phase III Conispherical Tank Fuel Sloshing at
50 Percent Fraction Fill ($\sigma = 0.335$)

5-23

a) Time Constant Group Versus Reynolds Number

Figure 5-9. Phase III Conispherical Tank Fuel Sloshing at 30 Percent
Fraction Fill ($\sigma = 0.335$)

5-24

REYNOLDS' NUMBER $(\frac{Ad^2}{\nu})$

b) Energy Group Versus Reynolds Number

Figure 5-9 (continued). Phase III Conispherical Tank Fuel Sloshing at 30 Percent Fraction Fill ($\sigma = 0.335$)

5-25

The interesting behavior noted in Figure 5-9a is that Froude number convergence is not so obvious. The explanation for this gravity effect is not known. The Reynolds number behavior is similar in curvature but increased in magnitude over the 50 percent fill.

The 30 percent fill shows a behavior very similar to the small amplitude behavior at 50 percent. However, the energy levels differ by about a factor of 20. It appears at 30 percent that not only is the dissipation down because there is less mass and less wetted area but also because the fluid is almost entirely in the conical section where the restriction to motion is maximum. This is demonstrated more conclusively when the conisphere and sphere are compared at 30 percent.

5.3.7 Summary of Phase III Conispherical σ = 0.335 Data

During the discussion of the data in the previous sections, certain behaviors and facts were pointed out which represent the key results of the test. The major results have been reduced to a simple graphical summary shown in Figure 5-10.

What has been done in plotting Figure 5-10 is to take only the maximum Froude number curves for each fraction fill and coplot the respective energy groups versus Reynolds number. If the data were dependent on nutation level, this fact is also included. In looking at this plot, the following facts are observed, some of which may have been mentioned already.

Starting at 100 percent fraction fill, the energy dissipation rate increases by nearly a factor of 20, peaking at 66 percent and then falling off first slowly to 50 percent and then rapidly to 30 percent. The obvious peaking of the dissipation rate strongly suggests some type of resonance phenomenon occurring at or near 66 percent fraction fill. In the Edwards model of the fluid motion, this peaking is interpreted as a geometrical resonance characteristic of the shape of the container and the vehicle (i. e. , the inertia ratio, σ). While the model remains crude at this time, the region of resonance for the conispherical tank agrees quite well with the test result. More interestingly, the model predicts for the spherical tank a similar resonance around 54 percent fill. As will be seen in the next section, this is also good agreement with the test data. And finally at σ = 0.1, the model predicts a resonance in the conisphere at or near 90 percent fill. The test data again agree with this prediction, however, the data are not sufficient to state conclusively that the 90 percent fill is the worst case.

The issue of Reynolds number dependence is not clearly understood. It is perhaps sufficient to say that in all of the data the Reynolds number dependence is weak relative to the other variables such as fraction fill, inertia ratio, and container shape. While the data may be interpreted as containing a Reynolds number transition, the attendant $\dot{E}$ level shifts are small and quite unlike laminar-turbulence transitions in other fluid dynamics phenomena. At this time it is not worthwhile belaboring the Reynolds number behavior.
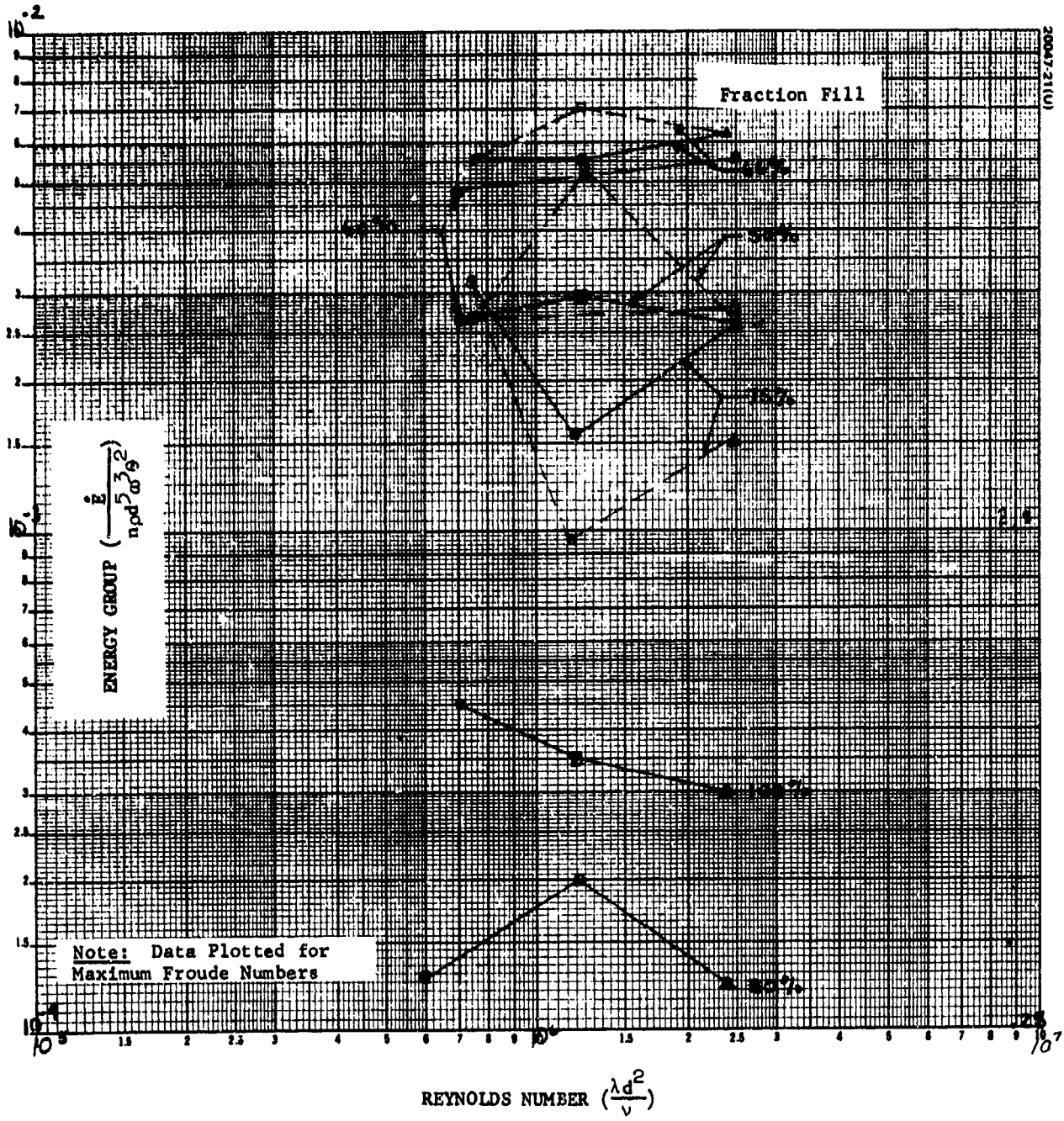
Figure 5-10. Comparative Energy Groups for Various Fraction
Fills of Conispherical Tank (σ = 0.335)

To establish a dimensional perspective on the energy dissipation rates being measured in this test, Figure 5-11 is a dimensional version of Figure 5-10. Here, the data in Figure 5-10 have been used for an Intelsat IV condition, i.e., $n = 4$, $d = 1.44$ feet, $\rho = 1.92$ slug/ft^3, and $\omega_s \approx 50$ rpm. The energy levels are seen to vary from 0.3 mw (at 30 percent FF) to 20 mw (at 66 percent FF). These rates have been computed at 1 degree nutation. In the laboratory, the energy dissipations are comparable to these values.

5.3.8 Comparison of Phase I and III Conispherical Data at $\sigma = 0.335$

An interesting graph can be constructed by coplotting the Phase I and III conispherical data at the various fraction fills tested. Even though the vehicles are different dimensionally and physically, it is possible to normalize the data by the same dimensionless groups and, hopefully, arrive at the same group constants for the respective fill fractions. If the group levels agree, then dimensional scaling by d^5 is established. Figure 5-12 presents the available data at 100, 66, 50, and 30 percent fraction fills. Only the energy groups are plotted since the time constant group is redundant. The following discussion examines these curves in the above order. (The entire set of Phase I data can be found in Appendix A.)

At 100 percent fill, Figure 5-12a, it is immediately obvious that the energy group are discrepant by nearly an order of magnitude. The Phase I data show neither good Froude number convergence nor any Reynolds number dependence.

It is suspected that the Phase I data contain not only the Phase III data, which are believed to be correct due to flight confirmation but also an additional parasitic dissipation mechanism not subtracted from the data. As it turns out, this secondary dedamper is sufficiently strong to mask the Reynolds number dependence of the fuel sloshing. The reason then for poor Froude number convergence is that the data scatter is a consequence of the other dedamper. However, the other dedamper is not sensitive to the 1 g field since the levels do not change appreciably.

At 66 percent fill (Figure 5-12b), the Phase I data above the Phase III data, and likewise, at 50 and 30 percent fills. In each case, the situation is the same; and, therefore, the above conclusion is the same.

The Phase I tests appear to consistently contain the new Phase III data plus another dissipator. The magnitude of the dissipator can be found by simply subtracting the levels of the two curves at each fill fraction. That subtraction has been carried out and is plotted in Figure 5-13. The secondary dissipator peaks out at 50 percent fraction fill. The apparent parabolic shape of this curve suggests an mr^2 type relationship.
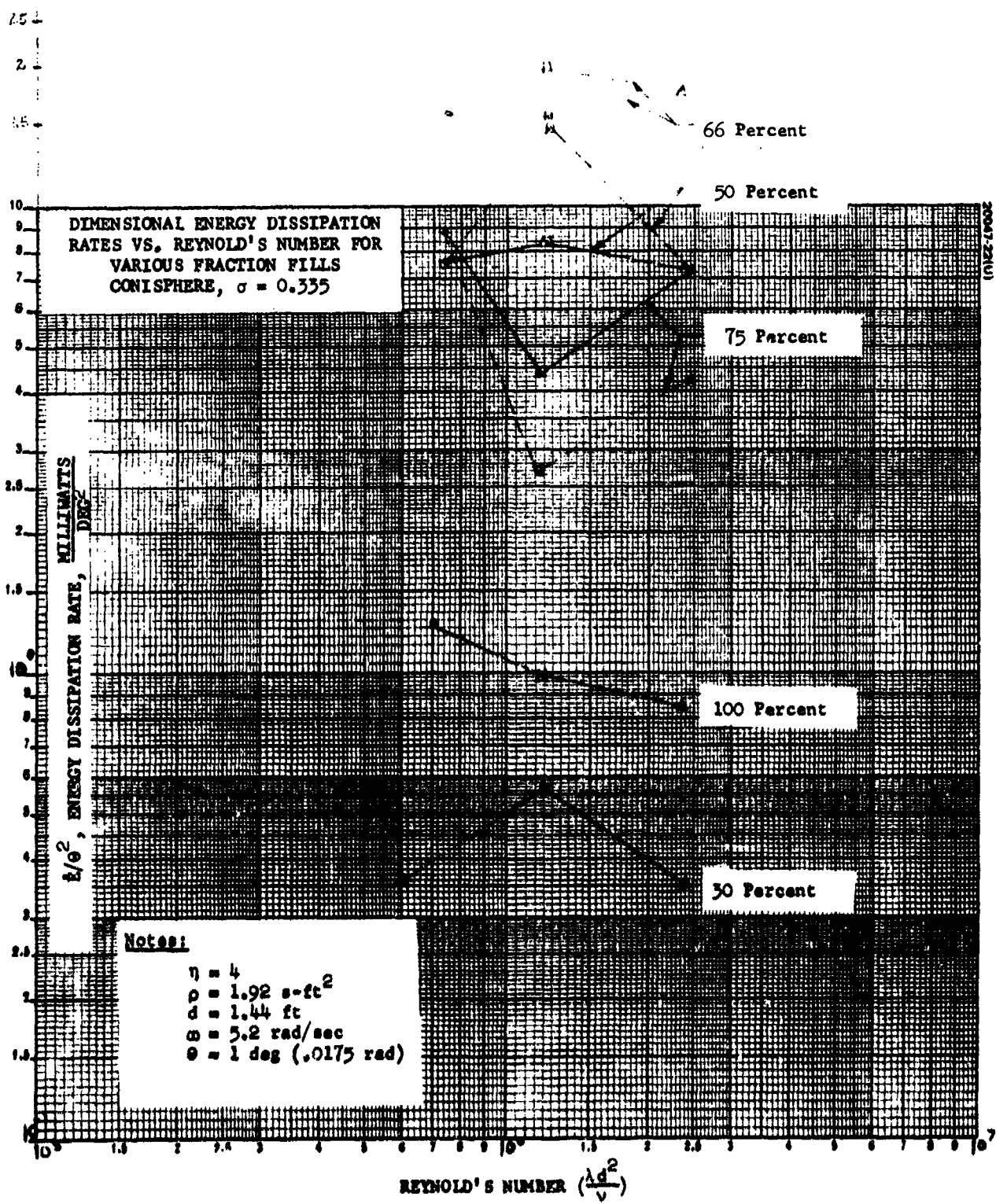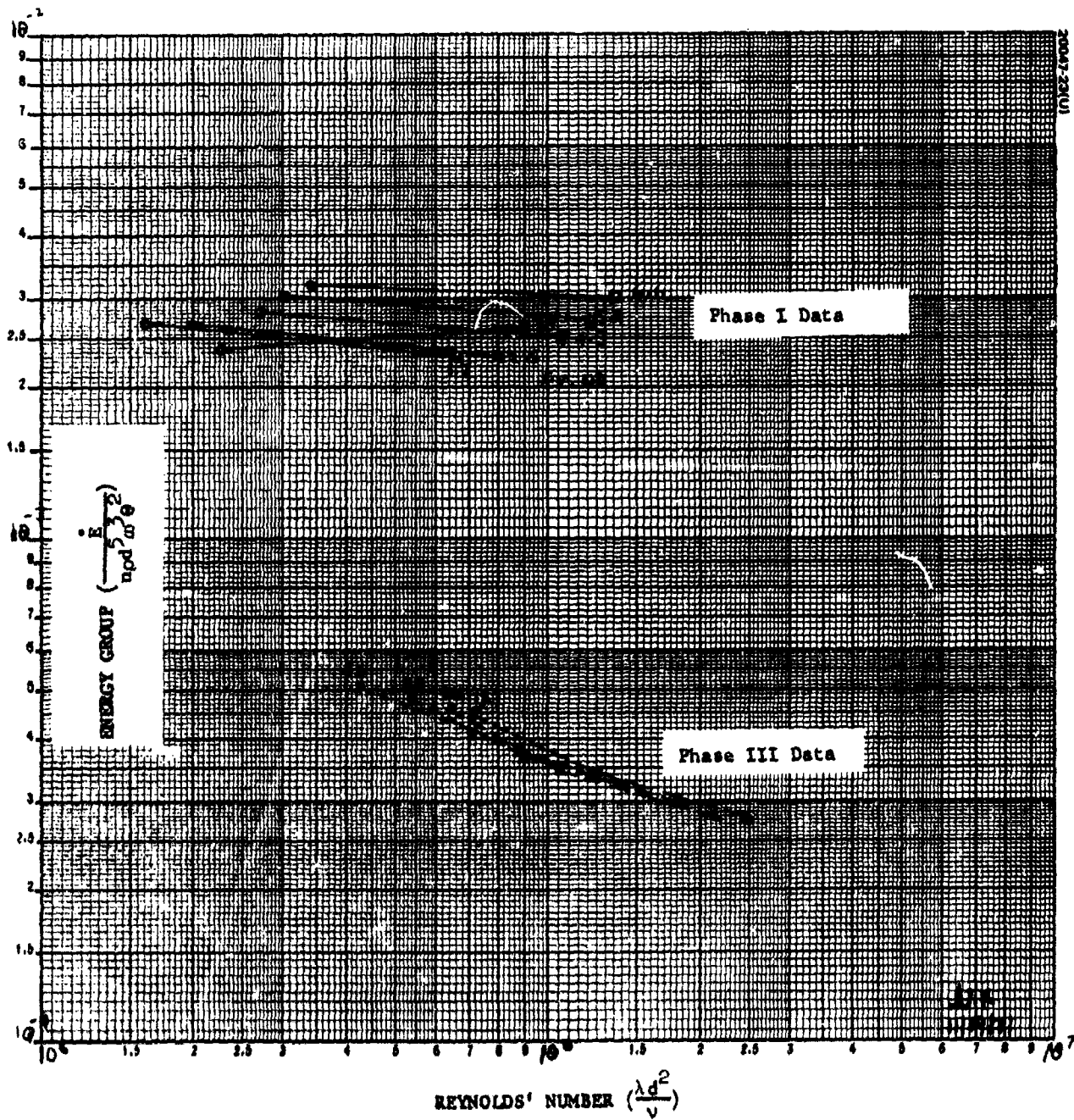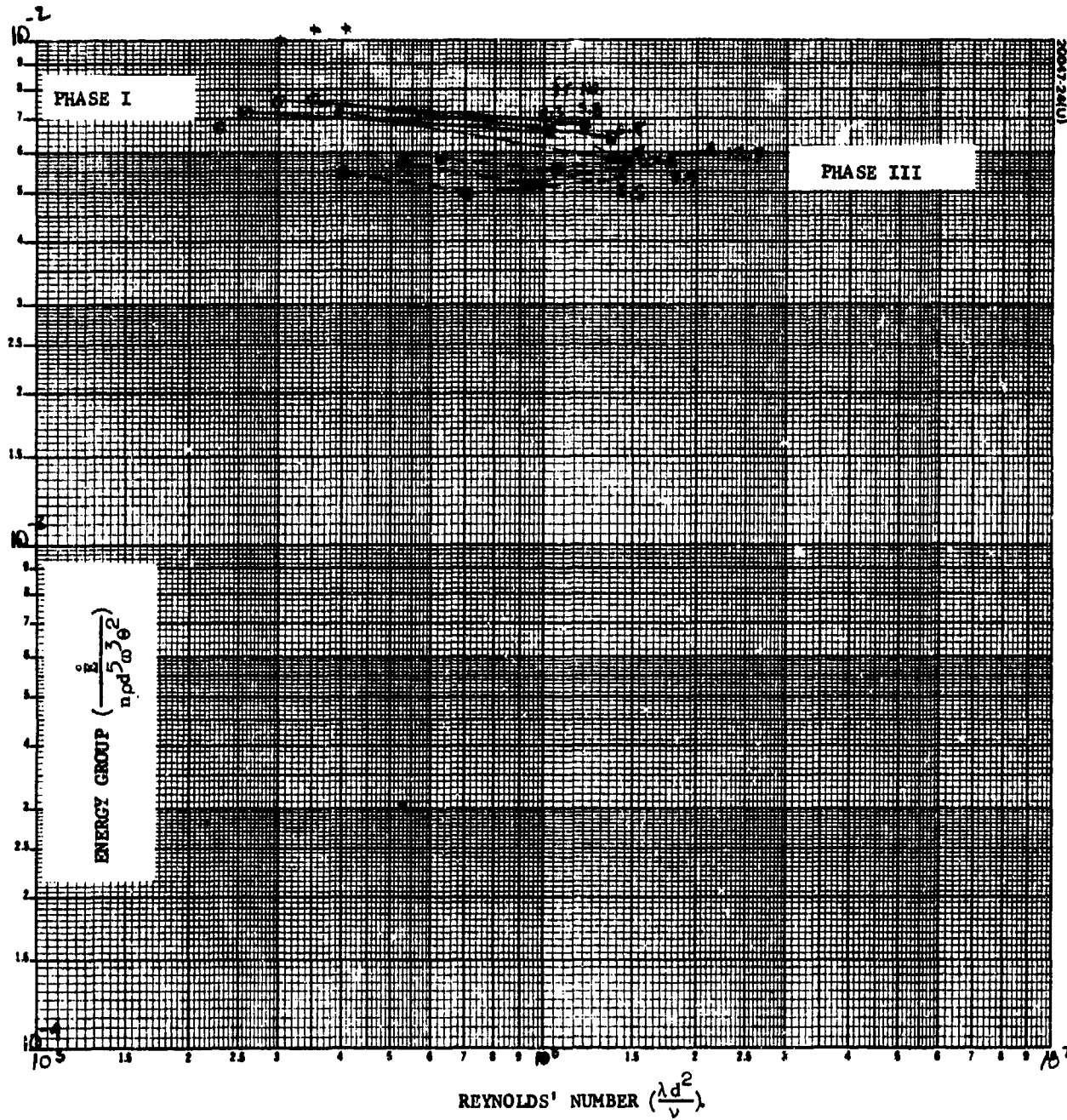
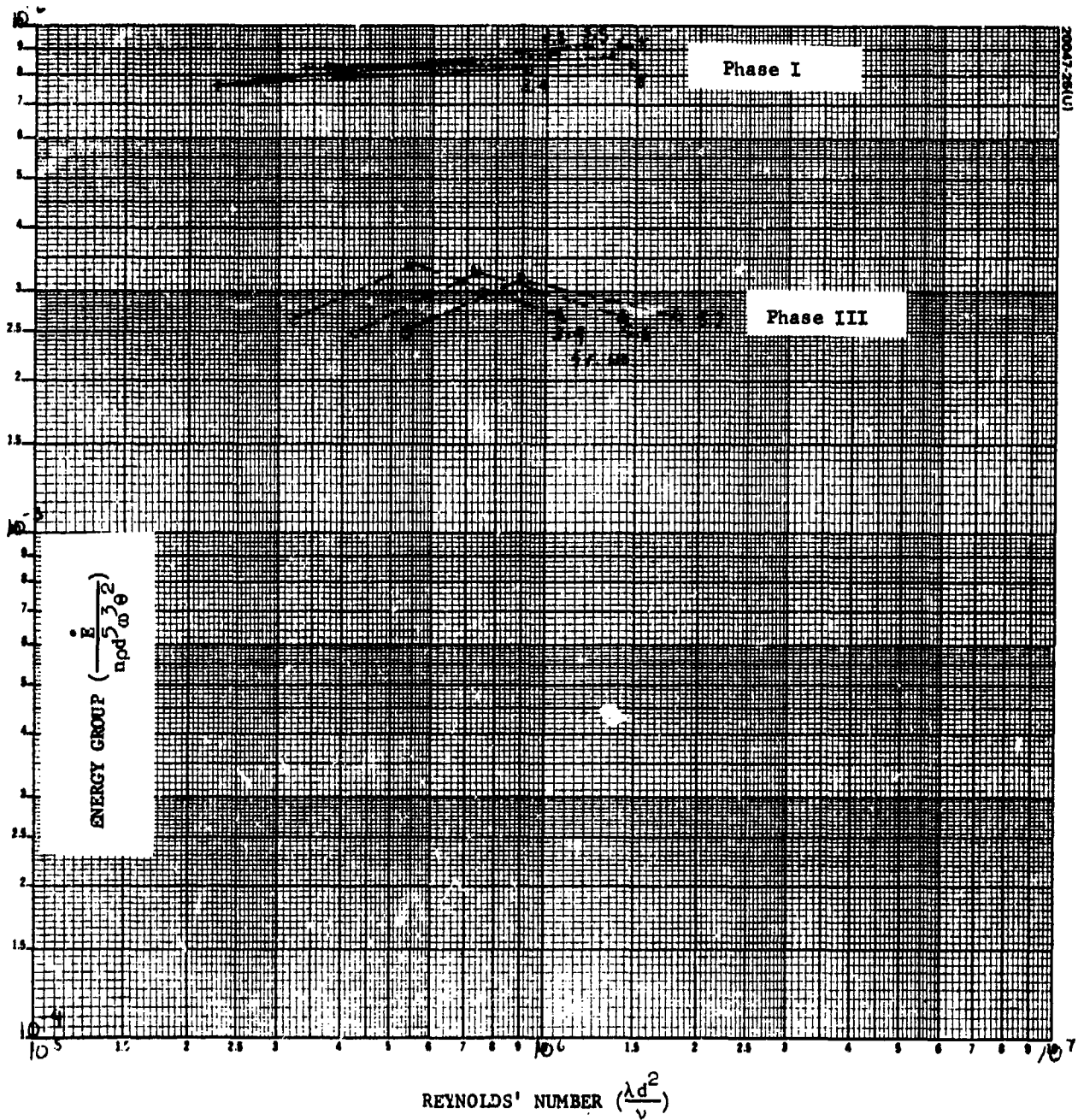Figure 5-11. Dimensional Energy Dissipation Rates Versus Reynolds Number for Various Fraction Fills of Conispherical Tank

5-29

a) 100 Percent Fraction Fill

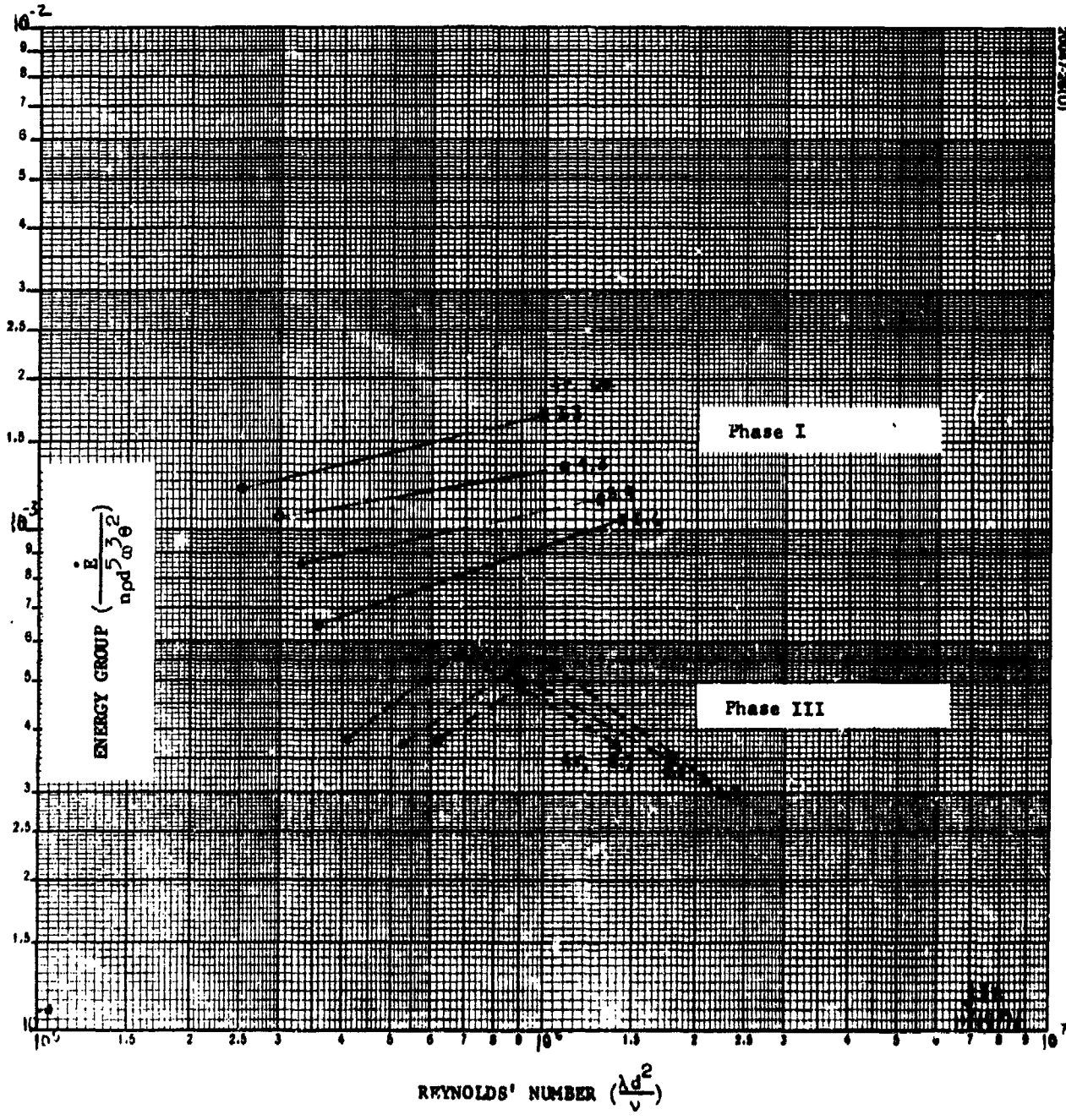Figure 5-12. Comparative Energy Groups for Various Fraction Fills of Conispherical Tank ($\sigma = 0.35$)

PHASE I

PHASE III

ENERGY GROUP $\left(\dfrac{\overset{\circ}{E}}{n\rho d^5 \omega^3 \theta^2}\right)$

REYNOLDS' NUMBER $\left(\dfrac{\lambda d^2}{\nu}\right)$

b) 66 Percent Fraction Fill

Figure 5-12 (continued). Comparative Energy Groups for Various
Fraction Fills of Conispherical Tank (σ = 0.35)

c) 50 Percent Fraction Fill

Figure 5-12 (continued). Comparative Energy Groups for Various
Fraction Fills of Conispherical Tank (σ = 0.35)

d) 30 Percent Fraction Fill

Figure 5-12 (continued). Comparative Energy Groups for Various
Fraction Fills of Conispherical Tank (σ = 0.35)
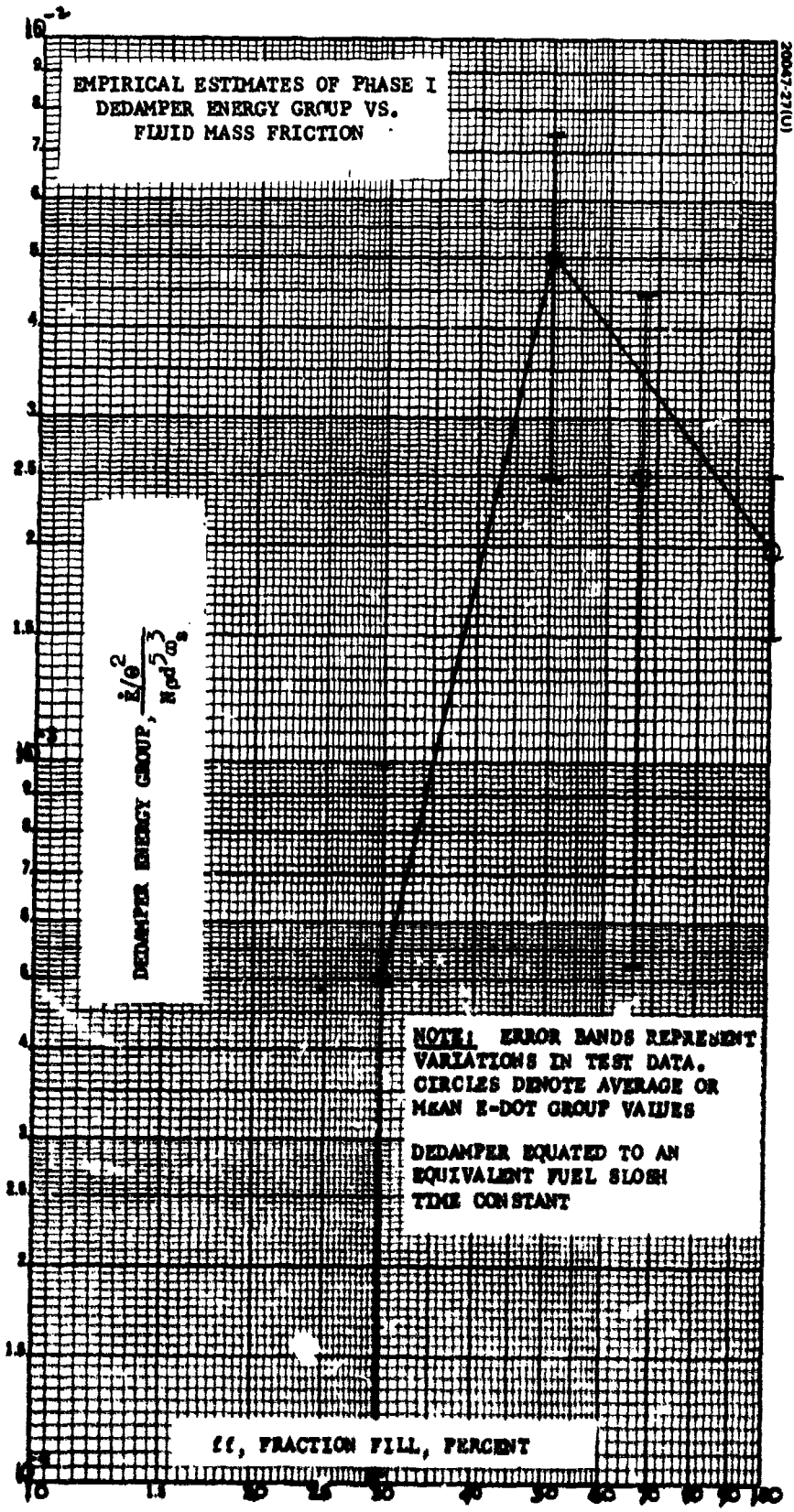
Figure 5-13. Empirical Estimates of Phase I Dedamper Energy Group
Versus Fluid Mass Friction

It is believed that the cause of this additional dissipation was excitation of the tank support structure by the pendulous fluid motion in forced response to the nutation. This mode of structural working was not calibrated during the parasitic test runs. During those tests, a static load representative of the fluid mass was attached to the mounting point. However, when the fluid was free to oscillate about the tank center, a moment was produced at the attach points which must compensate for the torque created by the fluid motion. Since the frequency is that of rotor nutation, the extra dissipation would add in phase to create additional divergence.

Even though the Phase I data appear to be corrupted by an additional dedamper, one critical result is evident. Dimensional scaling by d^5 appears to be valid. The test demonstration is strongest at 66 percent fill, where the parasitic dedamper in Phase I is on the order of the fuel slosh. Figure 5-12b indicates that the dimensionless groups are about the same value. Even 50 percent and 30 percent agree within a factor of 2. And finally, the good flight correlation with the test data which intrinsically applies the d^5 scaling laws adds critical evidence to support the above conclusions.

The above test results imply that if Intelsat IV increased in size from 8 to 10 feet radius and the radial location and tank diameter were scaled proportionately, the energy dissipation would be a factor of 3 higher than at present. At 66 percent fraction fill, assuming no damper changes, the system would be neutrally stable or unstable. The resulting dedamper time constant would be between 20 and 30 seconds. On the other hand, if Intelsat IV were to shrink 25 percent, tank sizes included, the time constant would be increased by a factor of 3.

Energy dissipation scaling by ρd^5 could explain why both ATS V and TACSAT I were not plagued by fuel slosh as major dedampers. For those vehicles, the tank diameters were 11 inches compared with Intelsat IV's 18 inch tanks. (The fact that they were spherical is ignored.) Thus, on a dimensional basis, the energy dissipation alone would be down by $(11/18)^5$, or nearly an order of magnitude. Therefore, the heat pipes and bearing and power transfer assembly (BAPTA) were the dominate dedampers in the two vehicles, with fuel slosh effects hidden in the noise.

5.4 SPHERICAL TESTS, $\sigma = 0.335$ DATA

During the Phase III test series, the conispherical tank was inverted to simulate a spherical tank geometry. Figure 3-4 indicates the physical relationship of the tank with respect to the conispherical position. For fraction fills below 75 percent, the tank geometry presents a spherical boundary to the fluid. Unfortunately, it was not possible to run a 100 percent fill since a comparative result with the conisphere at the same fill would provide some insight to assist in development of the empirical model.

The following set of figures, 5-14 through 5-18, present the spherical data taken at the 0.335 inertia ratio. Figure 5-19 is a summary energy group curve where the various fraction fills are coplotted for maximum Froude numbers. This curve is the companion to Figure 5-11 for the conispherical case.

5.4.1 75 Percent Fraction Fill

Figure 5-14 presents the 75 percent fraction fill data. Here, the behavior versus Reynolds number is somewhat similar to the equivalent conispherical case. The definite energy level shift again suggests that the test may be occurring in a sensitive Reynolds number region. The Froude number behavior is also similar to the conisphere. While the data appear to converge, there may be some complicated Froude number/Reynolds number interrelationship.

5.4.2 66 Percent Fraction Fill

The 66 percent fill, Figure 5-15, indicates a slight Reynolds number dependence with a peaking around 10^6. Again, the curves for constant Froude number appear to be translated as Reynolds number increases.

5.4.3 60 Percent Fraction Fill

At 60 percent fraction fill, the dissipation is more linear than in the conisphere. While only two test fluids were run, Figure 5-16 shows the curves both converge with Froude number. The data are best fit by one time constant.

5.4.4 50 Percent Fraction Fill

At 50 percent fill, the sphere experiences its maximum dissipation rate. This is not too surprising inasmuch as previous nonspinning spherical sloshing tests indicate that maximum sloshing occurs at 50 percent. The energy dissipation rates are about four times less in the spherical tank at resonance, as in the conisphere at 66 percent.

Figure 5-17 shows that dissipation is virtually independent of Reynolds number. Recall that this was also observed to be the case for the conisphere at 66 percent. It seems reasonable to conjecture that the same lossy mode of dissipation is present in the sphere, which when excited gives rise to dissipation on the same order as the conisphere.

5.4.5 30 Percent Fraction Fill

The 30 percent fill for the sphere is an interesting case for several reasons. First, between 50 and 30 percent, the sphere becomes worse than the conisphere. As it turns out, this crossover is of little engineering significance since the energy dissipation rate is sufficiently below the critical value. A possible explanation for the crossover is the following. As the fill

fraction decreases to the value where the remaining fluid is almost entirely in the conical section of the tank, the presence of the cone acts to inhibit the fluid movement when excited by nutation. The sphere, on the other hand, experiences no such impediment; and the slug of fluid is free to exhibit forced oscillatory motion. Since the liquid amplitude would be greater, the energy dissipation rate would also be increased.

Figure 5-18 shows the behavior of the test data at this fill fraction. Several observations can be readily made. First, the dissipation shows a Reynolds number dependence. The data also show a time constant change. The data indicate the time constant is smaller in the small amplitude regions. This again suggests some saturation mechanism.

The data also contain the characteristic Froude number behavior of the other fill fraction. The family of curves of constant Froude number appear to be translation along the Reynolds number axis. The explanation for this behavior is not known.

5.4.6 Summary of Spherical Data

Figure 5-19 is a plot of the high Froude number energy groups for the fraction fills tested. This is a companion curve to Figure 5-10. Here, peaking is seen at 50 percent. The Reynolds number behavior with fraction fill is somewhat similar to the conispherical case. The curves appear convex for fill fractions greater than resonance and concave for fills lower than resonance.

In comparison, it has been experimentally verified at the 0.335 inertia ratio that spherical tanks are quantitatively better than conispherical tanks insofar as energy dissipation is concerned. However, the advantage is not so significant that future designs must necessarily employ a spherical tank propellant system. A figure of merit must be placed on the two designs when considering a new propulsion design. As it turned out, in the Intelsat IV case, it was an easier engineering modification to increase the composite damper performance a factor of four than it would have been to redesign the propulsion system. Future designs may also find it more attractive to design more efficient nutation dampers than to compromise the efficiency of the propulsion system.

5.5 CONISPHERICAL TESTS, $\sigma = 0.1$ DATA

Most of the Phase II testing and the initial part of the Phase III series was conducted at the HS-318 spacecraft inertia ratio of 0.1. All the testing was conducted with conispherical tanks except for one spherical test at 66 percent fill. The results of that test are presented after the presentation of the conispherical data.
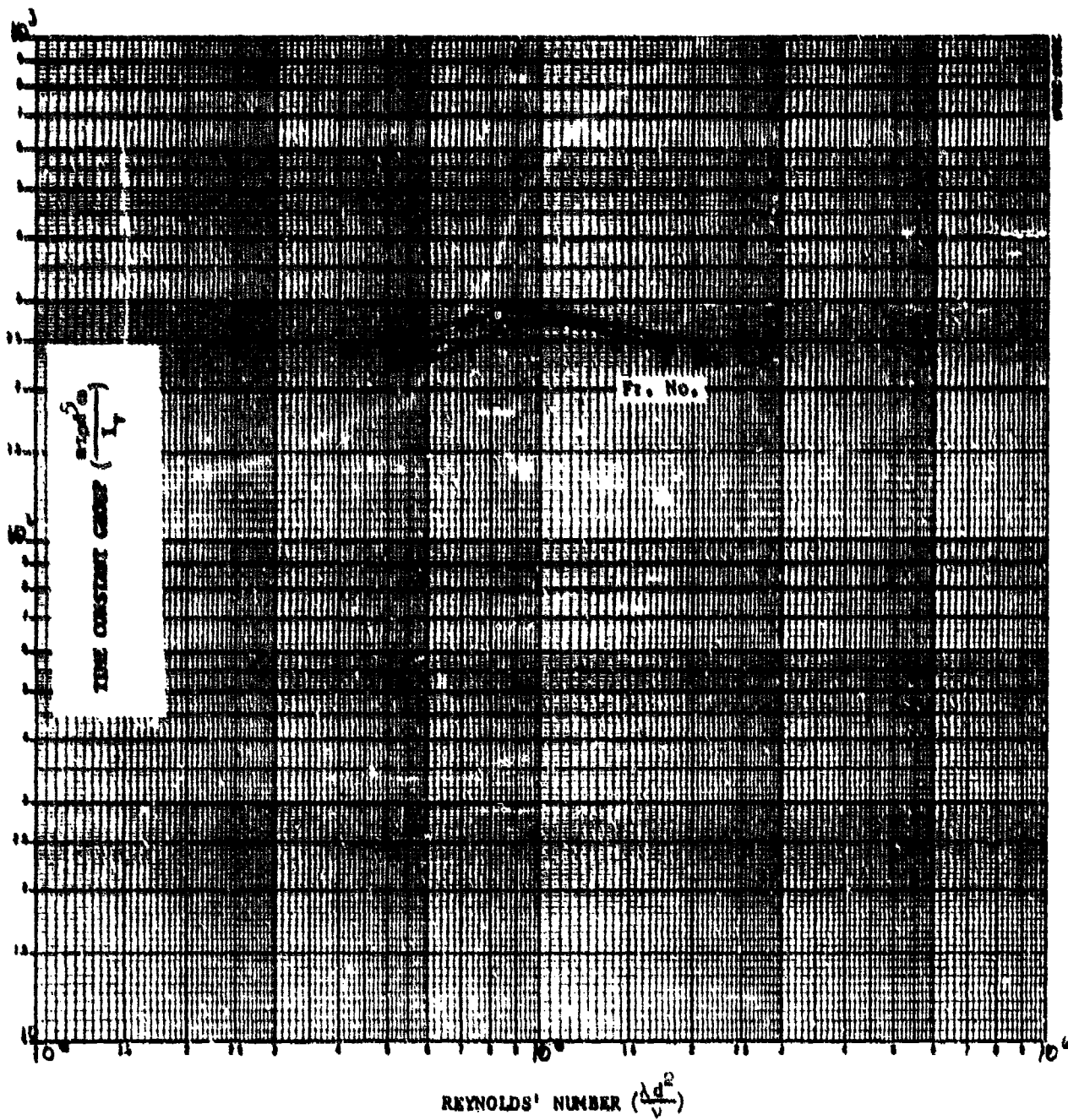
REYNOLDS' NUMBER $(\frac{Ad^2}{\nu})$
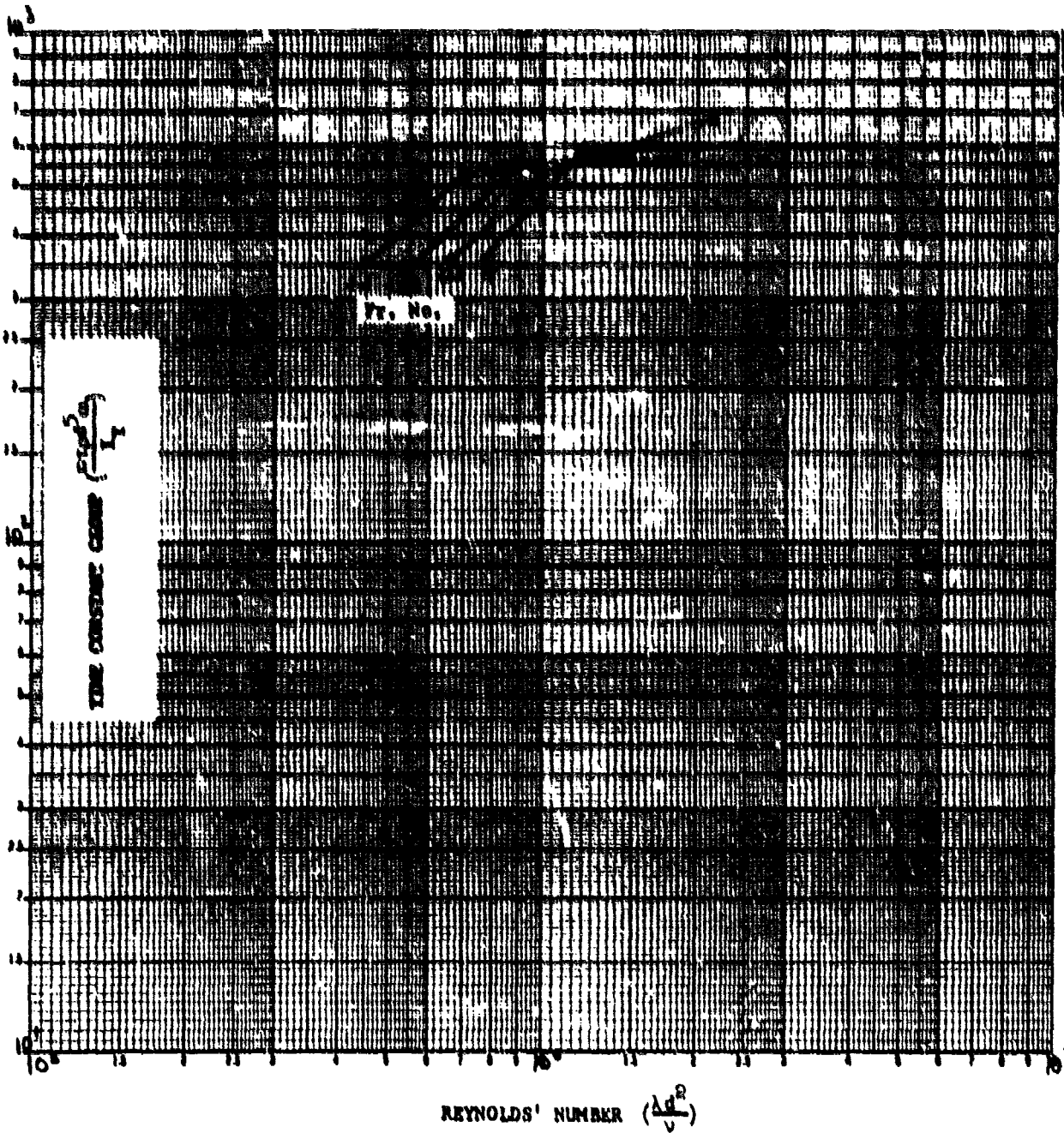
a) Time Constant Group Versus Reynolds Number

Figure 5-14. Phase III Spherical Tank Fuel Sloshing at 75 Percent Fraction Fill (σ = 0.335)
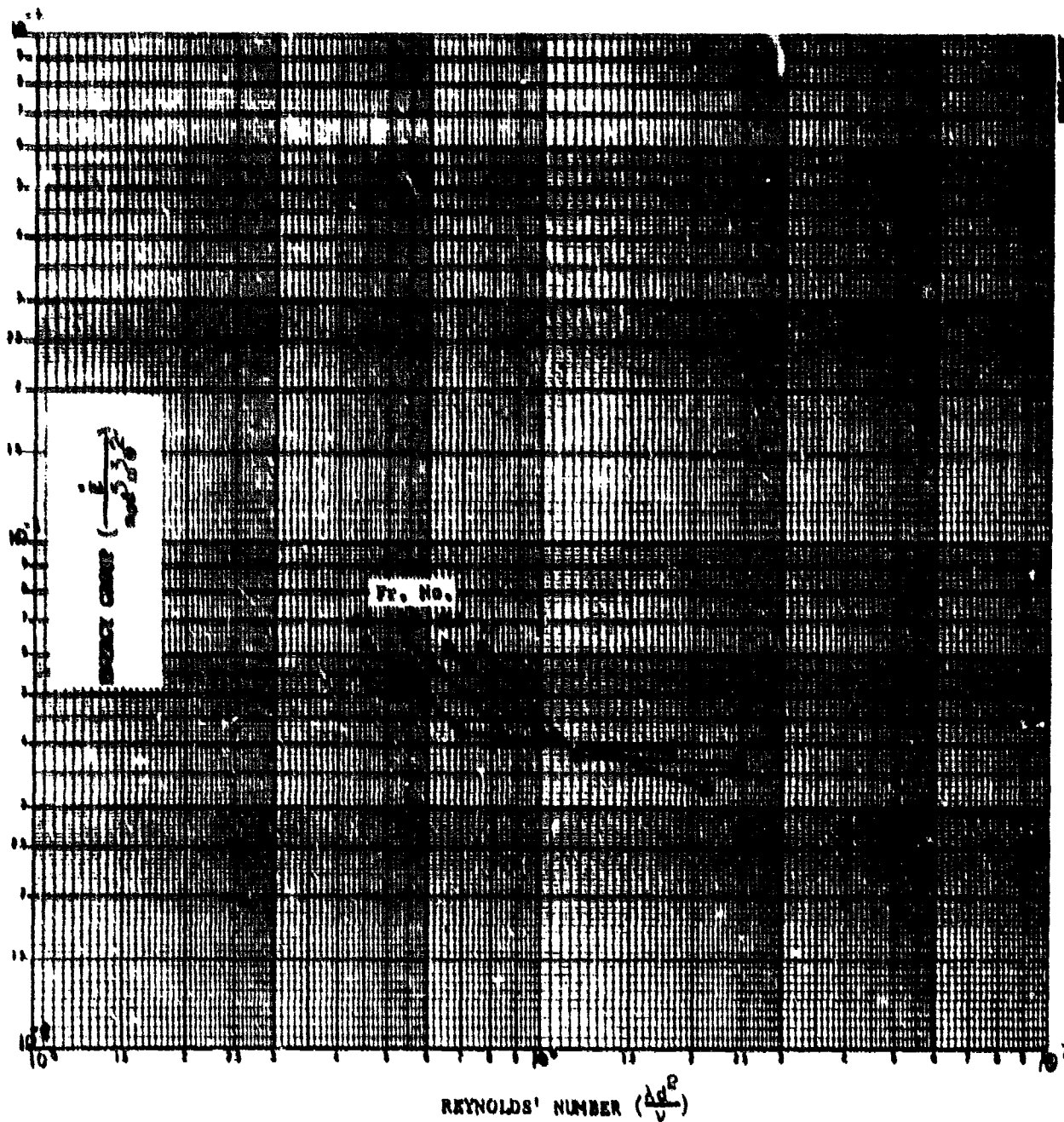
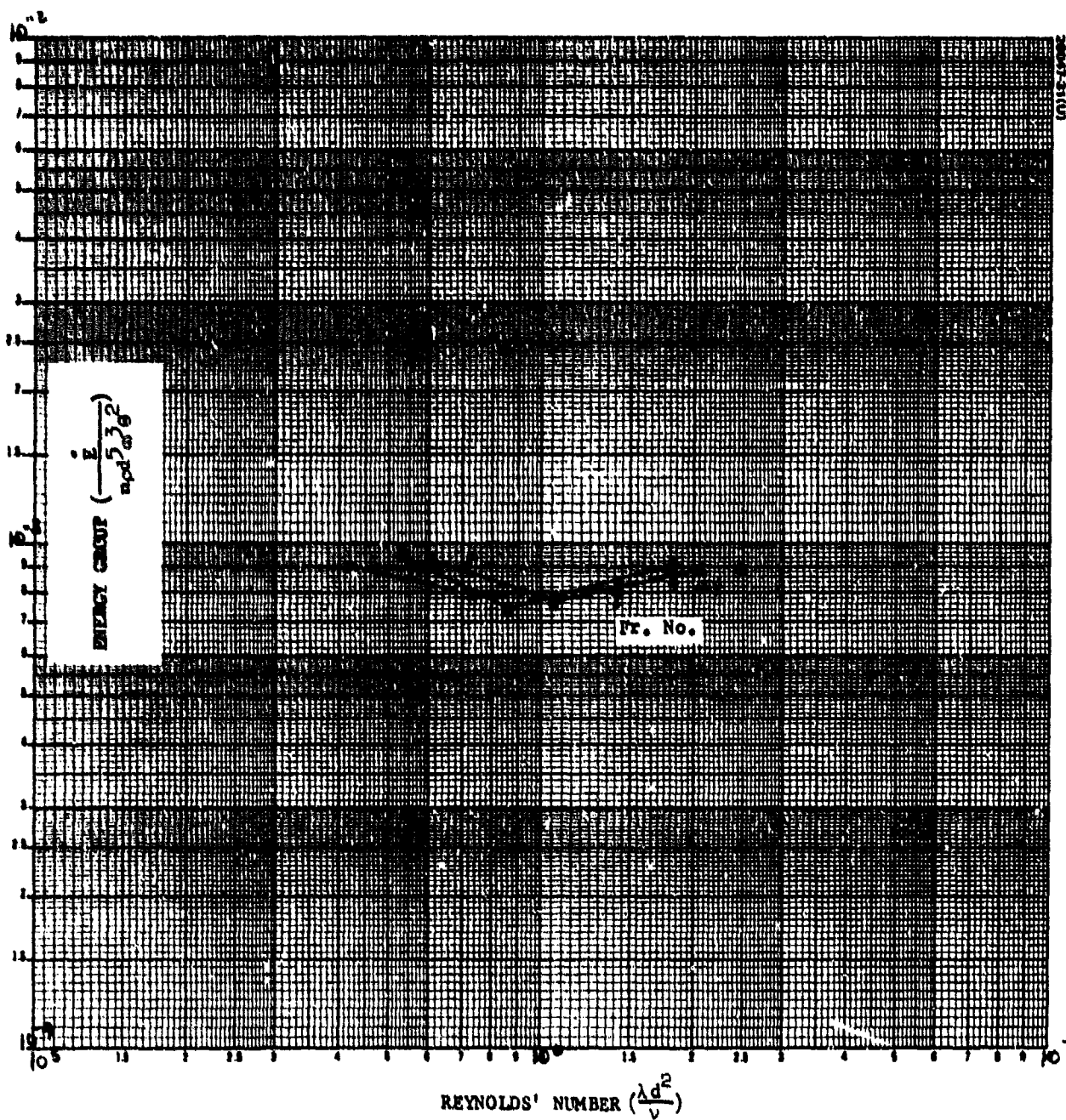REYNOLDS' NUMBER $(\frac{\Delta d^2}{\nu})$

b) Energy Group Versus Reynolds Number

Figure 5-14 (continued). Phase III Spherical Tank Fuel Sloshing at 75 Percent Fraction Fill ($\sigma = 0.335$)
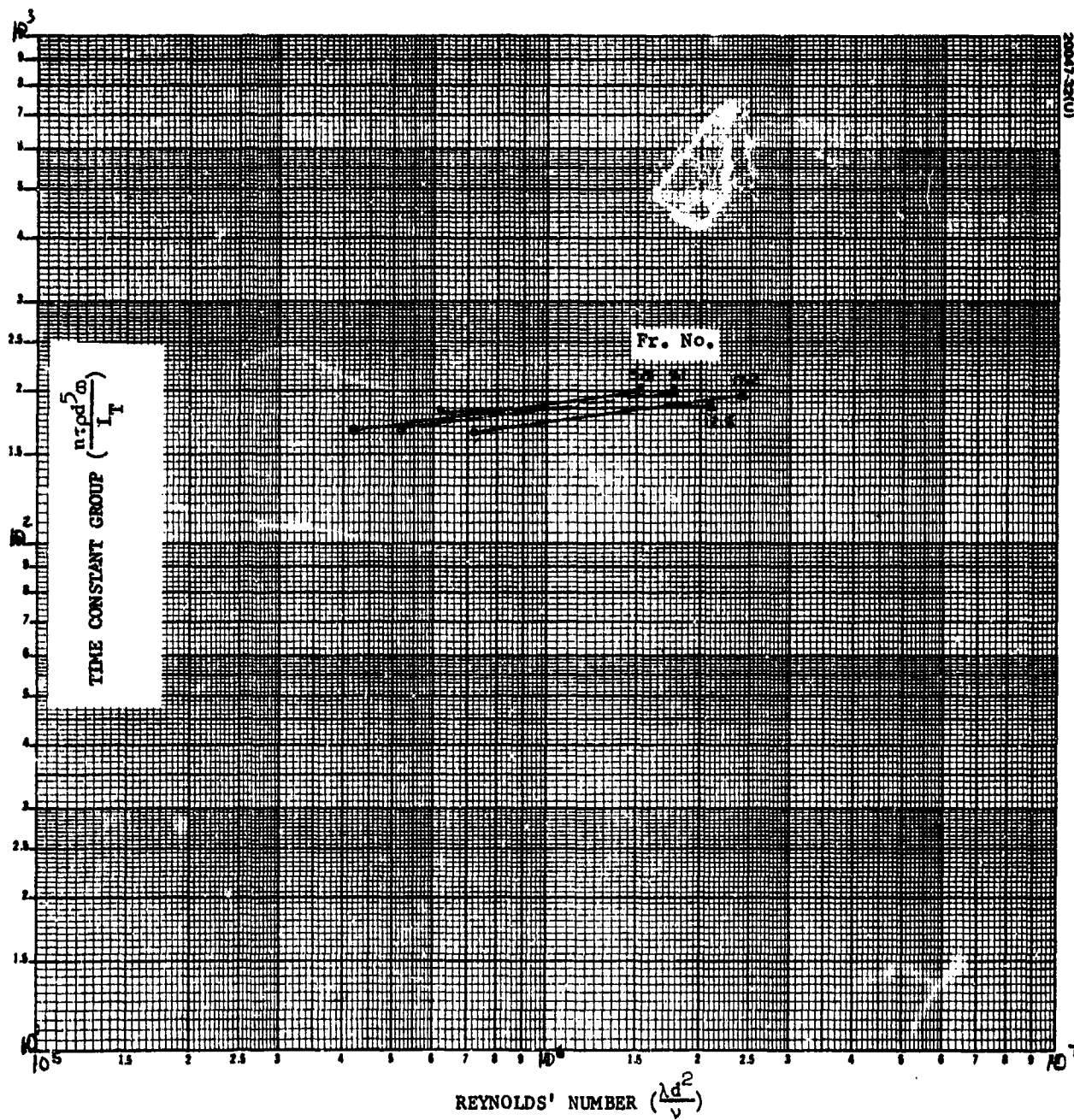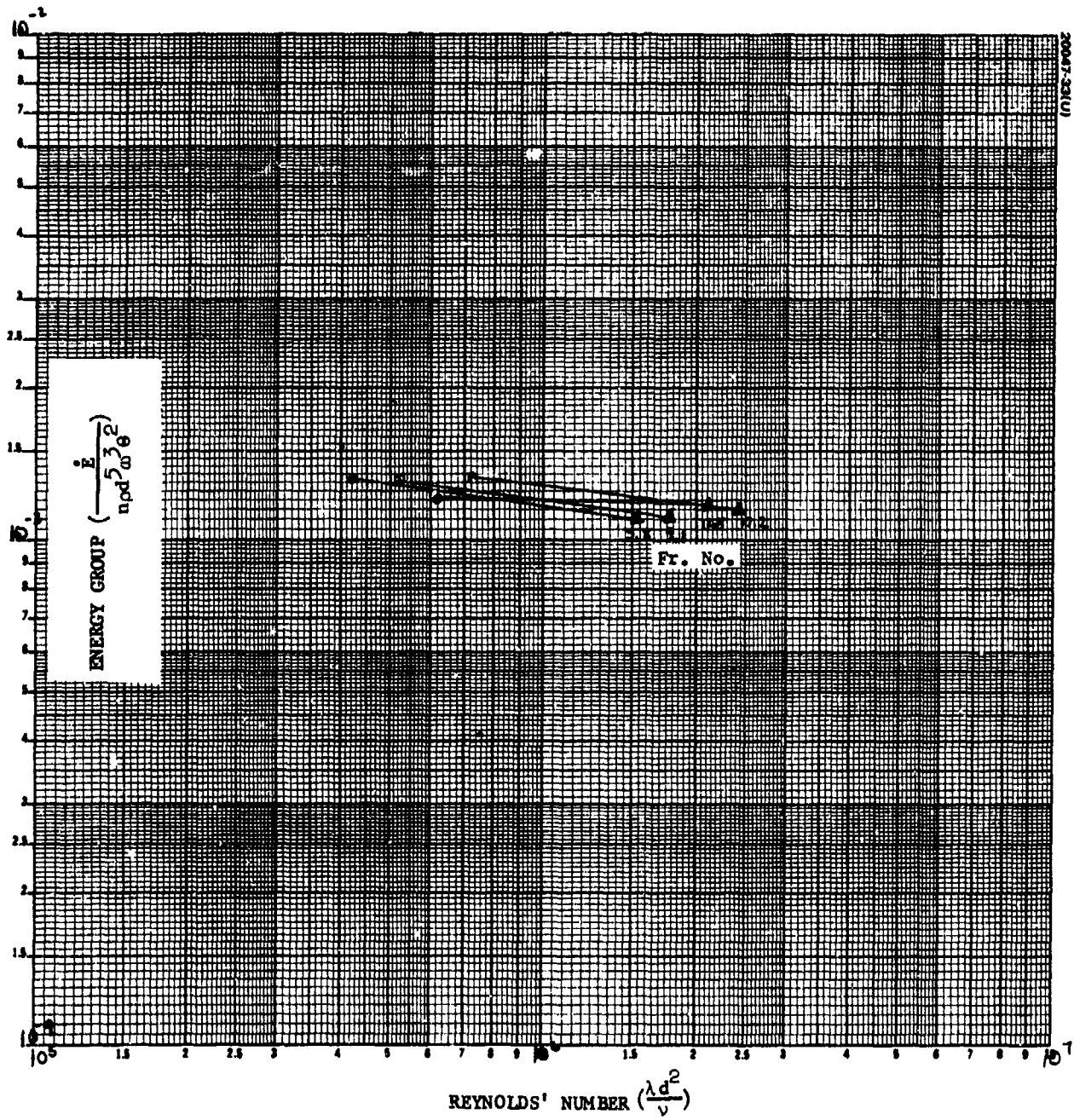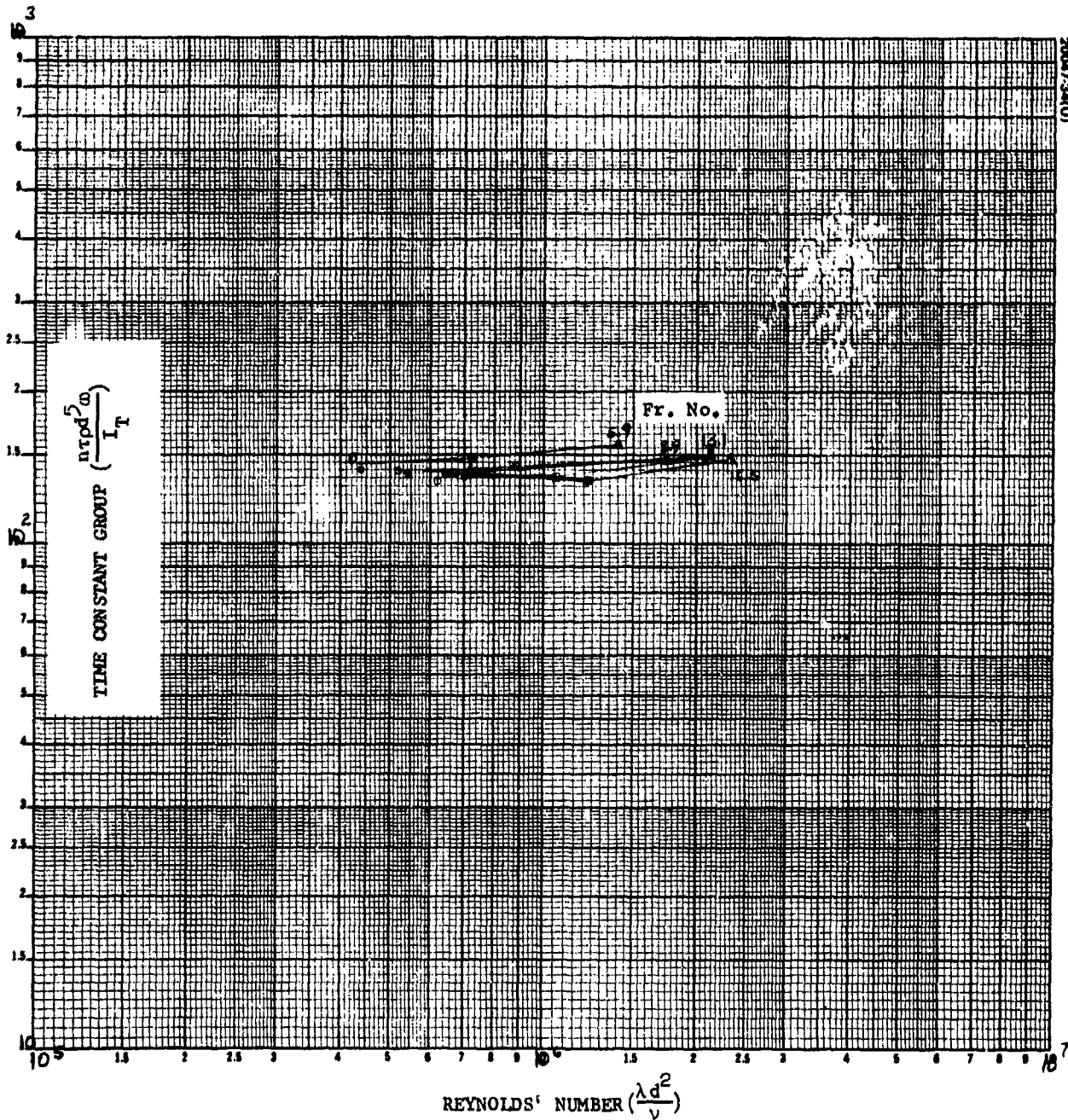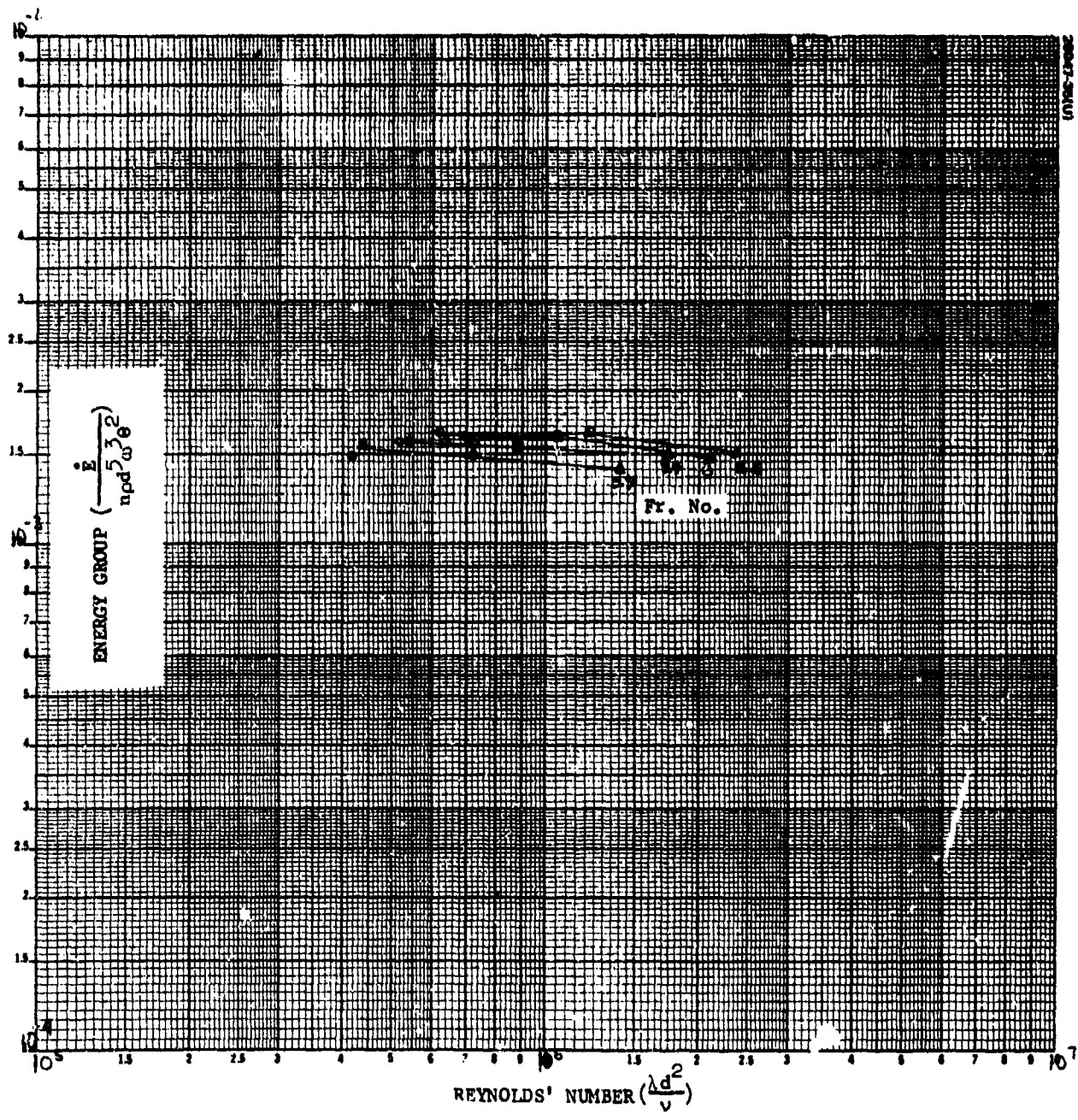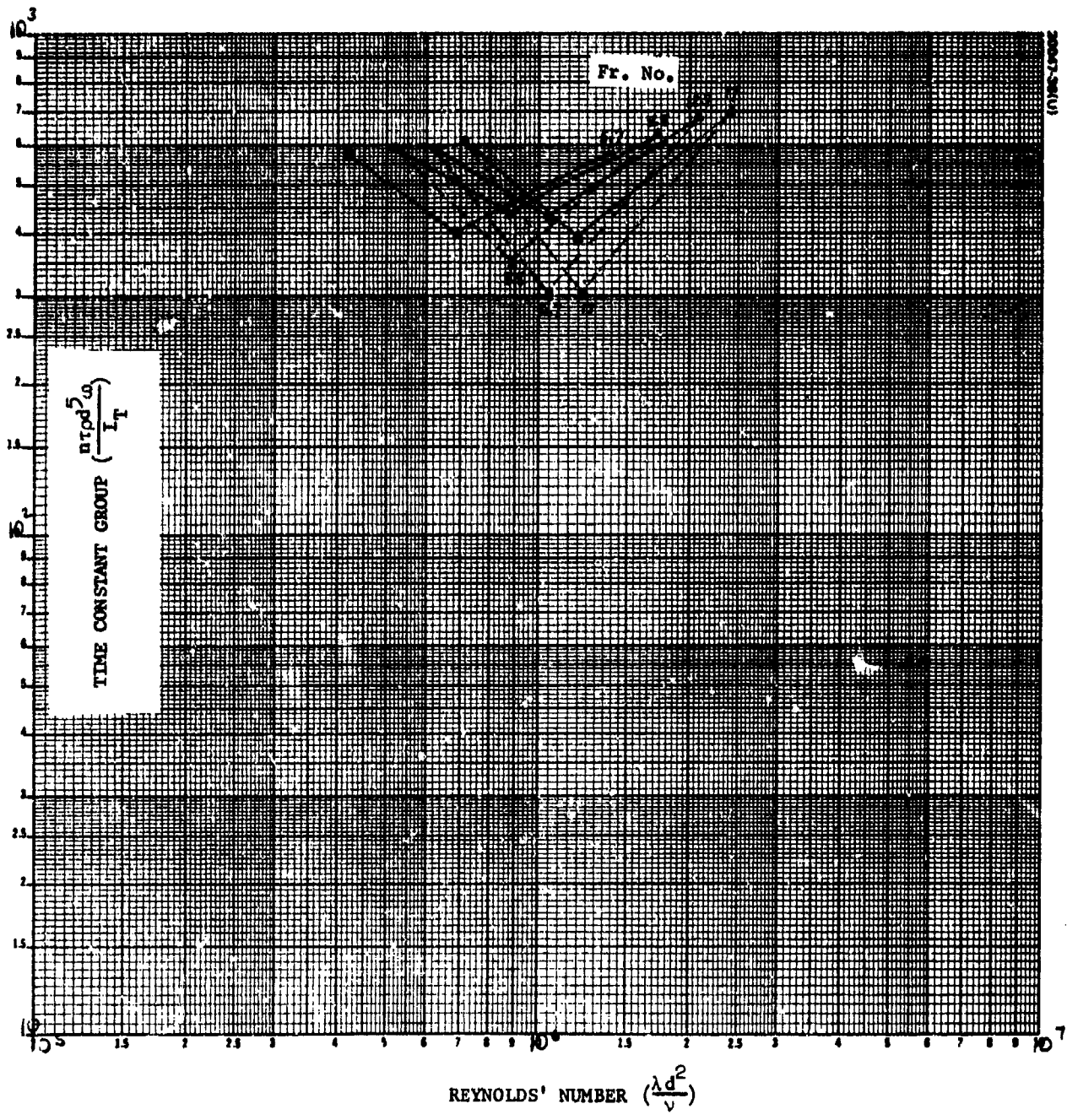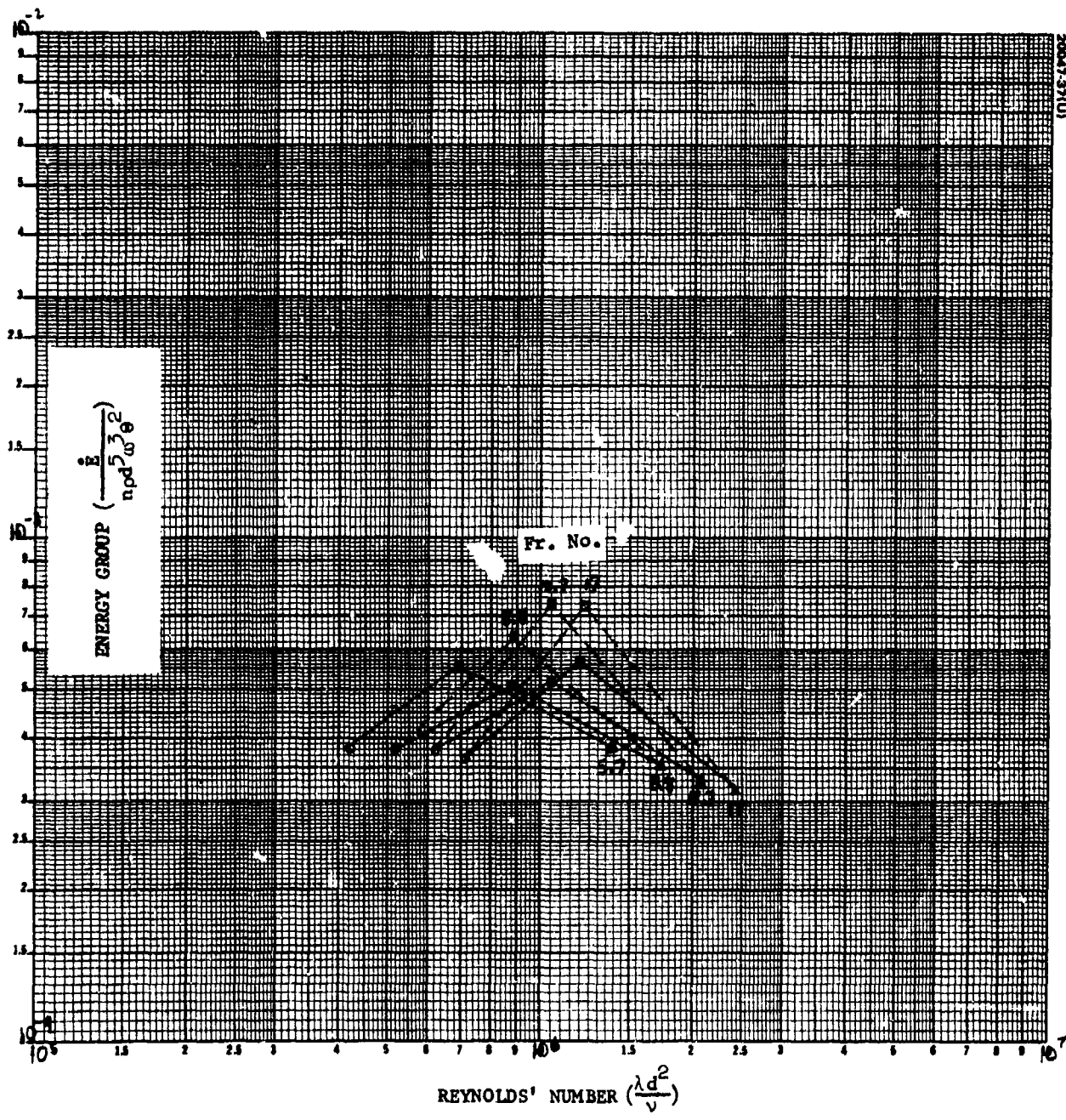
a) Time Constant Group Versus Reynolds Number

Figure 5-15. Phase III Spherical Tank Fuel Sloshing at 66 Percent
Fraction Fill ($\sigma = 0.335$)

b) Energy Group Versus Reynolds Number

Figure 5-15 (continued). Phase III Spherical Tank Fuel Sloshing at 66 Percent Fraction Fill (σ = 0.335)

a) Time Constant Group Versus Reynolds Number

Figure 5-16. Phase III Spherical Tank Fuel Sloshing at 60 Percent
Fraction Fill (σ = 0.335)

5-42

b) Energy Group Versus Reynolds Number

Figure 5-16 (continued). Phase III Spherical Tank Fuel Sloshing at
60 Percent Fraction Fill ($\sigma = 0.335$)

5-43

a) Time Constant Group Versus Reynolds Number

Figure 5-17. Phase III Spherical Tank Fuel Sloshing at 50 Percent
Fraction Fill ($\sigma = 0.335$)

b) Energy Group Versus Reynolds Number

Figure 5-17 (continued). Phase III Spherical Tank Fuel Sloshing at
50 Percent Fraction Fill ($\sigma = 0.335$)

5-45

Figure 5-18. Phase III Spherical Tank Fuel Sloshing at 30 Percent Fraction Fill ($\sigma = 0.335$)

a) Time Constant Group Versus Reynolds Number

b) Energy Group Versus Reynolds Number

Figure 5-18 (continued). Phase III Spherical Tank Fuel Sloshing at
30 Percent Fraction Fill (σ = 0.335)
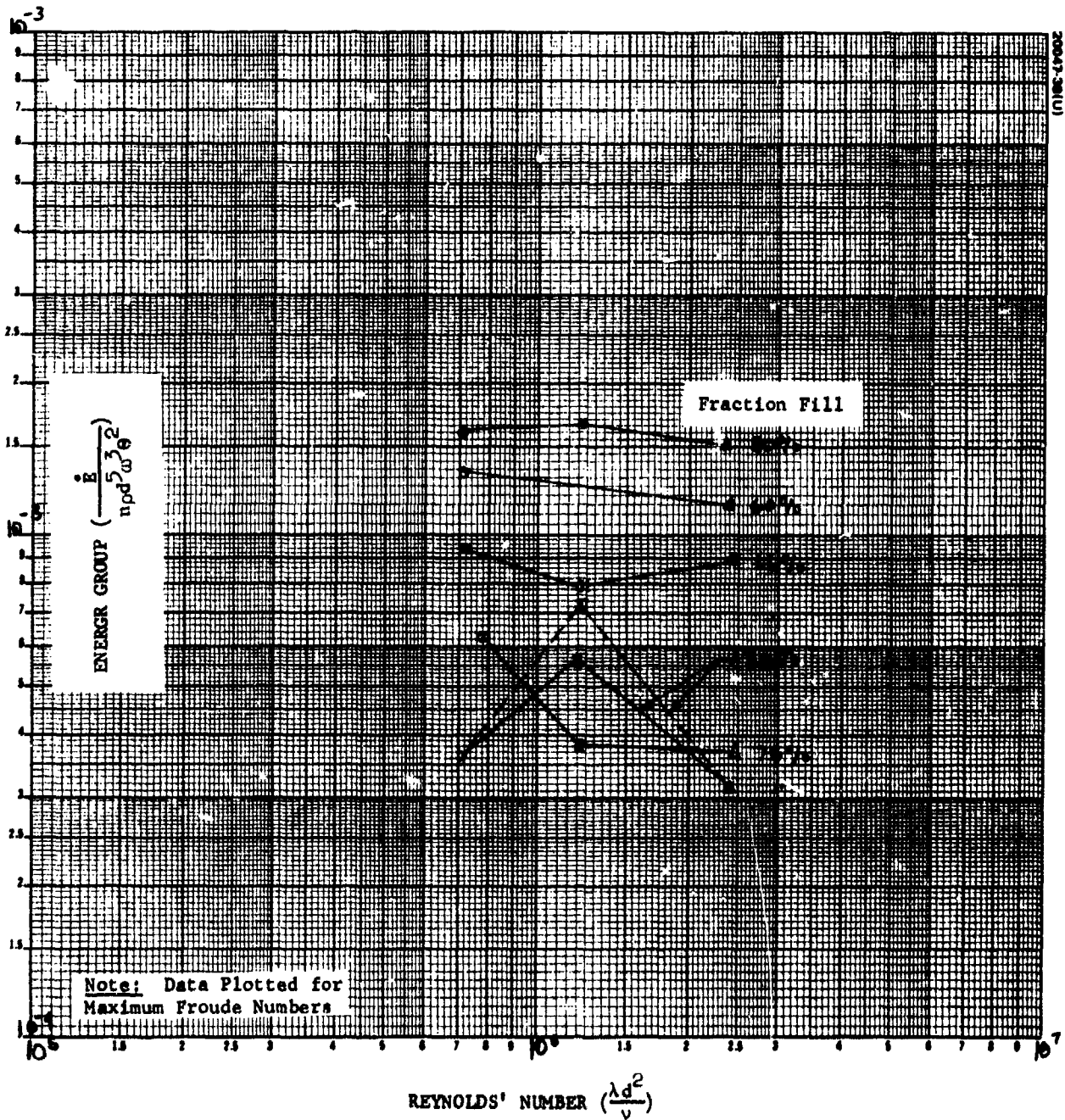
Figure 5-19. Comparative Energy Groups for Various Fraction Fills of Spherical Tank ($\sigma = 0.335$)

5-48

The test matrix for the 0.1 inertia ratio (Table 5-3) is not nearly as complete as for the 0.335 inertia ratio. The primary reason for this, as will be seen shortly, is that the fuel sloshing effects at this inertia ratio are not nearly as serious as at 0.335. From an engineering standpoint, therefore, extensive mapping of the parameter space at this ratio was not warranted. The primary purpose of conducting tests at this ratio was to achieve a satisfactory bound on the dissipation rate. It was recognized that there was no reasonable way to extrapolate the 0.335 results to the 0.1 case since the data obtained at the former value defied numerous modeling attempts.

Since the data in this section are therefore sketchy and incomplete, it is necessary to view the data in light of the discussion presented in the last section. Certain characteristic trends and behaviors can be correlated between the two sets of data, which, hopefully will ultimately lead to an empirical model.

The data are presented here in the same format as established in the last section. The companion time constant and energy groups are presented for each fraction fill. As will be noted at two fill fractions, i. e. , 80 and 50 percent, the graphs only contain one set of data. These data will be used to establish the approximate energy levels at these fill fractions.

It should be noted that the scale on the ordinate parameter on most of these graphs has been shifted by an order of magnitude. The time constant group is increased by a factor of ten and the energy group is correspondingly decreased by the same amount. This is, perhaps, the most significant observation of the following data in comparison to the data presented in the last section. The second most significant point is the lack of convergence; and, finally, the fraction fill dependence is noticeably different from the 0.335 inertia ratio.

5.5.1 100 Percent Fraction Fill

The 100 percent fraction fill data are presented in Figure 5-20. Several familiar trends can be observed. The data, while somewhat noisier than the 0.335 data, indicate that the energy dissipation rate is independent of gravity. This is seen by the family of constant Froude number curves falling on top of each other. As has been pointed out, this behavior is expected for the completely filled case.
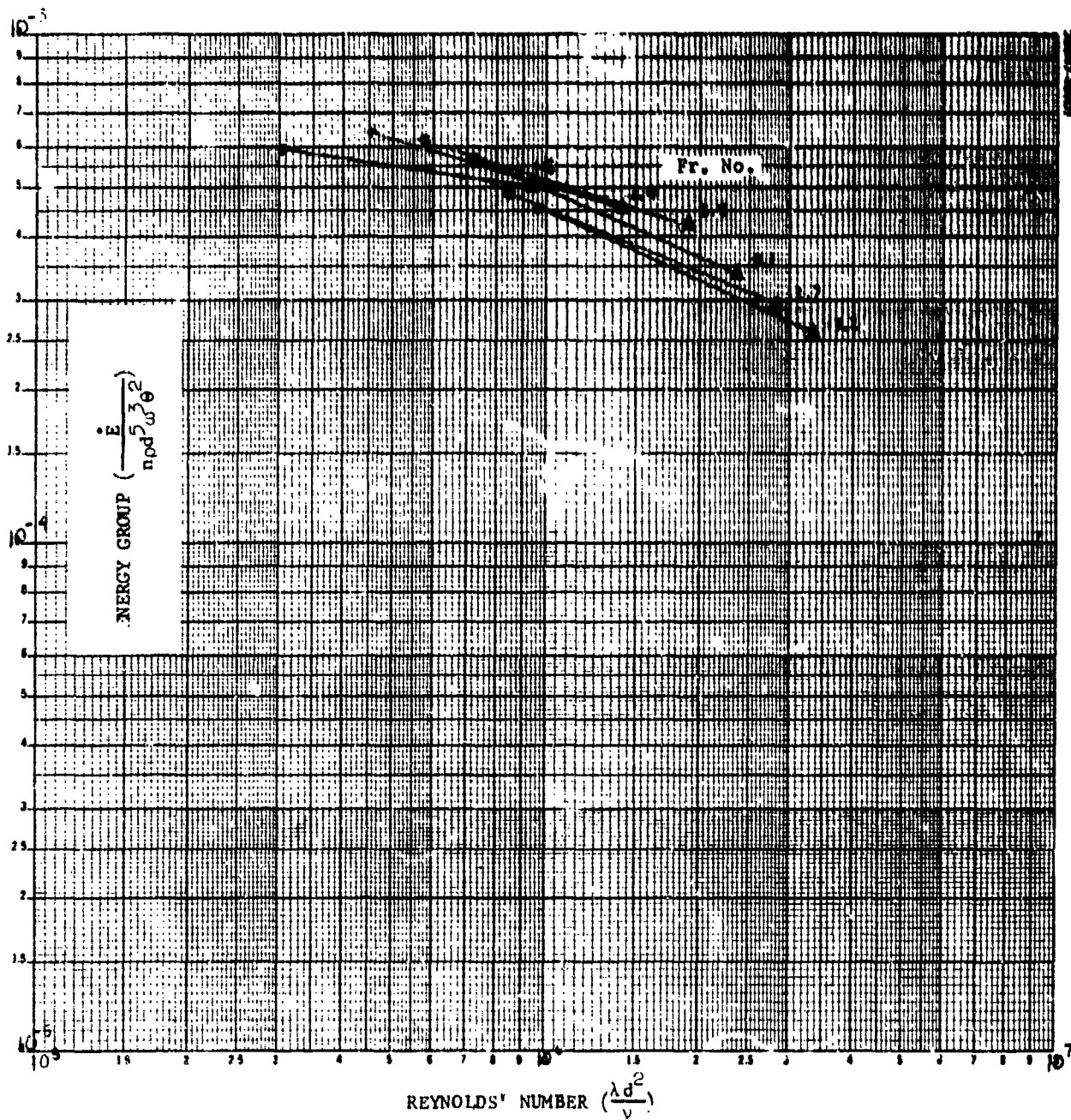
Another observation is that the energy dissipation appears to be approximately inversely proportional to the square root of the Reynolds number. This is the same Reynolds number dependence observed at $\sigma = 0.335$ 100 percent fraction fill.

If the energy groups at 0.1 and 0.335 are compared on a relative basis, it is seen that the 0.1 data lie about 30 percent above the 0.335. This case, it turns out, is an exception to the comment that 0.335 energy dissipation is worse than at 0.1. The reason for this behavior is not clear.
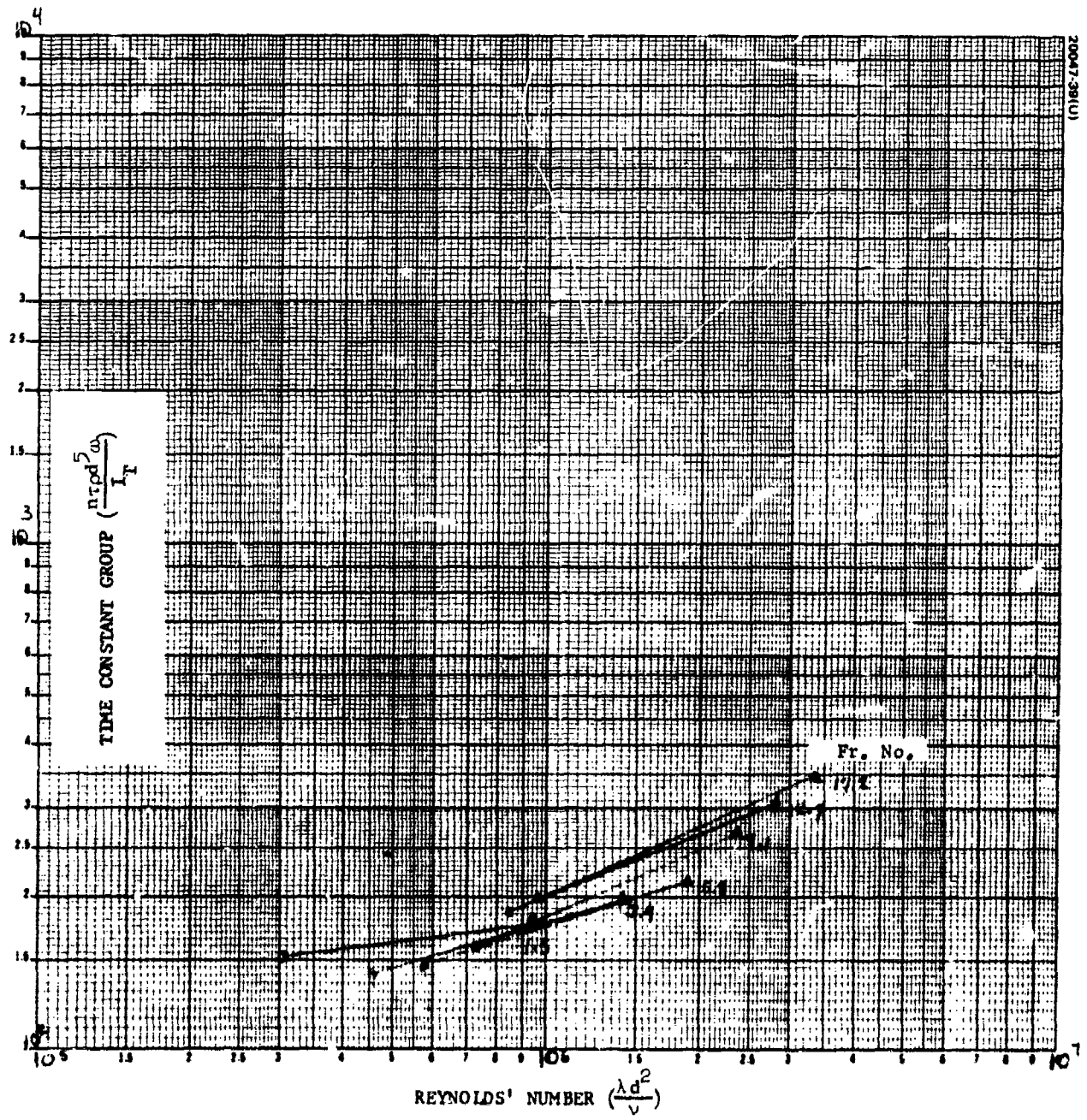
a) Time Constant Group Versus Reynolds Number

Figure 5-20. Phase III Conispherical Tank Fuel Sloshing at 100 Percent Fraction Fill ($\sigma = 0.1$)

5-50

Y-axis label: ENERGY GROUP $\left(\dfrac{\dot{E}}{n_p \rho d^5 \omega^3 \theta^2}\right)$

X-axis label: REYNOLDS' NUMBER $\left(\dfrac{\dot{\lambda} d^2}{\nu}\right)$

Fr. No.

b) Energy Group Versus Reynolds Number

Figure 5-20 (continued). Phase III Conispherical Tank Fuel Sloshing at 100 Percent Fraction Fill (o ⪡ 0.1)

5-51

However, since the Edwards model predicts a resonance at or near 90 percent fill for $\sigma = 0.1$, the proximity of the 100 percent fill to this peak could result in comparable dissipation rates with the $\sigma = 0.335$, 100 percent fill case.

5.5.2 80 Percent Fraction Fill

The 80 percent fill, Figure 5-21, contains the result of only one test conducted with the freon solution. The data indicate one behavior fundamentally different from the 0.335 data. As the Froude number increases, so does the time constant group. That is to say, as gravity effects become less significant the resultant dissipation rates due to nutation increase rapidly.

The only other comment about the 80 percent data is a comparison with the 0.335, 75 percent data. Comparing the energy groups at the highest Froude number and comparable Reynolds number, it is observed that the 0.1 group levels are down nearly an order of magnitude from the 0.335 tests.

5.5.3 66 Percent Fraction Fill

The 66 percent fraction fill, Figure 5-22, contains some very interesting behaviors. The most obvious difference between the 0.1 and 0.335, 66 percent data is that the critical spin speed ω_s^N has not been reached and Froude number convergence has not occurred.

One word of caution, however; only two test fluids were run, and therefore it is only possible to draw a straight line between them. As pointed out in Section 4 and observed in the previous section, the introduction of a third fluid permits drawing a second-order polynomial through the data. It is entirely possible that, as in the case of 30 percent fill at $\sigma = 0.335$, the water tests are critical in establishing curvature to the family of constant Froud number curves and changing the observed behavior from one of no convergence to one of, at least, quasi-convergence. Such may be the case here. Perhaps at some later date the missing data can be obtained.

For the time being, it suffices to say that the gravity dependence is significant at $\sigma = 0.1$ even to the highest Froude number obtainable in the test. One comment is, perhaps, worth making. While the Froude number is a significant parameter which measures the relative magnitude of centrifugal to gravitational forces, it is also important to keep in mind the ratio of the nutational to gravitational acceleration. If the fluid motion is to be driven by the nutational acceleration, obviously this acceleration must dominate gravity. As is generally known, those nutational accelerations are related to the centrifugal accelerations only by a constant proportional to $\sigma(2-\sigma)$ and θ, i.e., $a_{NUT} = \sigma(2-\sigma)R\omega_s^2$. Gravity, on the other hand, sinusoidally excites the orthogonal axis to the nutational excitation when the vehicle is nutating. (Refer to Appendix D for further clarification of

this point.) The magnitude of this gravity excitation is proportional to $\mu\theta$. Thus the ratio of the two excitations is significant, i.e., the ratio $\sigma(2-\sigma)R\omega^2/g$ which is just $\sigma(2-\sigma)(\text{Froude number})$. At the same Froude number, this ratio becomes 1/6 the value at 0.335. What this suggests is that at 0.1 the spin speed must be increased to suppress the gravity excitation. To satisfy this condition, the spin speed would have to be increased over a factor of 2 at $\sigma = 0.1$ to correspond to the equivalent nutation-gravity ratio at 0.335. Unfortunately, the test machine cannot withstand such speeds; so this hypothesis cannot be easily tested. Perhaps the Phase IV tests at 0.6 and 1.1 inertia ratios will shed more light on this matter.

It is interesting to observe that, in the case of $\sigma = 0.335$, gravity tended to mask the dissipation due to nutation. In the case of $\sigma = 0.1$ gravity effects dominate the dissipation giving the data an appearance of being much worse than they really are. In all the analyses and simulations conducted on this problem, the strong gravity dependence was not included nor really recognized. It is lack of a priori fluid dynamic insight into the problem which necessitates extensive testing.

A further observation about the 66 percent data is that the energy group at the maximum Froude number is nearly a factor of 60 below the comparable conditions at the respective fill for $\sigma = 0.335$.

Since the data at 66 percent do not indicate Froude number convergence the only possible way in which the data can be interpolated to space is to assume that the maximum Froude number curve represents a lower bound on the dedamping time constant. In this way, the time constant group number at the flight Reynolds number can be used to estimate the dedamper magnitude in flight.

5.5.4 50 Percent Fraction Fill

The 50 percent fill, Figure 5-23, represents the limited data available at the fraction. Very little can be said about the data. There is apparently a strong gravity effect still in the data. The comparative 0.1 and 0.335 energy groups show the 0.1 down by at least an order of magnitude.
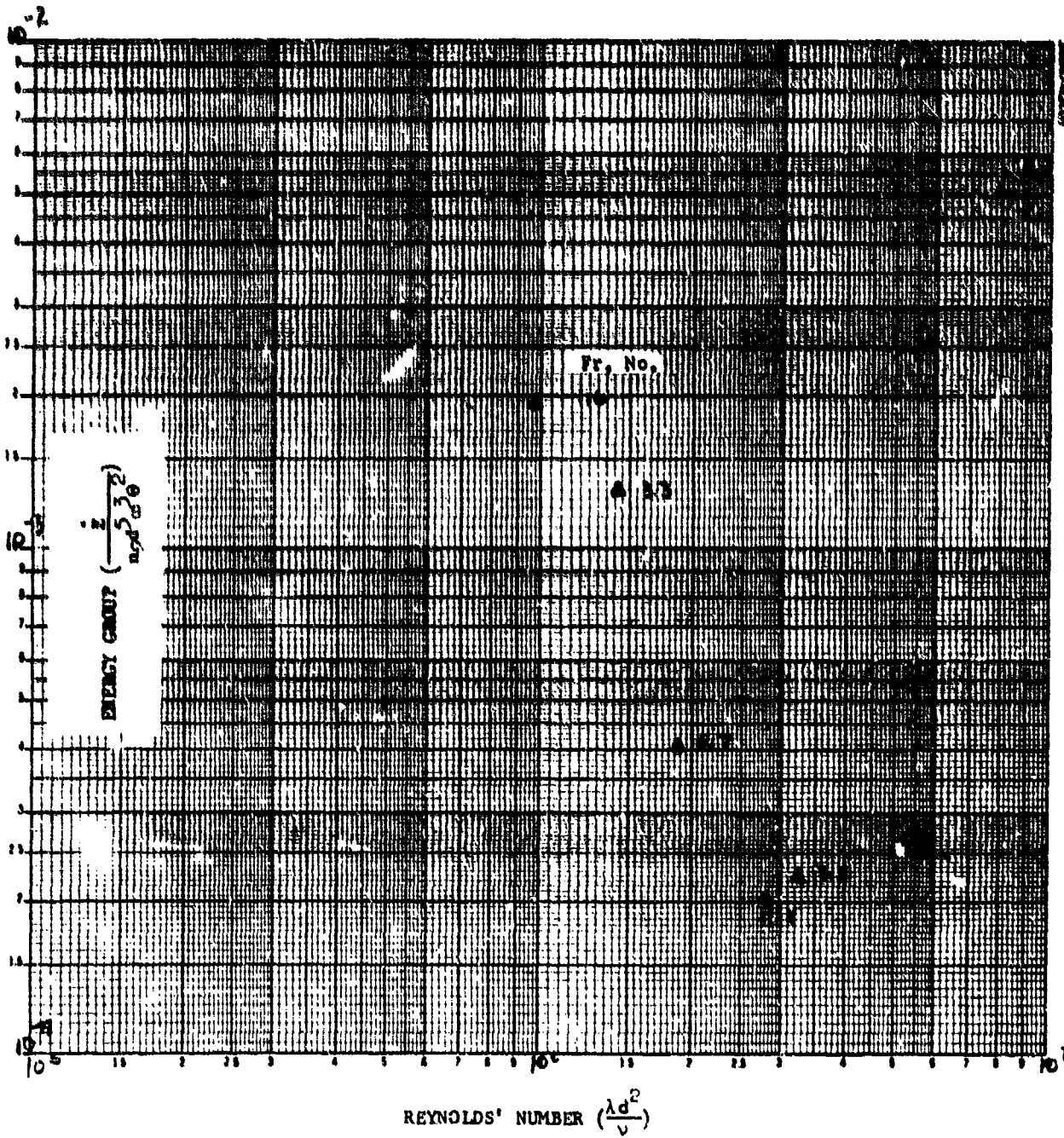
5.5.5 30 Percent Fraction Fill

Figure 5-24 presents the available 30 percent data at 0.1. Again there is the characteristic $\sigma = 0.1$ Froude number behavior. However, this time there is a crossover at 12.8 and 16.5 Froude numbers. While this may be partly due to scatter in the data, it is also suggesting that the limiting Froude number may have been reached at this fill. It is not clear why this would happen at 30 percent but, perhaps, the phenomena is complicated by the full occupancy of the conical segment.
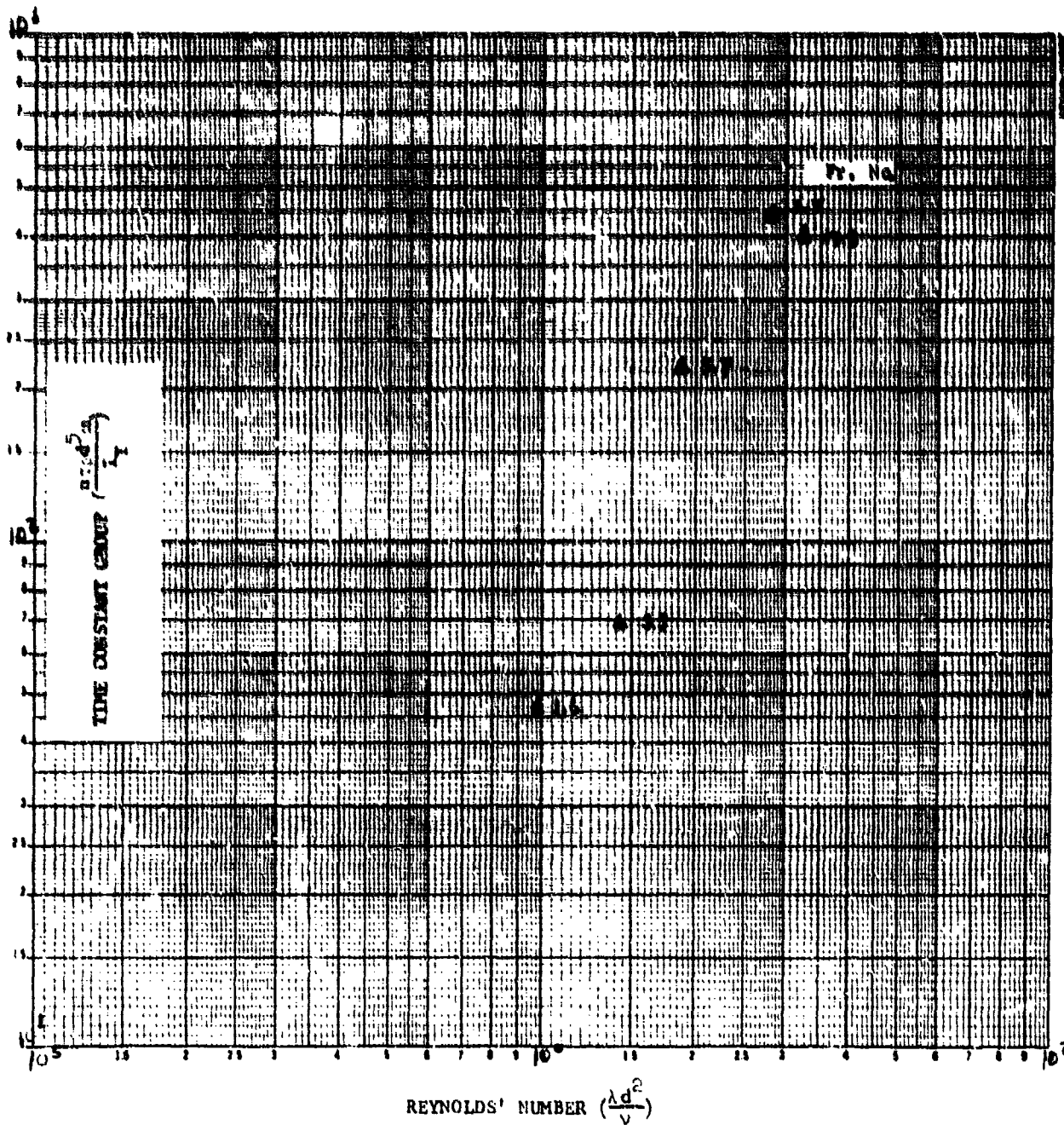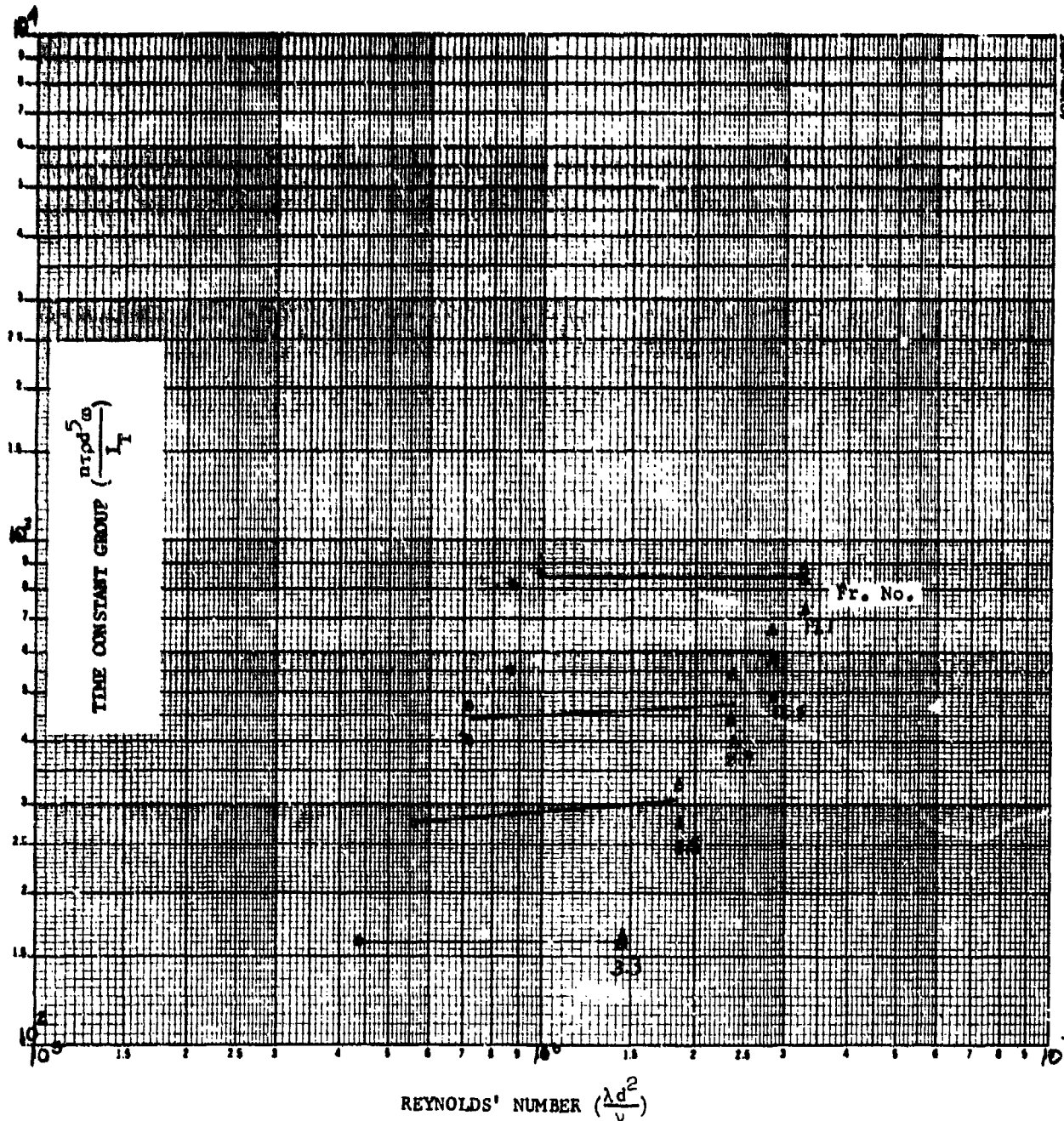
REYNOLDS' NUMBER $(\frac{\lambda d^2}{\nu})$

a) Time Constant Group Versus Reynolds Number

Figure 5-21. Phase II Conispherical Tank Fuel Sloshing at 80 Percent Fraction Fill ($\sigma = 0.1$)
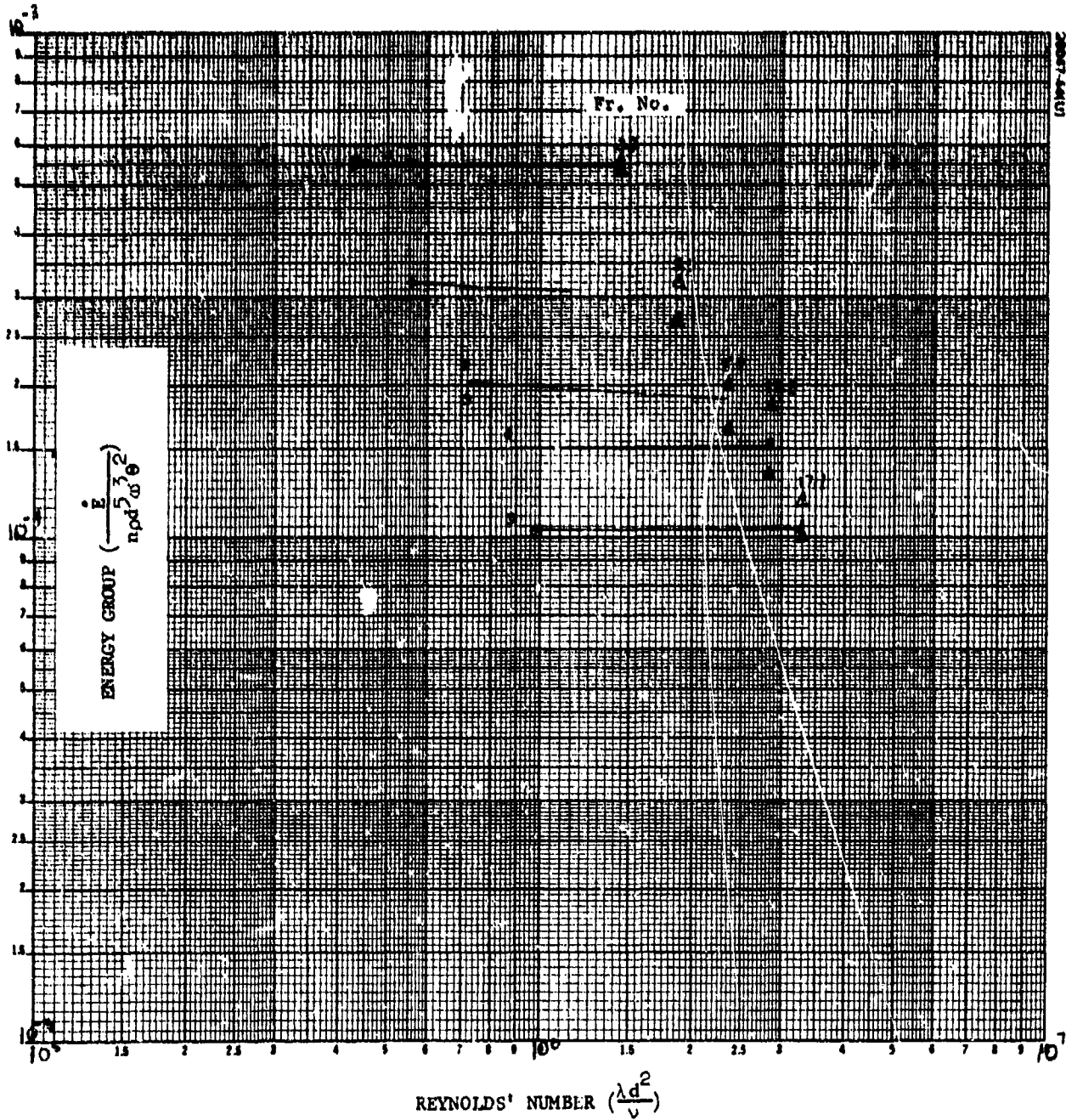
5-54

b) Energy Group Versus Reynolds Number

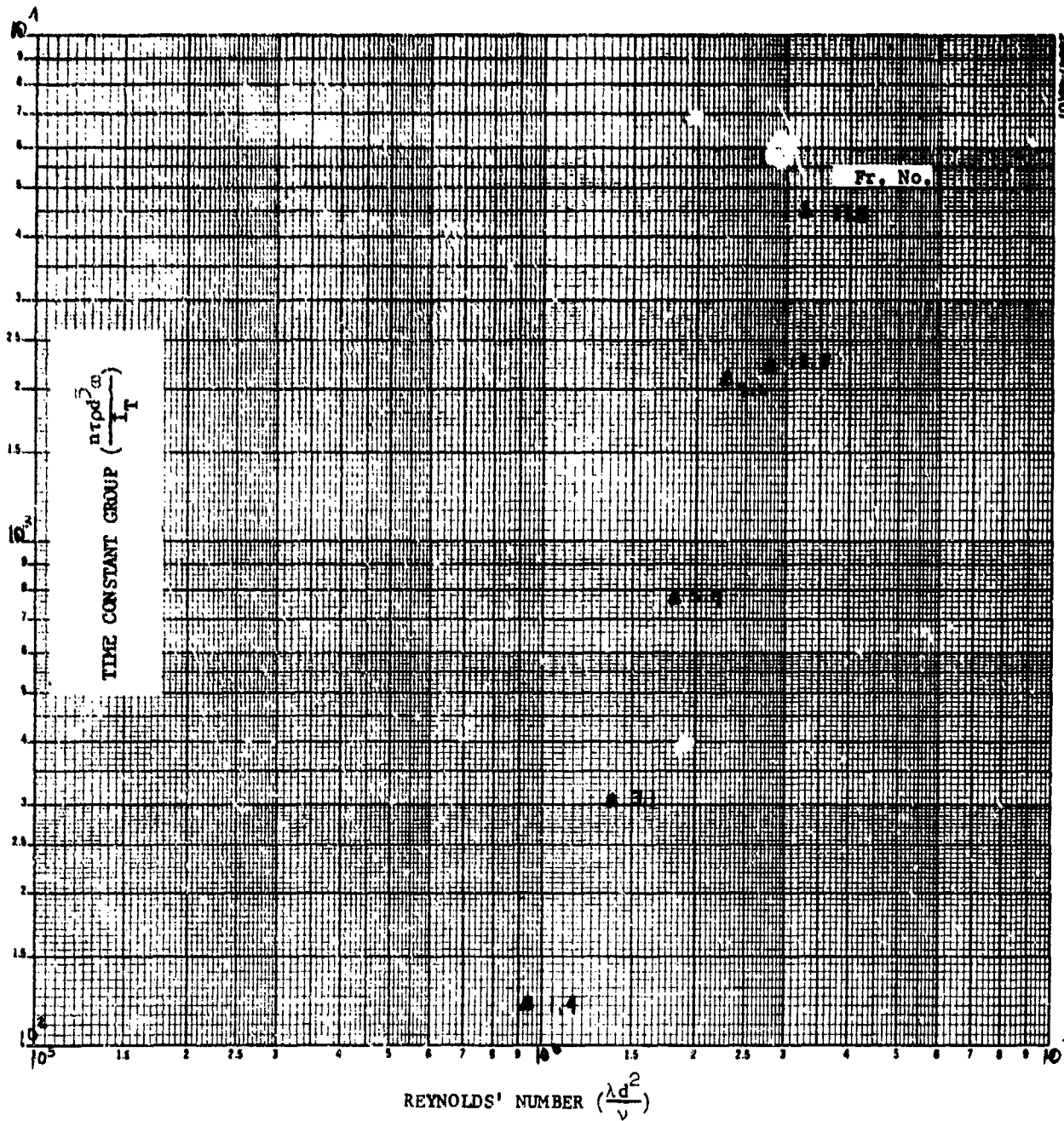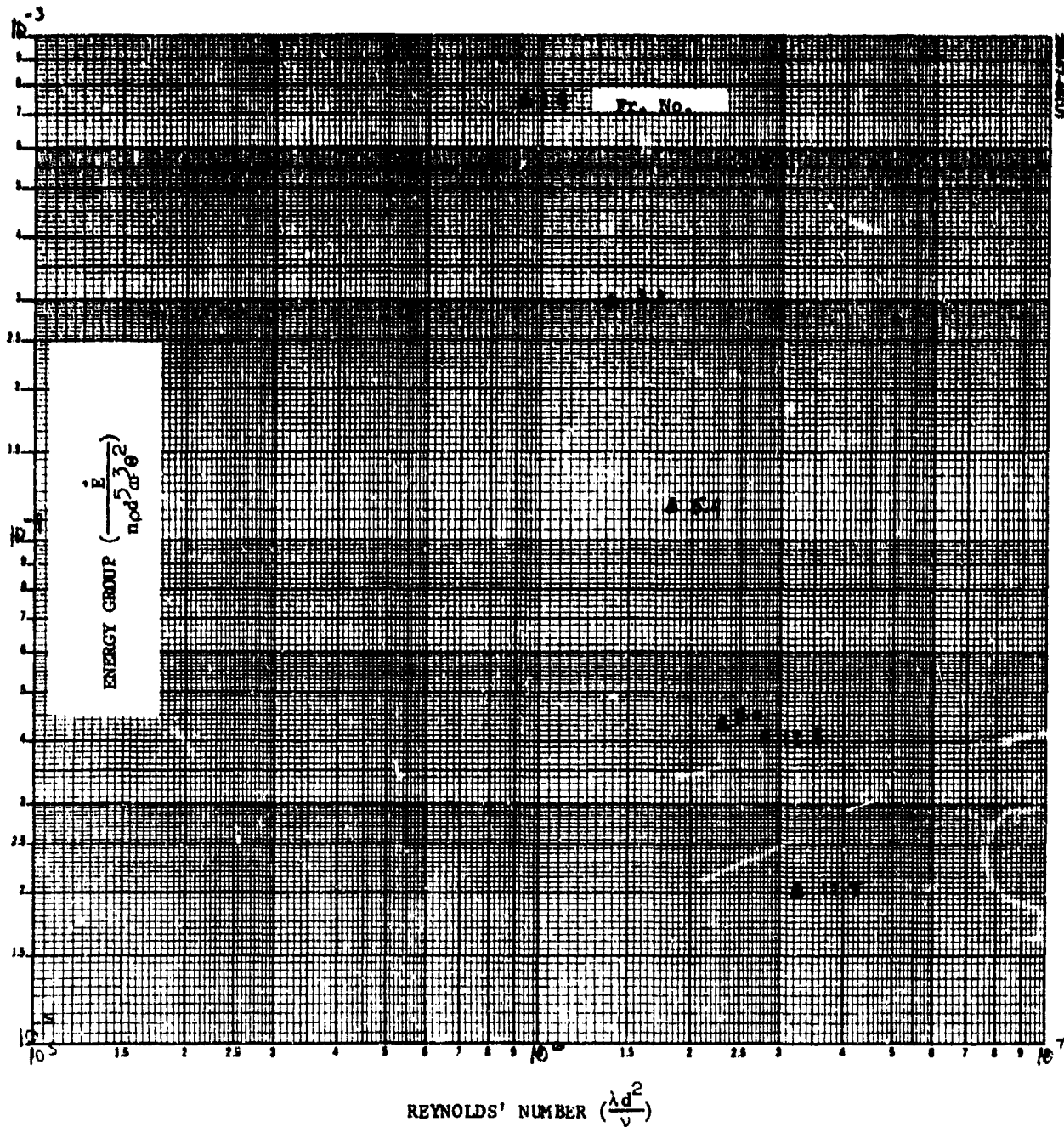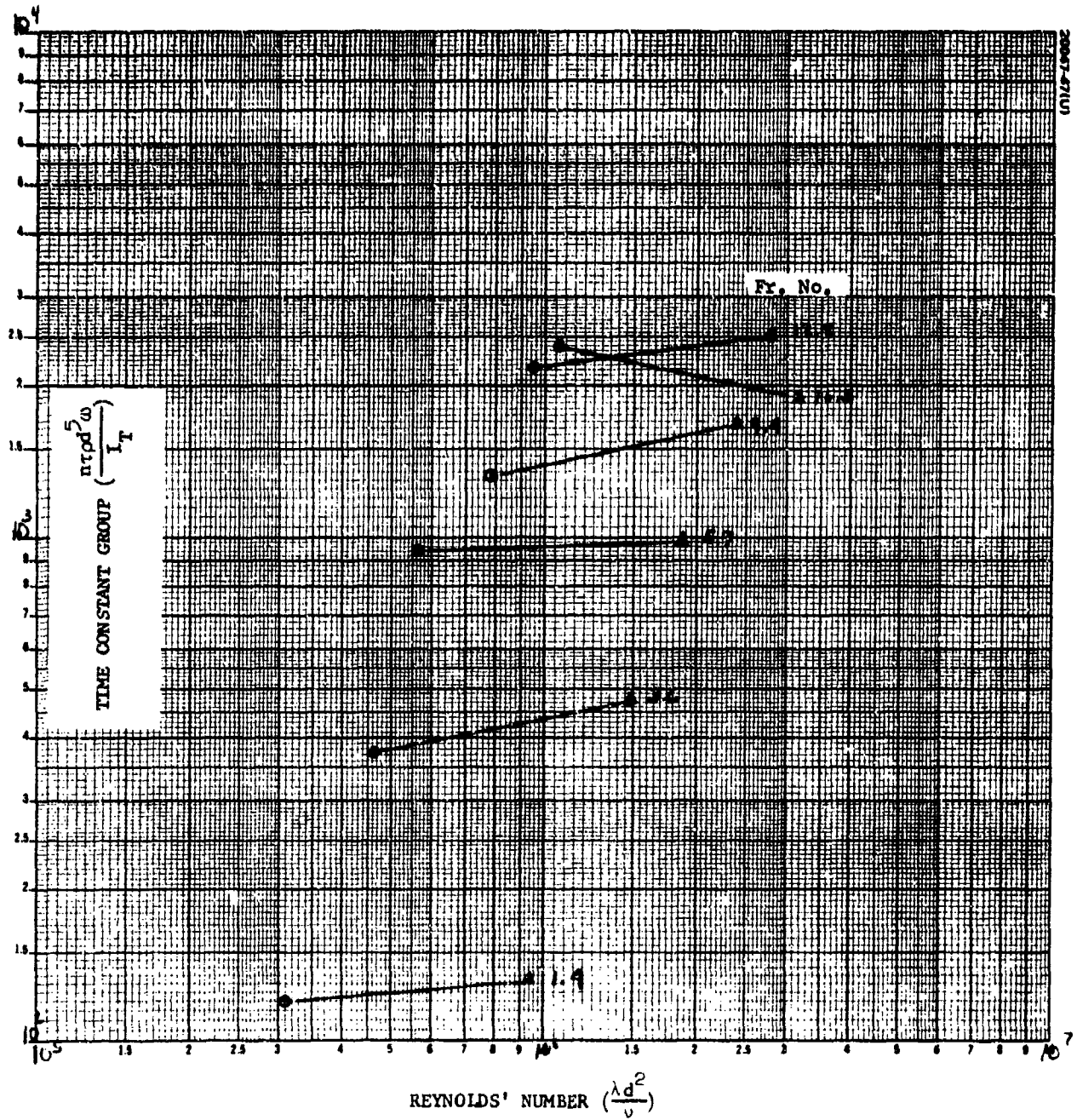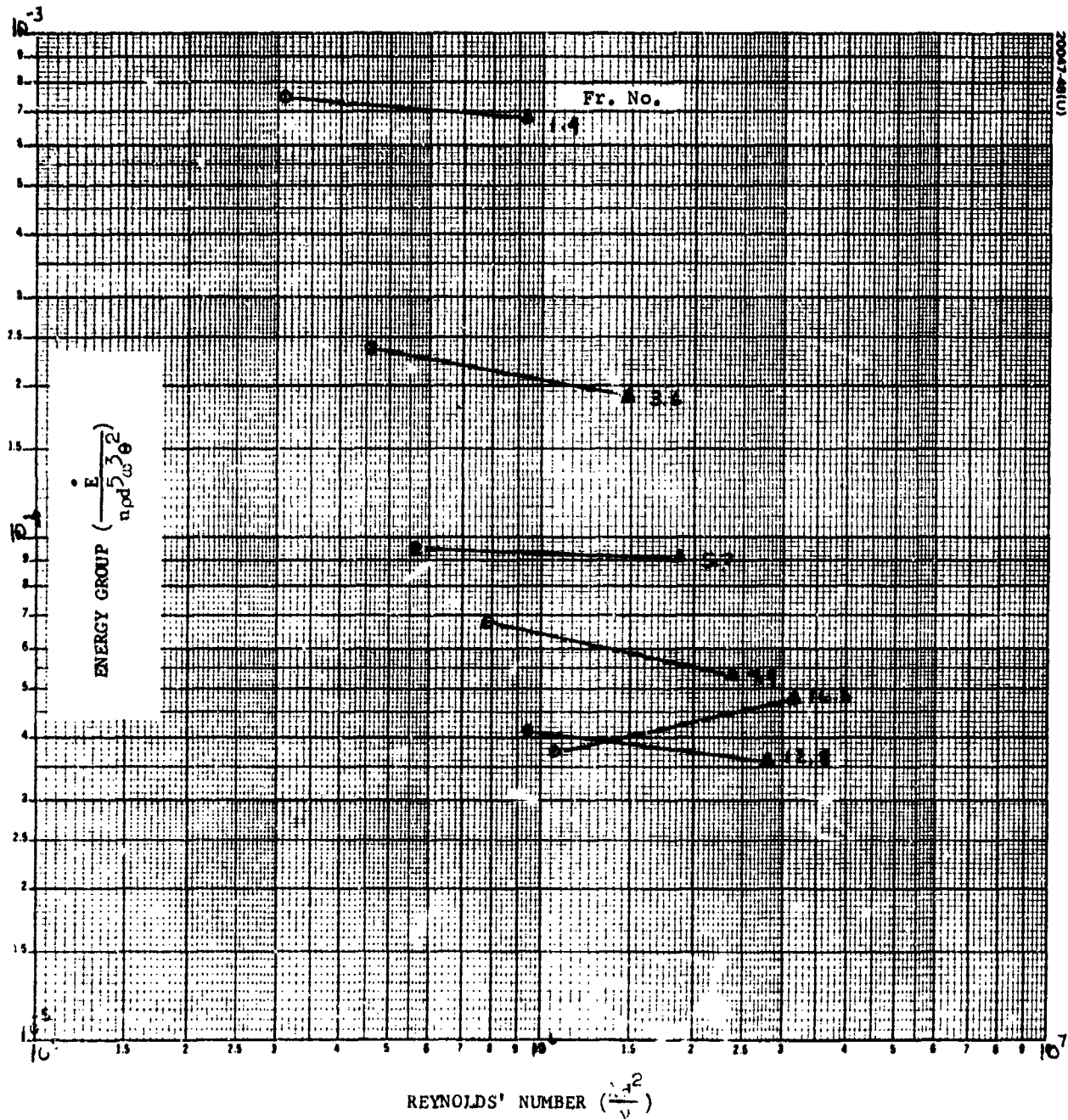Figure 5-21 (continued). Phase II Conispherical Tank Fuel Sloshing at 80 Percent Fraction Fill ($\sigma = 0.1$)

a) Time Constant Group Versus Reynolds Number

Figure 5-22.   Phase III Conispherical Tank Fuel Sloshing at 66 Percent
Fraction Fill ($\sigma = 0.1$)

b) Energy Group Versus Reynolds Number

Figure 5-22 (continued). Phase III Conispherical Tank Fuel Sloshing at 66 Percent Fraction Fill ($\sigma = 0.1$)

a) Time Constant Group Versus Reynolds Number

Figure 5-23. Phase II Co ispherical Tank Fuel Sloshing at 50 Percent Fraction Fill ($\sigma = 0.1$)

b) Energy Group Versus Reynolds Number

Figure 5-23 (continued). Phase II Conispherical Tank Fuel Sloshing at
50 Percent Fraction Fill (σ = 0.1)

a) Time Constant Group Versus Reynolds Number

Figure 5-24. Phase II Conispherical Tank Fuel Sloshing at 30 Percent Fraction Fill ($\sigma = 0.1$)

b) Energy Group Versus Reynolds Number

Figure 5-24 (continued). Phase II Conispherical Tank Fuel Sloshing at 30 Percent Fraction Fill ($\sigma = 0.1$)

5.5.6 Summary of Phase II and III Conispherical σ = 0.1 Data

The preceding data have been assembled into a summary plot similar to Figure 5-11 drawn for the respective 0.335 data. Unfortunately, the resultant graph, Figure 5-25, is more qualitative than quantitative. The curves represent the maximum Froude number curves at each fraction fill. The limited data at 80 and 50 percent only permit the establishment of approximate levels. The 50 percent data are highly suspicious because they lie below 66 and 30 percent.

The conclusions drawn from Figure 5-25 are few. It appears that the worst dissipation at σ = 0.1 occurs at or near the 100 percent fill. The energy levels are significantly below the respective 0.335 data, except for the 100 percent case as described earlier.

5.6 SPHERICAL TESTS, σ = 0.1 DATA

Only one spherical test was conducted at σ = 0.1; this was at 66 percent fraction fill. The data are presented in Figure 5-26. Several observations can be made with respect to the data.

First, the Froude number, or gravity effect, appears to be the same in the sphere as in the conisphere. Zero g convergence has apparently not been reached at 210 rpm.

If the sphere is compared with the conisphere at the same fill, Figure 5-22b, it is noted that the energy groups are quite similar at the Froude numbers tests. Therefore, the sphere and conisphere are comparable dedampers at σ = 0.1. It is not known whether this result applies across the entire fraction fill region or just at this point. As noted in the spherical 0.335 data, a crossover occurred near 40 percent fill. For 0.1 inertia ratio, the crossover could be at 66 percent.

Suffice it to say at a 0.1 inertia ratio the issue of sphere versus conisphere is not germane in an engineering sense. If the conisphere is not a problem, the sphere is not a problem.
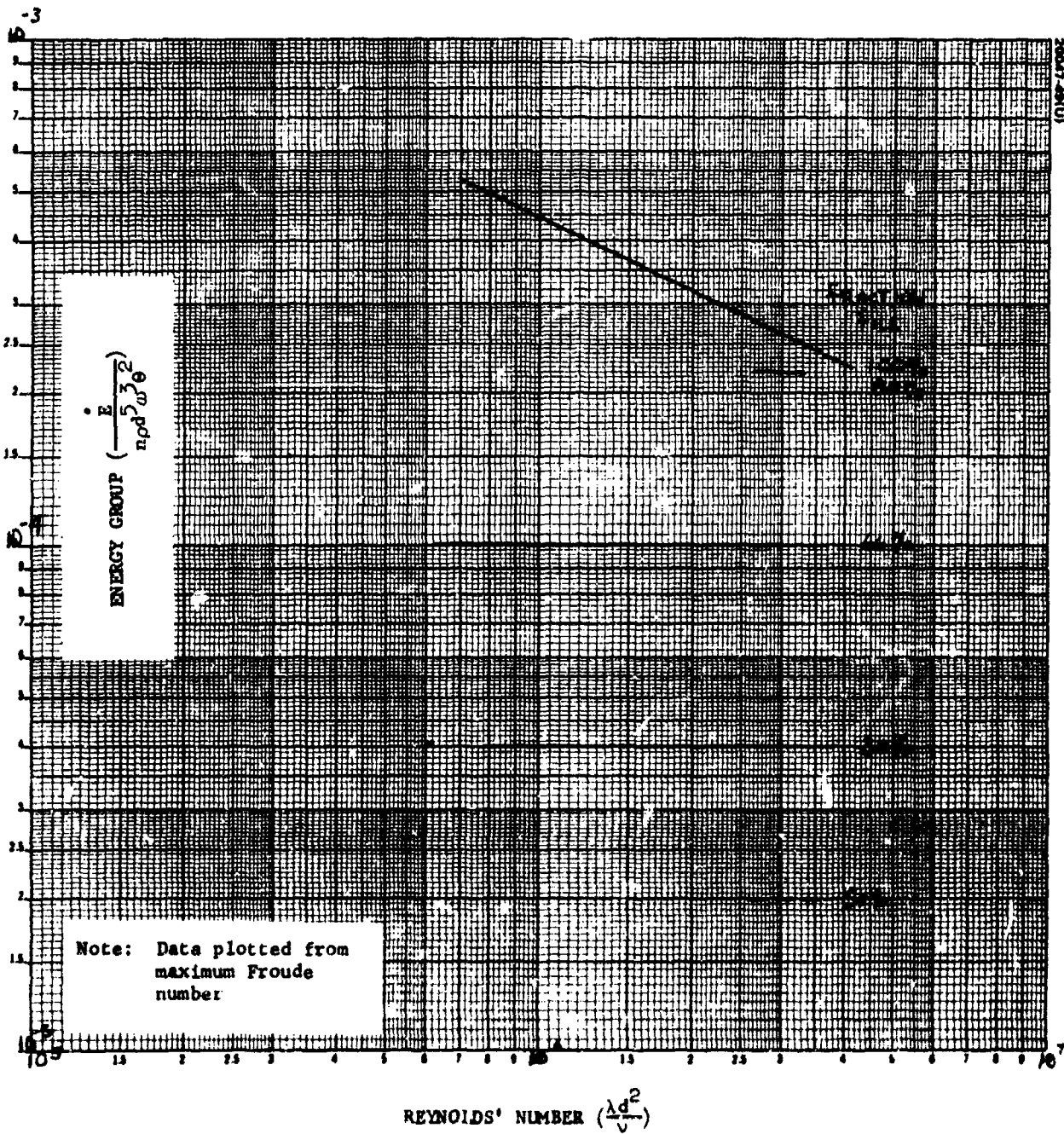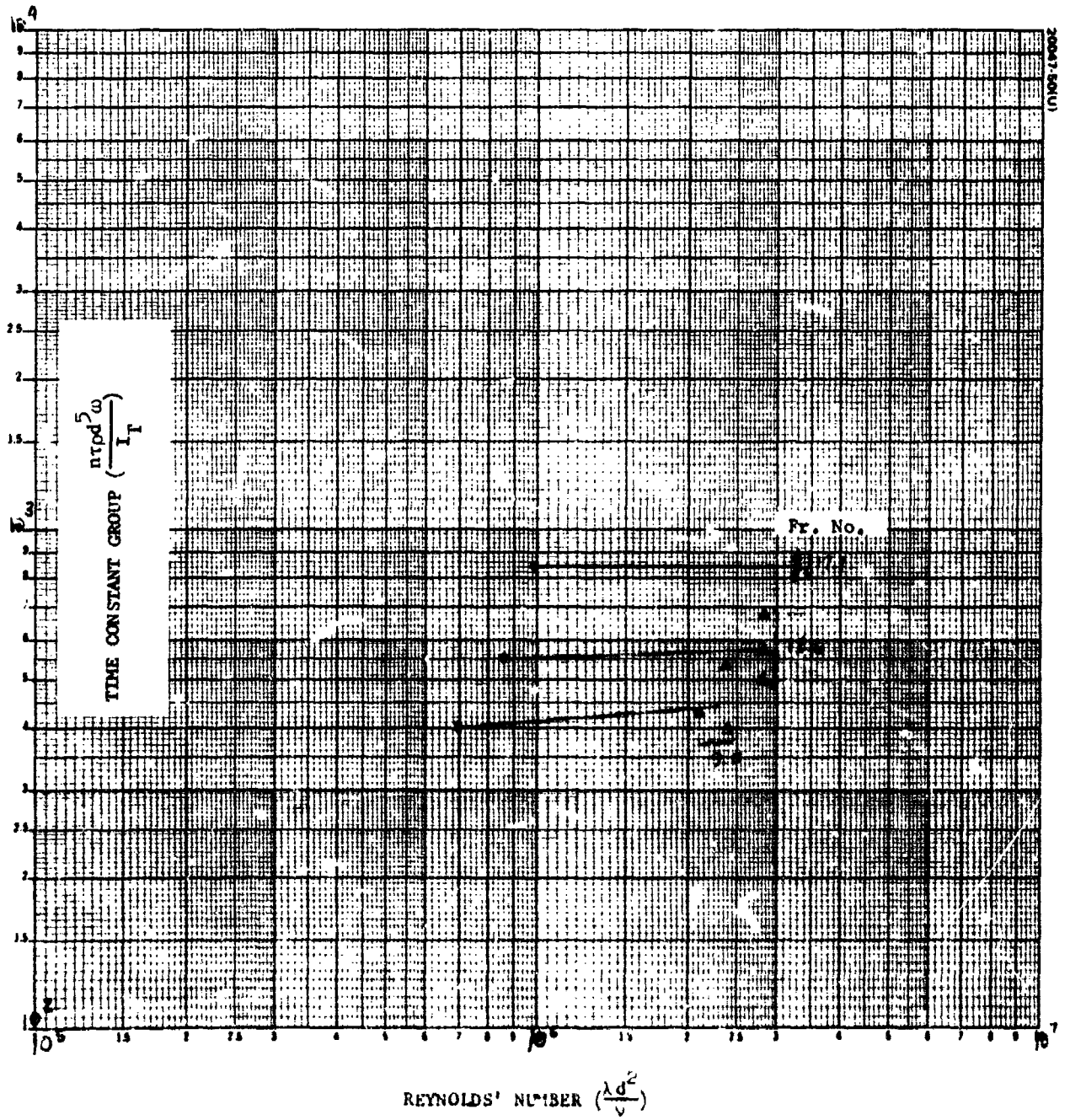
Figure 5-25. Comparative Energy Groups for Various Fraction Fills of Conispherical Tank ($\sigma = 0.1$)

The figure shows a log-log plot with:
- Y-axis: ENERGY GROUP $\left(\dfrac{\dot{E}}{n\rho d^5 \omega^3 \theta^2}\right)$
- X-axis: REYNOLDS' NUMBER $\left(\dfrac{\lambda d^2}{\nu}\right)$

Note: Data plotted from maximum Froude number

Figure axis labels: TIME CONSTANT GROUP $\left(\frac{n\tau\rho d^5 \omega}{I_T}\right)$, REYNOLDS' NUMBER $\left(\frac{\lambda d^2}{\nu}\right)$, Fr. No.

a) Time Constant Group Versus Reynolds Number

Figure 5-26. Phase III Spherical Tank Fuel Sloshing at 66 Percent Fraction Fill (σ 0.1)
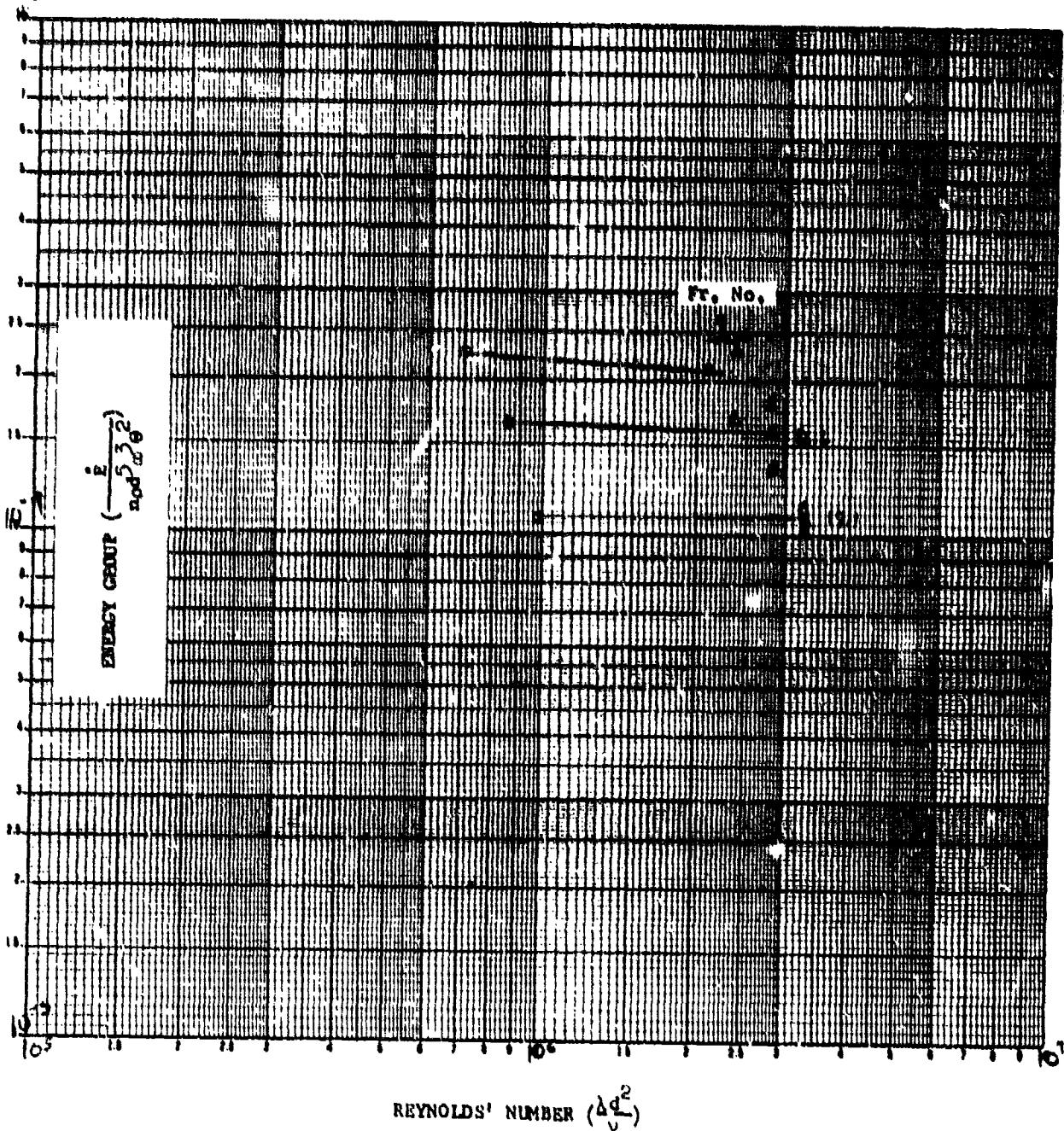
REYNOLDS' NUMBER $(\frac{\Delta d^2}{\nu})$

b) Energy Group Versus Reynolds Number

Figure 5-26 (continued). Phase III Spherical Tank Fuel Sloshing at 66 Percent Fraction Fill ($\sigma = 0.1$)

5-65

6. ZERO G EXTRAPOLATION AND FLIGHT EXPERIENCE

The substance of the laboratory test program is to arrive at estimated energy dissipation rates that are representative of the actual conditions in the 0 g scaling. Early analytical attempts were thwarted by the modeling complexities of the fluid dynamic motion. Based on the success of the ATS V heat pipe tests it was appreciated that a 0 g test condition could be obtained in the laboratory; however, there was no prior knowledge at which test spin speed the 0 g condition would be reached in the fuel slosh program. As has been seen in the previous section, at $\sigma = 0.335$ 0 g convergence is unquestionably a part of the data. At $\sigma = 0.1$ there is some question as whether a 0 g condition was obtained; yet lacking an unambiguous convergence signature it is still possible to establish a lower bound on the flight dedamping time constant.

The following discussion reviews the 0 g extrapolation for both Intelsat IV and HS-318, then reviews the flight confirmation of Intelsat IV. It finally uses the combined test and flight experience to scale $\dot{E}$ with σ.

6.1 INTELSAT IV FLIGHT PREDICTIONS

The dimensionless time constant group curves of Section 5.3 can be used directly to project the results to space. The procedure for 0 g scaling is the following:

1) Determine the equivalent flight Reynolds number for the flight vehicle. This may be a range of Reynolds number since both the spin speed and inertia ratio often change as a function of time.

2) Compute the time constant group coefficient for the flight vehicle, i.e., evaluate the function $I_t/n\rho \, d^5 \omega_s$. Again this value may vary as ω_s is often not constant.

3) Refer to the fraction fill curve or curves of interest and locate the flight Reynolds number (or range of numbers). Determine the value or range of values of the time constant group at the maximum Froude number curve plotted.

4) Multiply the value or values in (3) by the value obtained in (2). This then is the equivalent dedamper time constant. Due to the scatter in the data and the possible range of Reynolds number the projected flight time constant will turn out to be a band of values.

As a precaution it should be pointed out that it has been assumed that test data exist at the flight inertia ratio. No model for σ scaling presently exist so the test data are highly specialized at this time. It has been assumed that the propellant is equally distributed in the tanks. This assumption can be altered in step (2) if, for example, two tanks have 75 percent fill and the other two have 66 percent fill, the time constants can be separately determined using the above procedure, and the resulting values reciprocally added to determine the composite dedamper time constant.

In the case of Intelsat IV, the following evaluation is made. Table 6-1 lists the required spacecraft parameters for determining the dedamping time constant at the start of synchronous orbit operation.

TABLE 6-1. INTELSAT IV FLIGHT PARAMETERS

Parameter	Value
I_T	515 slug-ft^2
σ	0.355
ω_s	51.5 rpm
d	1.44 feet
ρ	1.94 slug-ft^3
n	4
FF	75 percent (initial load, 300 pounds)
θ	< 2 degrees
γ	10^{-5} ft^2/sec (hydrazine)

1) The equivalent flight Reynolds' number is first computed as follows:

$$\text{Reynolds' No.} = \frac{\lambda d^2}{\gamma} = \frac{(1 - \sigma)\omega_s d^2}{\gamma}$$

$$= \frac{(1 - 0.335)(5.4)(1.44)^2}{10^{-5}} = 7.2 \times 10^5$$

2) The time constant is now computed using the following
   relationship

$$\tau = k \frac{I_T}{n\rho d^5 \omega_s}$$

where k is the specific time constant group number obtained
from the curve. The expression $I_T/n\, d^5 \omega_s$ is evaluated and is
given as

$$\frac{I_T}{n\rho d^5 \omega_s} = \frac{515}{4 \times 1.94 \times 1.44^5 \times 5.4} = 2.0 \text{ sec}$$

Thus, for Intelsat IV synchronous orbit condition, merely
doubling the group number yields the expected time constant
for the fuel slosh.

3) For 75 percent fraction fill refer to Figure 5-5a. At the
   maximum Froude number of 17.6 the time constant group
   levels range between 70 and 110.

4) Multiplying 2 seconds times the above levels yields an estimated
   time constant of 140 to 220 seconds.

The other fraction fills are evaluated in the same manner just
described. The resulting estimates of the dedamping time constant versus
fraction fill is given in Figure 6-1. Here both the conisphere and sphere
results are coplotted subject to the four tanks, equal load assumption.

6.2 HS-318 FLIGHT PREDICTIONS

As has been noted in Section 5.5 the $\sigma = 0.1$ information forms an
incomplete set of data; however, it is sufficient to bound the flight time con-
stants. Also, the time constant group levels at the maximum Froude number
must be used since the zero g convergence has not been reached.

For HS-318 the flight Reynolds number is about 1.1×10^6. The time
constant group parameter (Step 2) is about 8.7 seconds. From the appropri-
ate fraction fill curves of Section 5.5, the projected flight dedamper time
constants are computed and plotted in Figure 6-2.

In comparing Figures 6-1 and 6-2 it is noted at the worse fraction
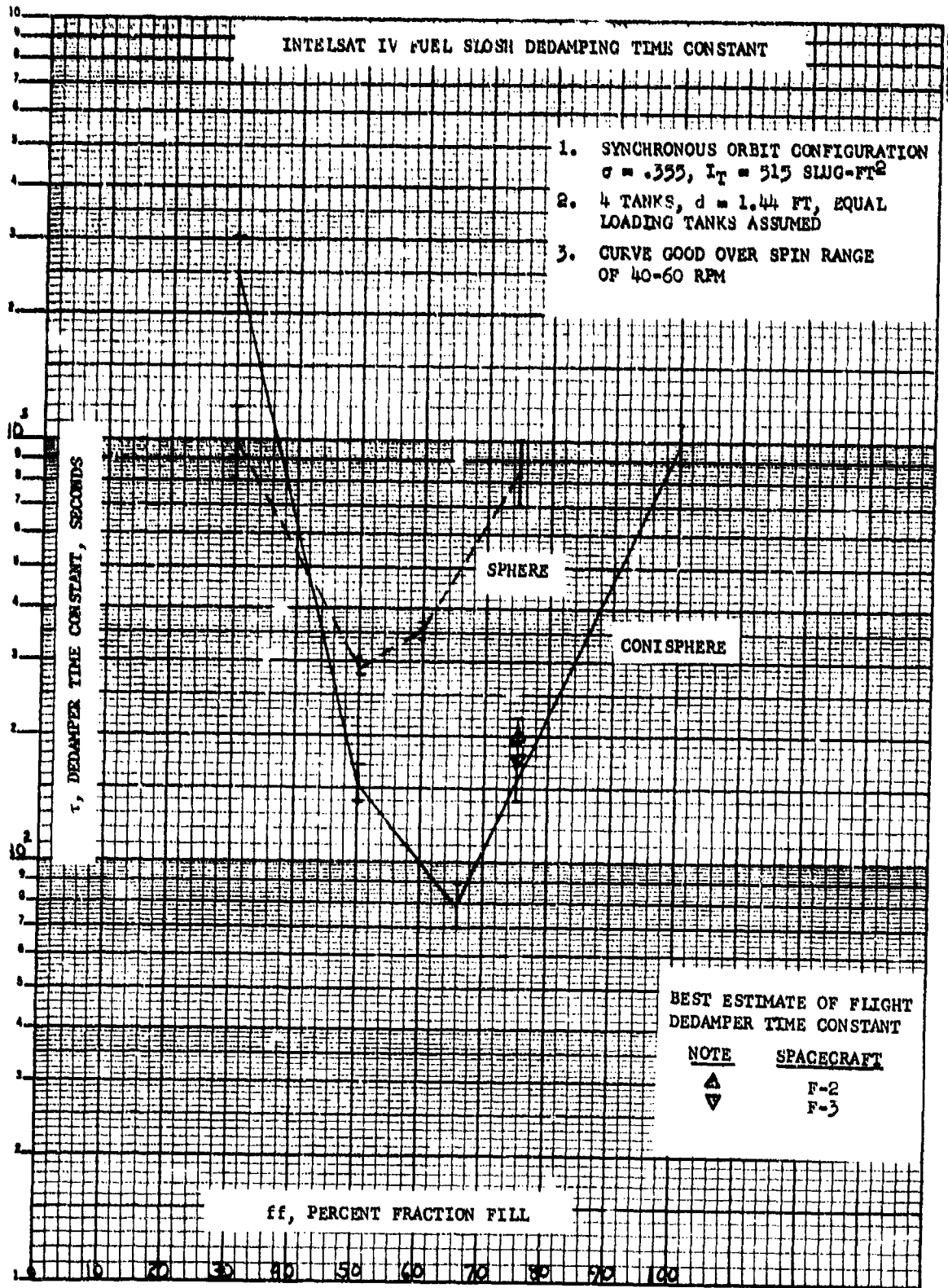fill, viz 66 percent, the Intelsat IV dedamping is nearly 60 times worse than
HS-318.

6-3

Figure 6-1.   Intelsat IV Fuel Slosh Dedamping Time Constant
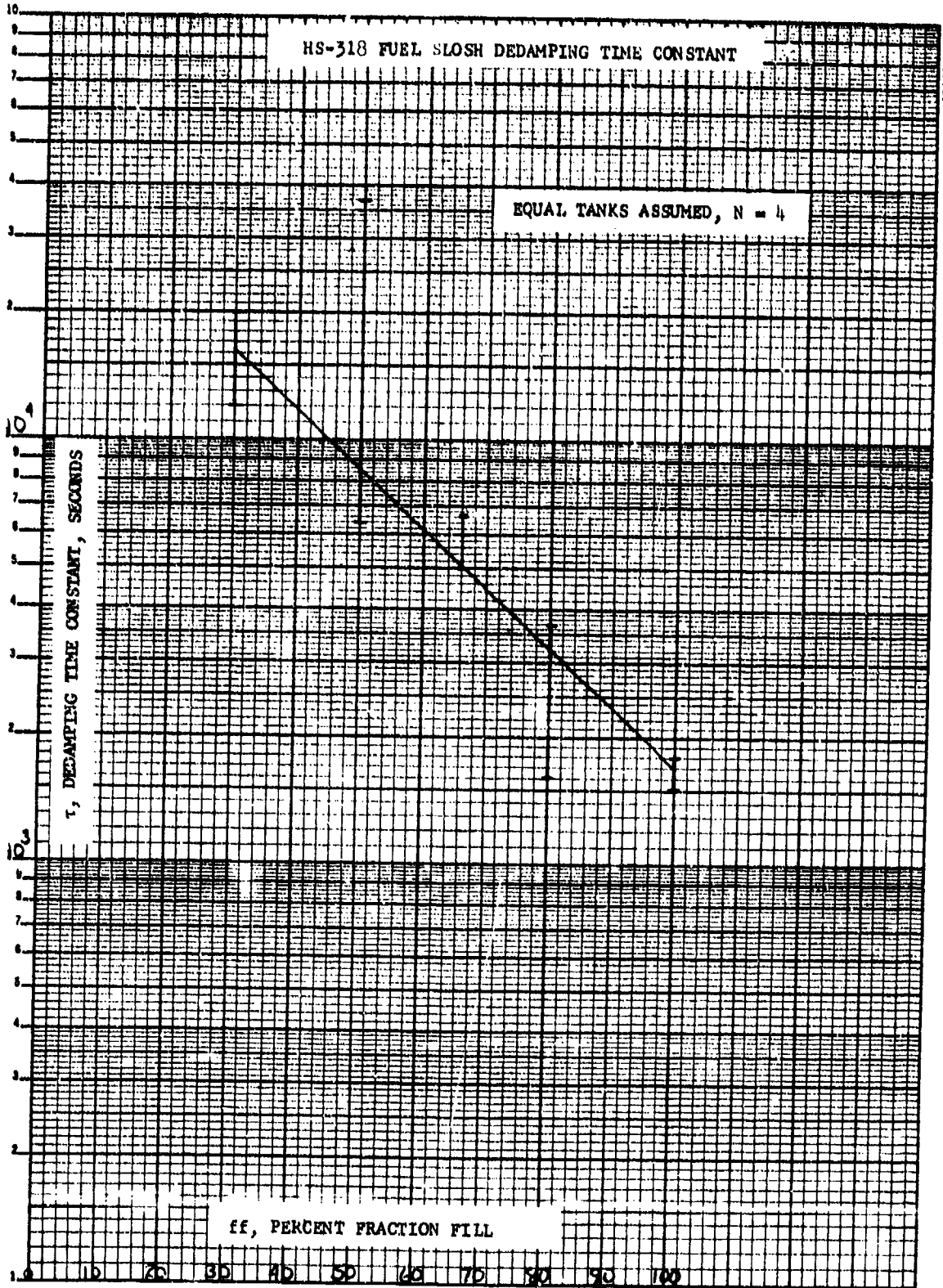
Figure 6-2. HS-318 Fuel Slosh Dedamping Time Constant

6.3 INTELSAT IV FLIGHT DATA

The best estimate for the flight dedamping time constant has recently been obtained from the F-3 launch for the synchronous orbit condition and F-4 in the transfer orbit condition. Following injection into synchronous orbit, a special dedamper test was conducted on the F-3 vehicle. The objective of the test was to determine if the time constant obtained from the F-2 launch was correct. As reported in Reference 29 following apogee motor fire a short time span of about 40 seconds existed during which the platform was counter-rotating at 4 rpm and the nutation angle was observed to remain constant. The conclusion arrived at was that the rotational effect had sufficiently detuned the dampers such that the presence of the dedamper could be noted. Postlaunch analysis concluded, as reported in the above reference that the best estimate of the dedamper time was about 200 seconds. However, substantial uncertainty existed in that estimate since the nutation signal was only observed for a fraction of a time constant. In fact, within the accuracy of the data the spacecraft could have been diverging with a very long time constant.

Subsequent to the F-2 launch and the determination of the 200 second dedamper, the third phase fuel slosh testing had taken place. The results of these tests were in agreement with the F-2 data — notwithstanding the large uncertainty in the F-2 data point.

If, in fact, the dedamper magnitude at 75 percent fraction fill agreed well with the laboratory test results at the same mass fraction, then it is reasonable to assume that the projected time constants at other fraction fills would also be correct. As seen in Figure 6-1, the initial mass fraction is not the worst case and as fuel is deleted in the course of normal on station maneuvering the region of maximum energy dissipation would be traversed. Operationally, then it may be required to adjust the spacecraft spin speed to maximize the damper performance during that portion of the mission. Once the fuel load is below 50 percent, the necessity to control spin speed can be relaxed.

Thus, to validate both the F-2 data point and the test results, a test on F-3 was planned to counterspin to 4 rpm, induce nutation, and monitor the time constant for an extended period of time — at least long enough to ensure reasonable accuracy in the data reduction. In light of the possibility of being unstable at this platform rate, the test was begun at the nominal despun condition. A time constant was established by manually inducing nutation. The resultant value thus served as a reference point from which to proceed. The next measurement was made at a counterspin rate of 2 rpm. This value was selected along with 3 rpm as desired intermediary reference points to determine whether or not it would be required to go to 4 rpm. As it turned out, the 4 rpm case was run. As expected, the dedamper could be measured quite accurately — at least as accurate as the estimate on the composite damper time constant, i.e., about 10 percent.

The incremental increase in the net damping time constant starting despun and progressing to 4 rpm with checks at 2 and 3 rpm are, in sequential order, 42 ±3, 67 ±4, 167 ±5, and 1150 ±50 seconds. The respective composite damper time constants are estimated to be 40 ±2, 62 ±2, 104 ±4, and 156 $^{+14}_{-4}$ seconds. The computed dedamping time constant is about 175 ±15 seconds (F-3 flight nutation data have not been documented).

The best estimates of the F-2 and F-3 flight dedamping time constants have been plotted on Figure 6-1. As seen, the agreement is quite good and well within the test and flight data uncertainties (on the order of 10 percent).

In the transfer orbit, the inertia ratio is 0.278. The flight data for F-2 gave an estimated value of 28 $^{+\infty}_{-20}$ minutes; the F-3 dedamper was estimated to be 12 $^{+10}_{-5}$ minutes. Recently, the F-4 launch provided a much better value of the transfer orbit dedamper. A test was conducted similar in scope to the one described previously of the F-3 synchronous orbit condition. By forward spinning the platform to 4 rpm and inducing nutation the net time was determined to be 594 seconds. The best estimate for the composite damper time constant was 290 seconds. The resultant dedamper is therefore estimated to be about 560 seconds. The uncertainty on this number is estimated to be about 10 percent.

With the additional transfer orbit time constant data it is now possible to combine this data with the test data at 0.1 and 0.355 inertia ratio. and investigate the functional dependence of $\dot{E}$ on the inertia ratio.

6.4 FIRST ATTEMPT AT INERTIA RATIO SCALING (75 PERCENT FRACTION FILL)

With the recent results of the Intelsat IV F-4 transfer orbit dedamper test, a good estimate of the fuel sloshing at $\sigma = 0.278$ exists. It is therefore, possible to combine this result with the $\sigma = 0.355$ and $\sigma = 0.1$ test and flight data in a first attempt to scale $\dot{E}$ with σ.

In the following analysis, the time constant data have been normalized to a vehicle with a transverse moment of inertia of 515 slug-ft^2 (i.e., ocrresponding to Intelsat IV in the synchronous orbit). Thus, the transverse orbit time constant of 560 seconds is scaled by (515/830). At $\sigma = 0.1$ the time constant has a great deal of uncertainty primarily due to the lack of 0 g convergence. At best, then, the test data serve as an upper bound on the energy group. It is expected that the actual 0 g energy group would fall

below the value used here. The following summarizes the data used in the inertial ratio scaling:

σ	τ, Seconds	τ Group	$\dot{E}$ Group
0.355	175	87.5	2.62×10^{-3}
0.278	350	175	1.15×10^{-3}
0.10	1000	500	1.8×10^{-4}

The time constant group and energy group numbers are plotted in Figures 6-3 and 6-4, respectively. The interesting curve here is the energy group, 6-4. The slope of the $\dot{E}$ cur   tween 0.278 and 0.355 is experimentally determined to be 3.3. If   curve is extrapolated back to $\sigma = 0.1$, it is seen that the test data lie substantially above the $\sigma = 0.1$ intercept of the $\sigma^{3.3}$ curve. As mentioned it was expected that the 0.1 test data would over estimate the actual 0 g condition. This discrepancy could be real, or alternately, due to extrapolation of the $\sigma^{3.3}$ curve, beyond the range of applicability. The primary objective of the phase IV test program is to obtain test data at $\sigma = 0.6$ and $\sigma = 1.1$. It is intended that these tests will establish the shape of the functional dependence of $\dot{E}$ versus inertia ratio.

It is fair to conclude that for inertia ratios near those of Intelsat IV the energy group is proportional to $\sigma^{3.3}$. Therefore, the associated time constant equation is the following:

$$\tau = \frac{I_t \sigma (1 - \sigma) \omega_{\cdot s}^2}{\dot{E}/\theta^2} \quad \alpha \quad \frac{I_t (1 - \sigma)}{n\rho d\omega_s^5 \sigma^{2.3}}$$

The constant of proportionality is dependent on Reynolds number, fraction fill, tank shape, and the other geometrical ratios. In the case of Intelsat IV in the two orbital conditions (i.e., constant fraction fill), the time constant scales as
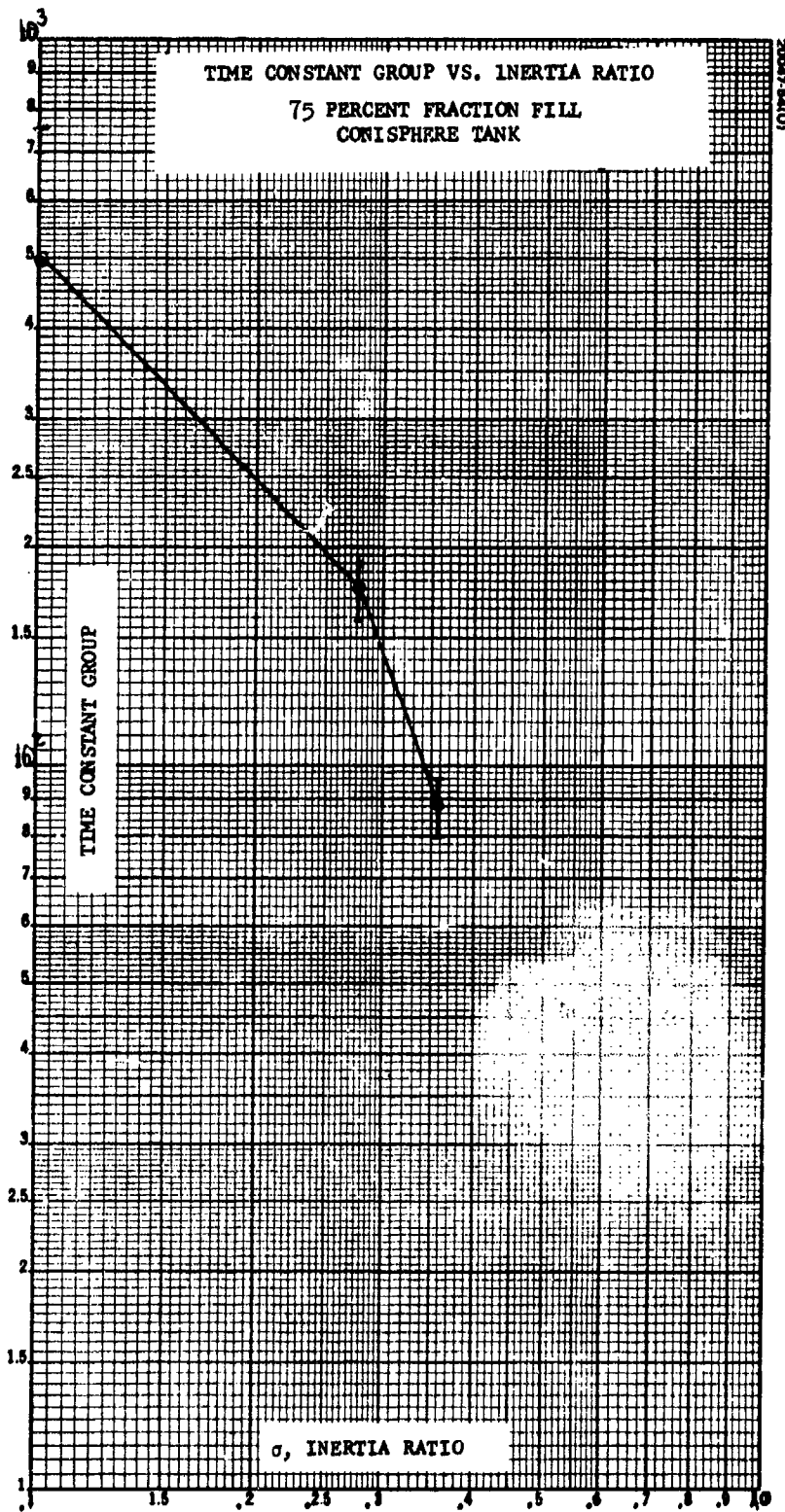
$$\tau \alpha \frac{I_t (1 - \sigma)}{\sigma^{2.3}}$$

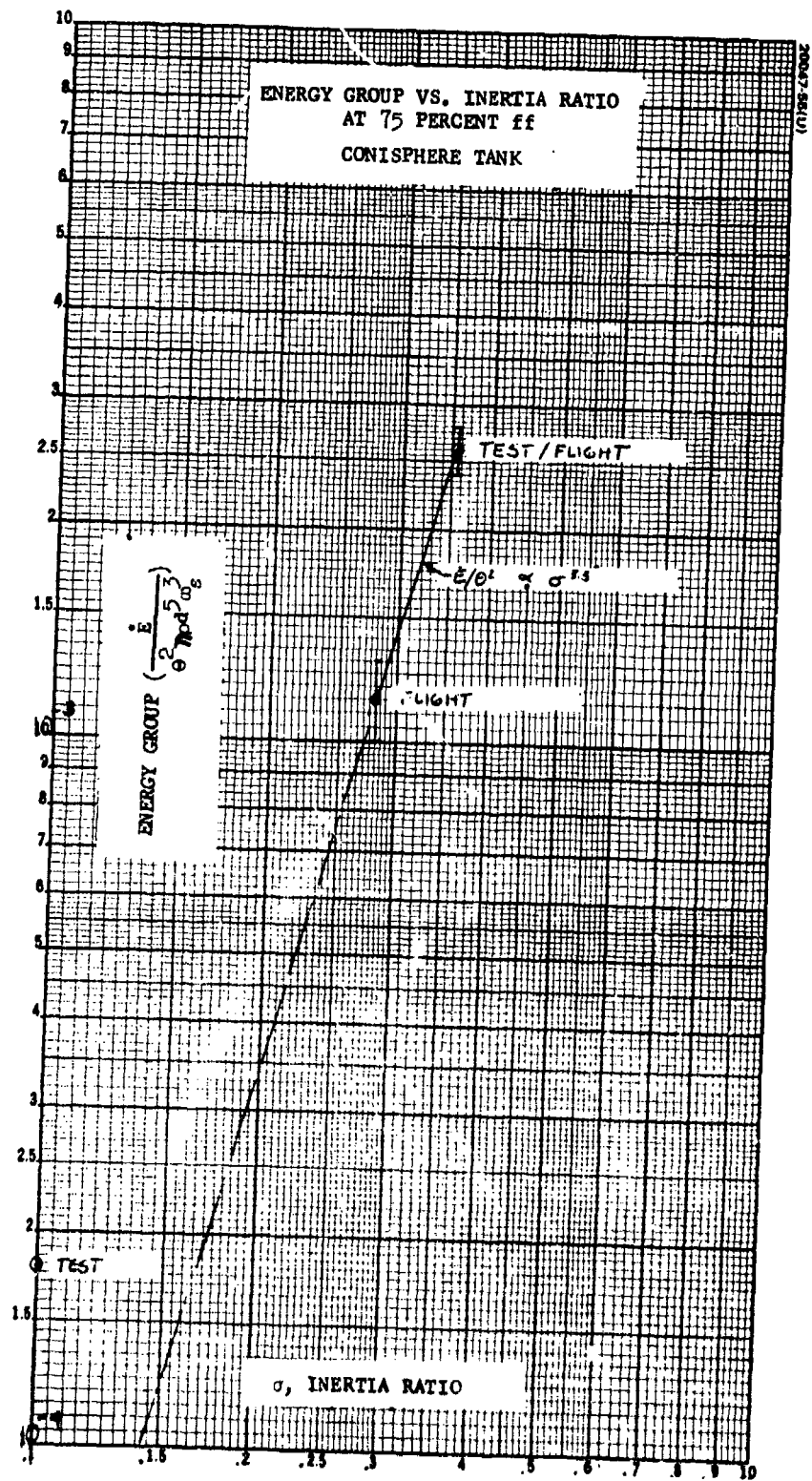Figure 6-3. Time Constant Group Versus Inertia Ratio

6-9

Figure 6-4. Energy Group Versus Inertia Ratio

7. CONCLUSIONS AND FUTURE PLANS

The test program to date has investigated the effect of fuel slosh on the nutation angle behavior of the Intelsat IV and HS-318 spacecraft. Test data have been obtained in laboratory conditions which closely approximate the space environment. Agreement between flight and laboratory observations has validated the empirical techniques employed.

General conclusions drawn from the testing to date are as follows:

1) The Williams fuel slosh model is invalid and underestimates the energy dissipation rates by nearly two orders of magnitude.

2) Fuel slosh dedamping time constants for Intelsat IV are on the order of a hundred seconds, while the time constants for HS-318 are on the order of thousands of seconds.

3) In the laboratory, gravity effects are significant at the nominal operating spin speeds for both Intelsat IV and HS-318. In the case of Intelsat IV, gravity masks the fuel slosh dissipation, making the dedamper appear less powerful than it really is. However, the test data do contain ah unambiguous 0 g convergence behavior which can be used to interpolate the test results to flight. In-orbit corroboration of the laboratory 0 g data supports these conclusions.

    For the HS-318 spacecraft, gravity has a different effect on the data. In the $\sigma = 0.1$ case, gravity effects tend to dominate nutational effects, making the data look worse than it is in space. While 0 g convergence was not reached at this inertia ratio, the data can be used to place a lower bound on the dedamper.

4) Phase I test data (old Culver City data) appear to contain all the results of Phase III tests plus an additional dissipator heretofore unrecognized. Therefore, the Phase I data are relegated to a lesser status than data obtained from the Phase II and III tests.

5)   Test data in the Phase II and III test series have proved to be repeatable and consistent.

6)   Peak dissipation occurs around 60 to 66 percent fraction fill for Intelsat IV and around 80 to 100 percent (with greater uncertainty) for HS-318.

7)   Energy dissipation in a spherical tank is on the same order as in a conispherical tank. Specifically, at $\sigma = 0.335$, the conisphere is about four times worse than the sphere at the worst fill fractions.

8)   Energy dissipation is dependent on Reynolds number for all fraction fills other than those near resonance or peak dissipation.

9)   At resonance, the energy dissipation rate has the form

$$E = K(\sigma, FF, S, d/R, z/R) \cdot n\rho d^5 \omega_s^3 \theta^2$$

where K is a function of the spacecraft geometrical parameters, i.e., roll-to-pitch ratio, fraction fill, shape, tank diameter to radial displacement, and tank axial displacement to radial displacement. The Phase I and III data, together with the Intelsat IV flight data support the d^5 dimensional scaling inherent in the above functional relationship.

10) The test and flight data have been combined at the 75 percent fraction fill to investigate the dependence of $\dot{E}$ on σ. The empirical functional dependence obtained suggests that $\dot{E} \propto \sigma^{3.3}$ Additional data at higher inertia ratios will prove or disprove this dependence.

11) Energy dissipation (at $\sigma = 0.35$) has two modes — a small nutation angle mode, $\theta_N < 2$ degrees, and a large nutation mode, $\theta_N > 2$ degrees.

It is now quite apparent that the fuel sloshing problem heretofore dealt within an analytic approach must be continued in a strongly experimental vein until sufficient data are generated to permit formulation of an empirical model which not only agrees with the test and flight data but also permits extrapolation to new spacecraft designs. The existing data can only be extended to a small class of vehicles which are closely similar to the Intelsat IV and HS-318 designs. In order to extend the usefulness of the data to designs substantially different from the existing ones, a Phase IV Test Plan is under way.

The primary objective of Phase IV is to investigate fuel slosh dissipation effects at inertias other than 0.1 and 0.35. The present plans call for values near 0.6 and 1.1. With the additional data, it will be possible to scale the fuel slosh time constants with σ and obtain a value which is hopefully valid to at least a factor of 2 accuracy.

APPENDIX A. PHASE I TEST DATA

The test results from the phase I program are presented here. The purpose of including the data in an Appendix has been discussed in Section 5.3.8. It has been suggested that these data not only contain the new information, which is believed to be the correct data, but also extra dissipation due to structural dedamper not correctly calibrated out of the data.

The data plotted here represent what is believed to be the best from Phase I. Several precursor comments are worth making with respect to the data.

Only two fluids were used during this series — water and a solution of glycerine and water. The latter solution is four times as viscous as water. Only one tank was used. This was decided after it was learned that the plexiglass tank itself contained structural dissipation on the same order as the fuel slosh. After establishing the tank superposition result, the plexiglass tank was removed and all subsequent tests conducted with the flight titanium tank. The tank was positioned in the flight orientation cone outboard ($\beta = 0$ degree to the old sloshers). Initially, the cone had been tipped down 23 degrees ($\beta = -23$ degrees) such that the fluid free surface, at 60 rpm, had the same geometrical position with respect to the cone as it would in space at the same spin rate. While the dissipation rate indicated some dependence on this angle, β, subsequent tests suggest the effect was more gravitational produced as opposed to a fluid dynamical origin. Since subsequent data in Phase II and III were obtained at high Froude numbers, on the order of 17, the free surface angle, α, closely approached the flight value of 90 degrees.

DISCUSSION OF THE DATA

Figure A-1 gives the basic test data time constant versus spin rate for the various fraction fills tested and the two fluids. In Figure A-1b it is seen that two sets of data are plotted for the 50 and 66 percent fraction fill case. The data correspond to both Culver City and El Segundo data. After the 50 percent runs, the vehicle was accidentally damaged and testing terminated for Phase I.
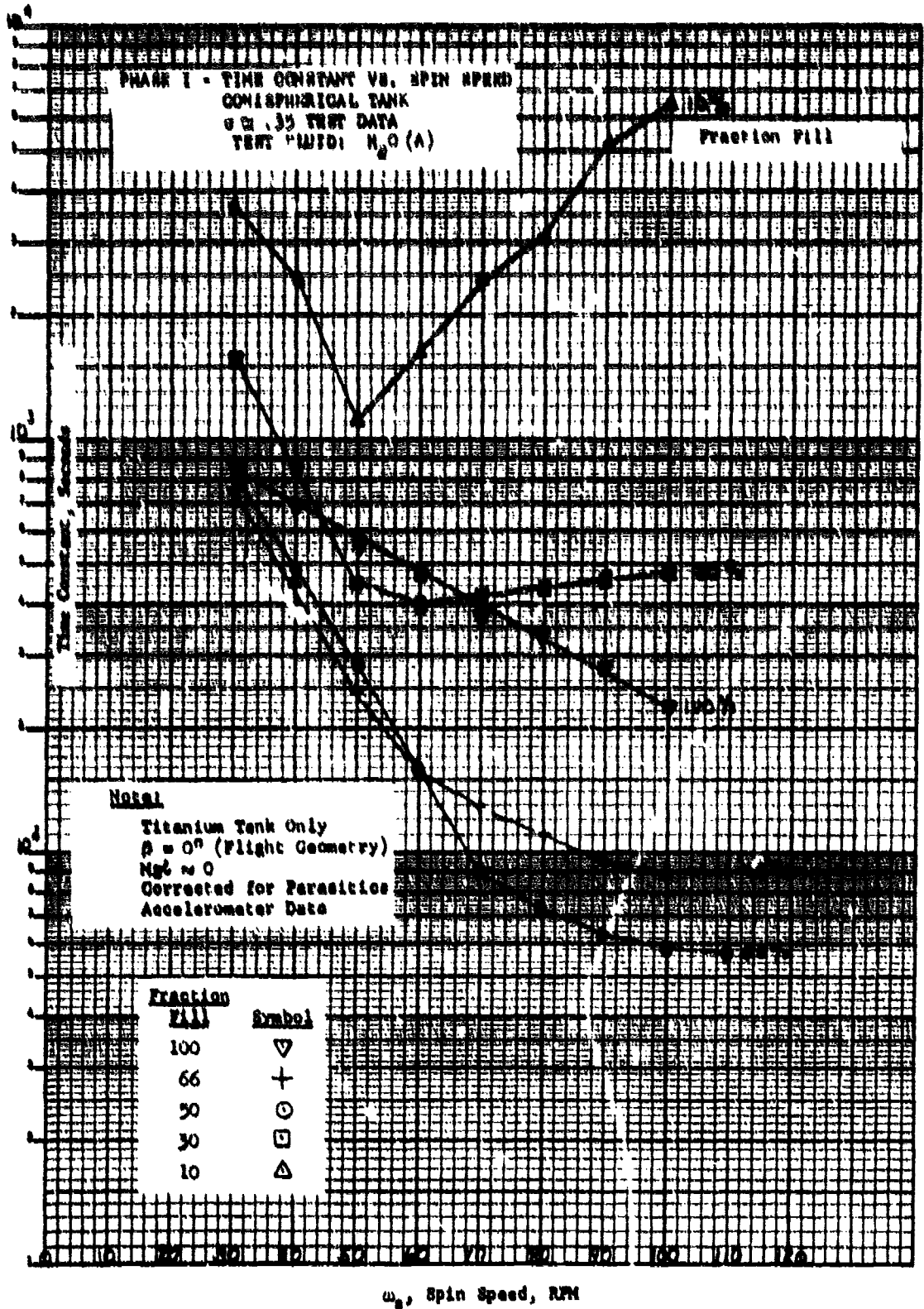
a) H_2O (A) Test Fluid

Figure A-1. Phase I Time Constant Versus Spin Speed for Conispherical Tank

A-2
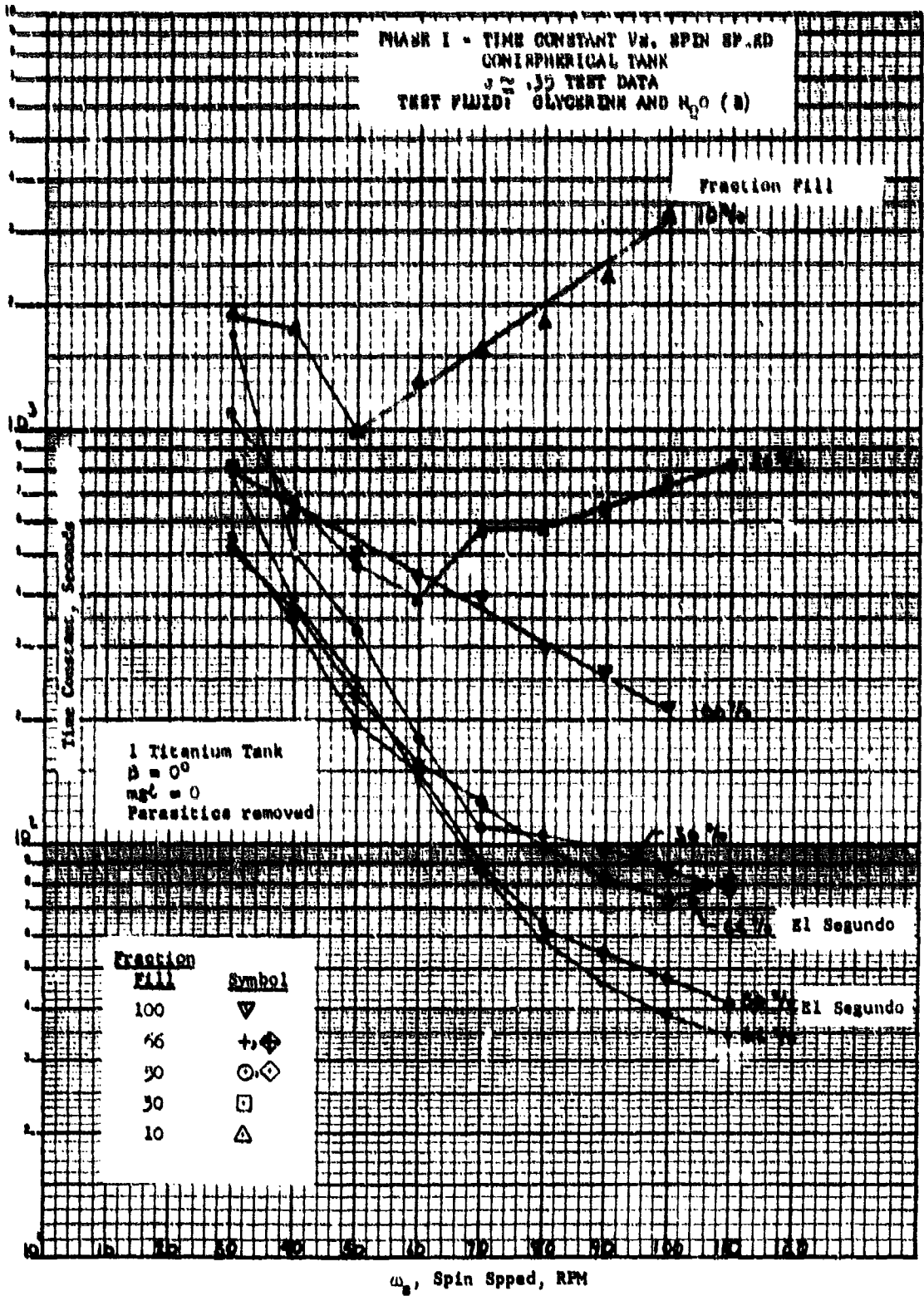
b) Glycerine and H_2O (B) Test Fluid

Figure A-1 (continued). Phase I Time Constant Versus Spin
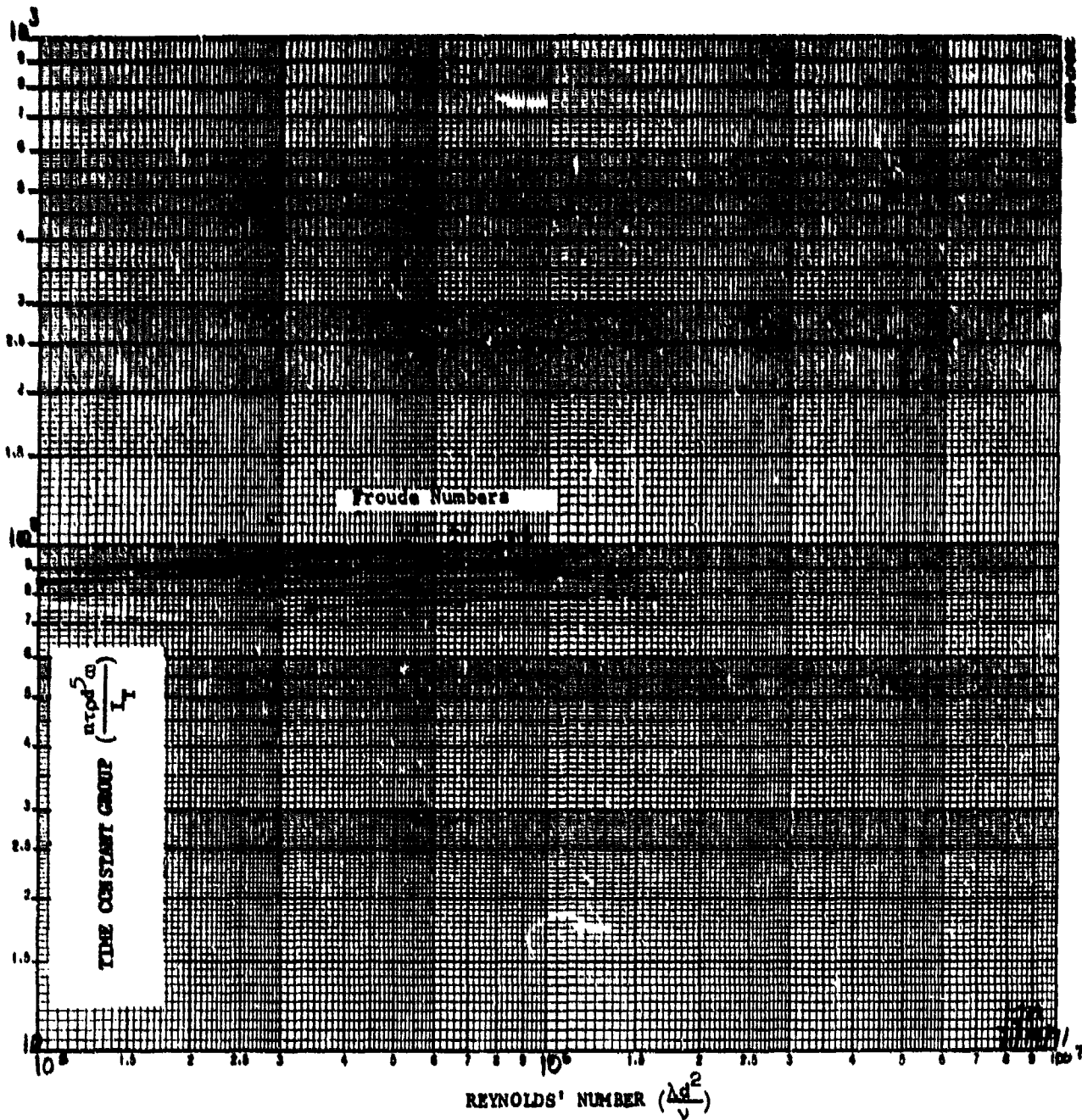Speed for Conispherical Tank

A-3

Figures A-2 through A-6 are the corresponding dimensionless time constant and energy groups for the appropriate fraction fills — 100, 66, 50, 30, and 10 percent.

Figure A-2 shows the 100 percent behavior. It is observed that the data has sizable scatter with Froude number. Apparently convergence has not been reached. The data also indicate no Reynolds number dependence. Both of the above behaviors are inconsistent with the Phase III results. The interpretation of these data is that the extra dedamper is masking the fuel slosh motion and concealing the Reynolds number dependence and Froude number convergence.

Figure A-3, the time constant group, for 66 percent fraction fill, indicates the discrepancy between the Culver City and El Segundo glycerine data. While the curves are drawn to the average value of the two data points, it is believed, in light of the phase III data, that the Culver City data are the more correct. The reasoning is associated primarily with the fact that Phase III 66 percent shows virtually no Reynolds number dependence of the test range of Reynolds number. The reason for the data discrepancy is not known for sure; however, it could be associated with the suspected parasitic damper.

A similar discrepancy is seen in A-4 for the 50 percent case. However, in light of the new data it appears that the best information would correspond to the average of the two glycerine tests. Using the average value of the data, the resulting curves show a weak Reynolds number dependence and a high Froude number convergence.

Thirty percent and 10 percent fraction fill cases, Figures A-5 and A-6, show the behavior as seen in Phase III. As the Froude number increases, the time constant group also increases, i.e., the energy dissipation rate decreases. In A-5 it appears that 0 g convergence has not been reached. This may be a consequence of having only two test fluids. A third fluid would most likely result in a Reynolds number dependence similar to the Phase III 30 percent test, i.e., a parabolic curve. The apparent peaking of the energy dissipation at 1.7 Froude number for both 30 and 10 percent would appear to be a gravity related phenomena as opposed to a real fluid resonance which would be present in space.

Froude Numbers

TIME CONSTANT GROUP $\left(\frac{\mu_T \rho d^5 \omega}{I_T}\right)$

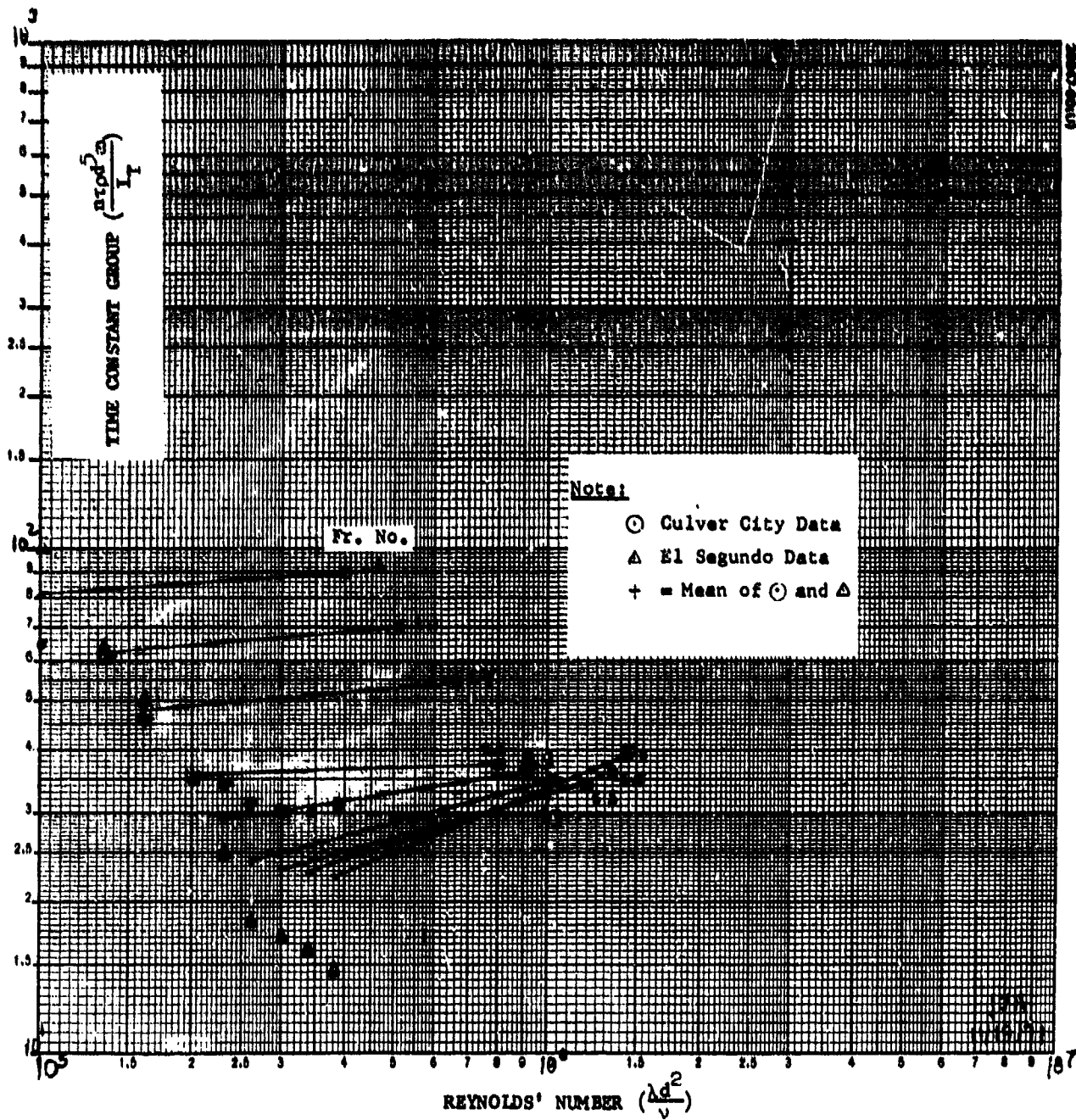REYNOLDS' NUMBER $\left(\frac{\lambda d^2}{\nu}\right)$

a) Time Constant Group Versus Reynolds Number

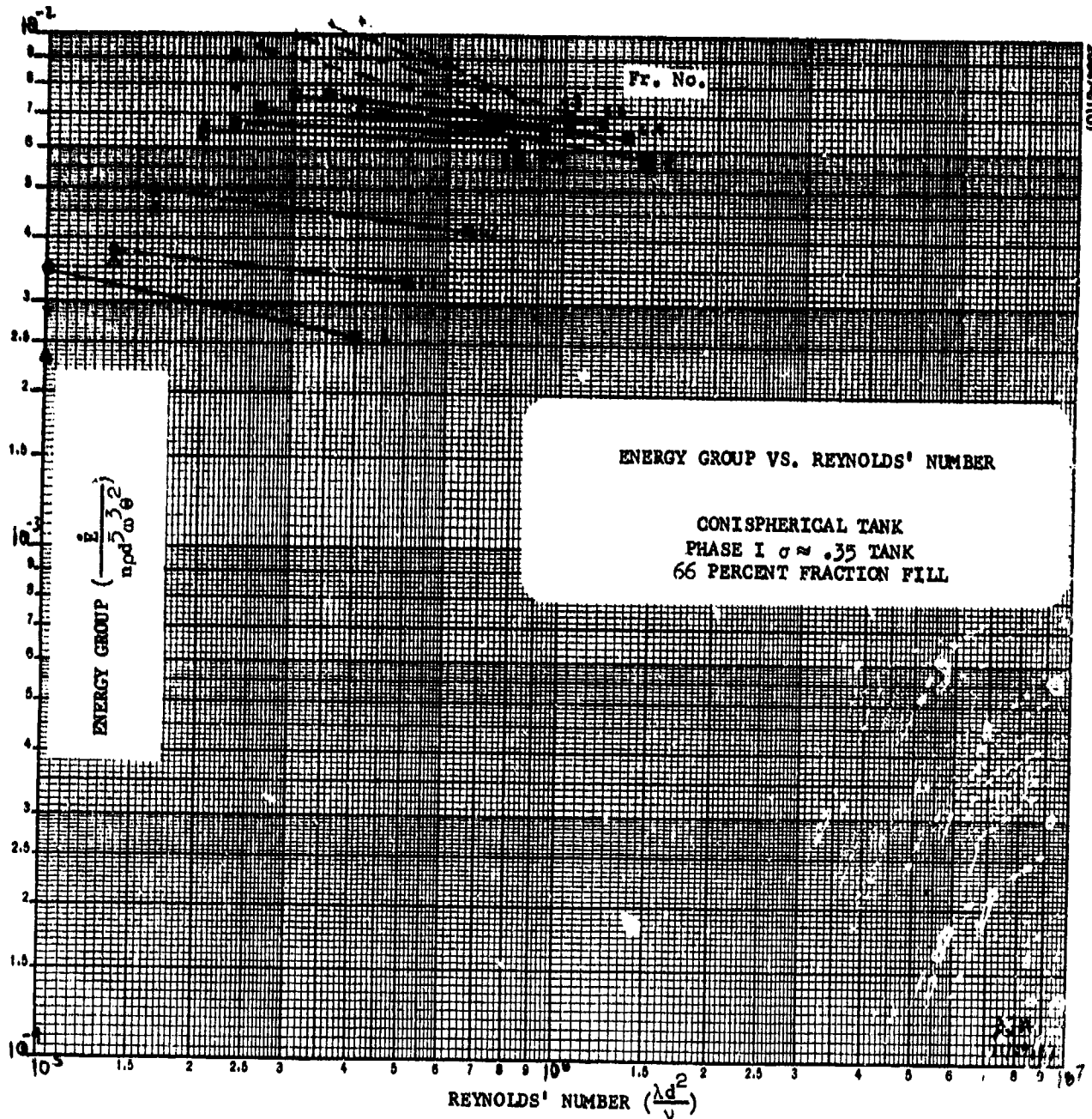Figure A-2. Phase I Conispherical Tank Fuel Sloshing at 100 Percent Fraction Fill ($\sigma = 0.35$)
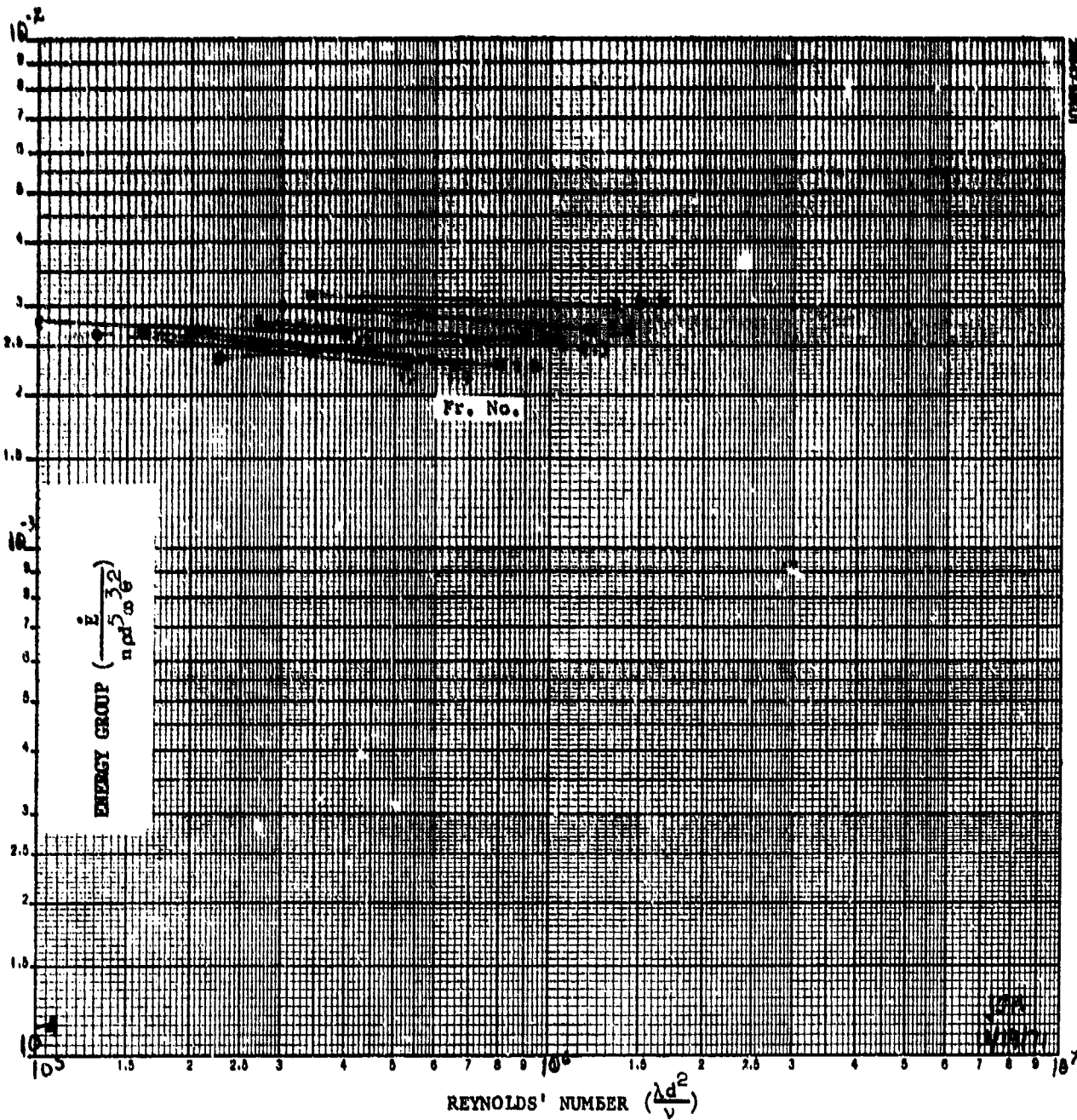
b) Energy Group Versus Reynolds Number

Figure A-2 (continued). Phase I Conispherical Tank Fuel Sloshing at
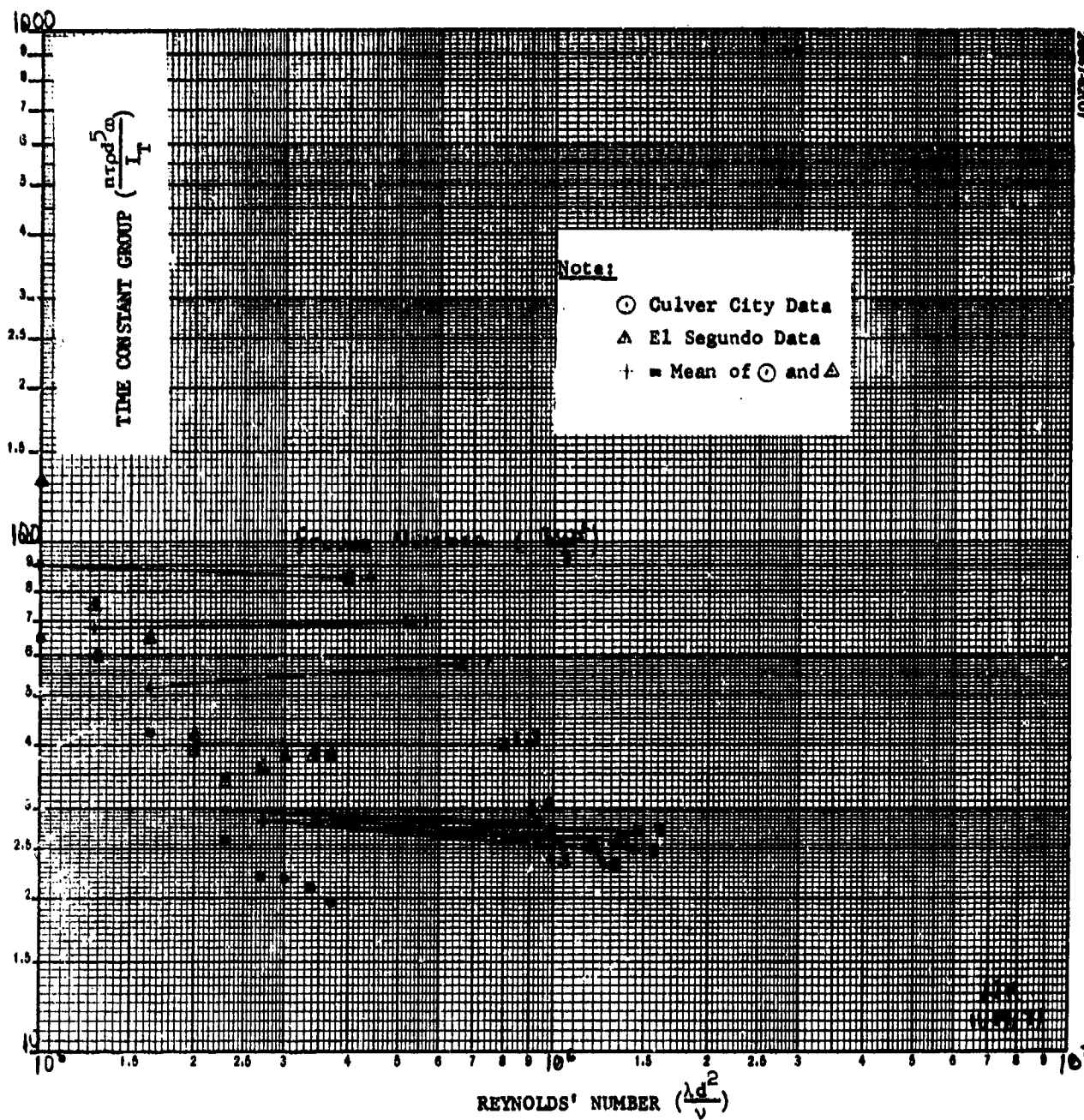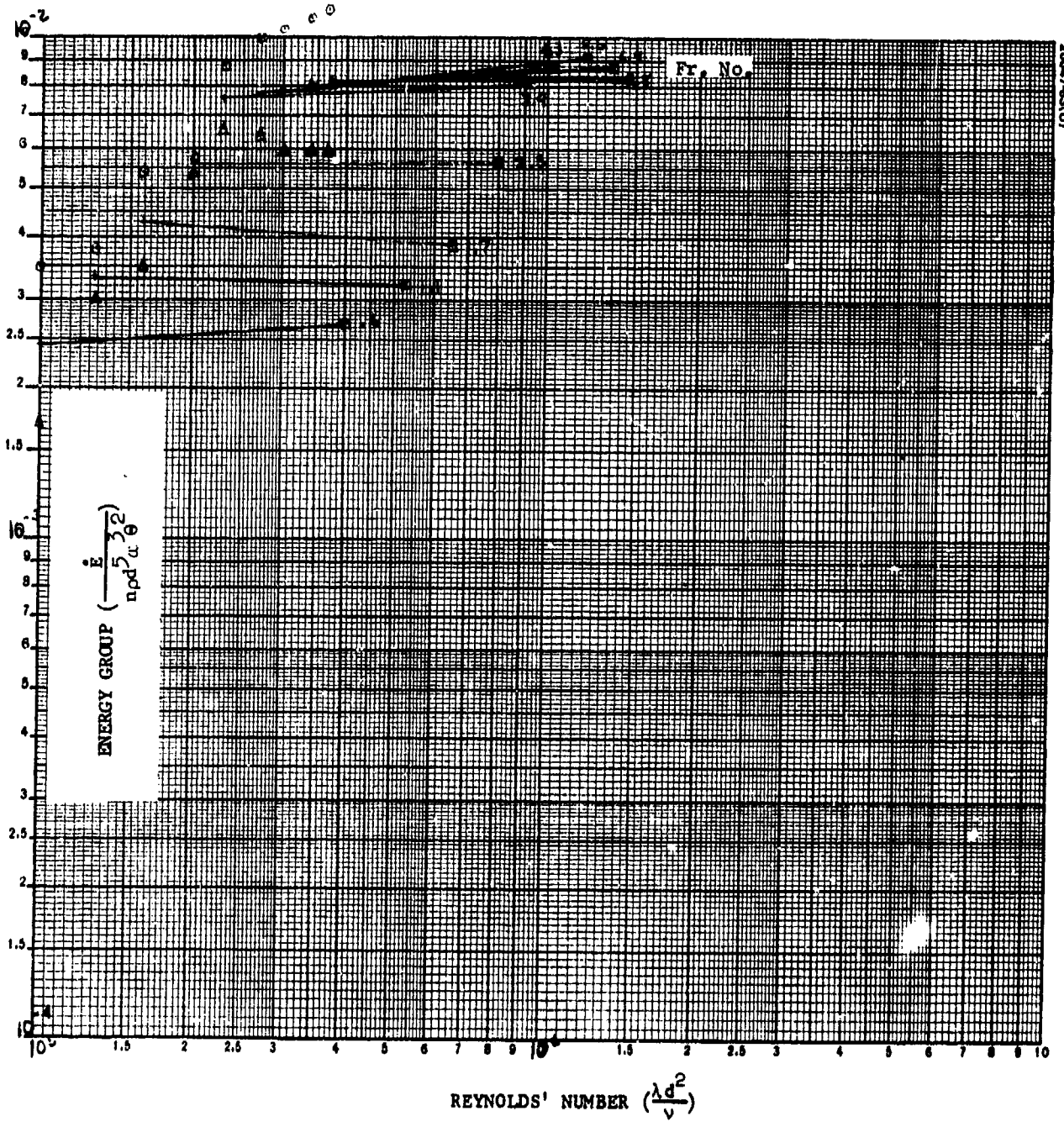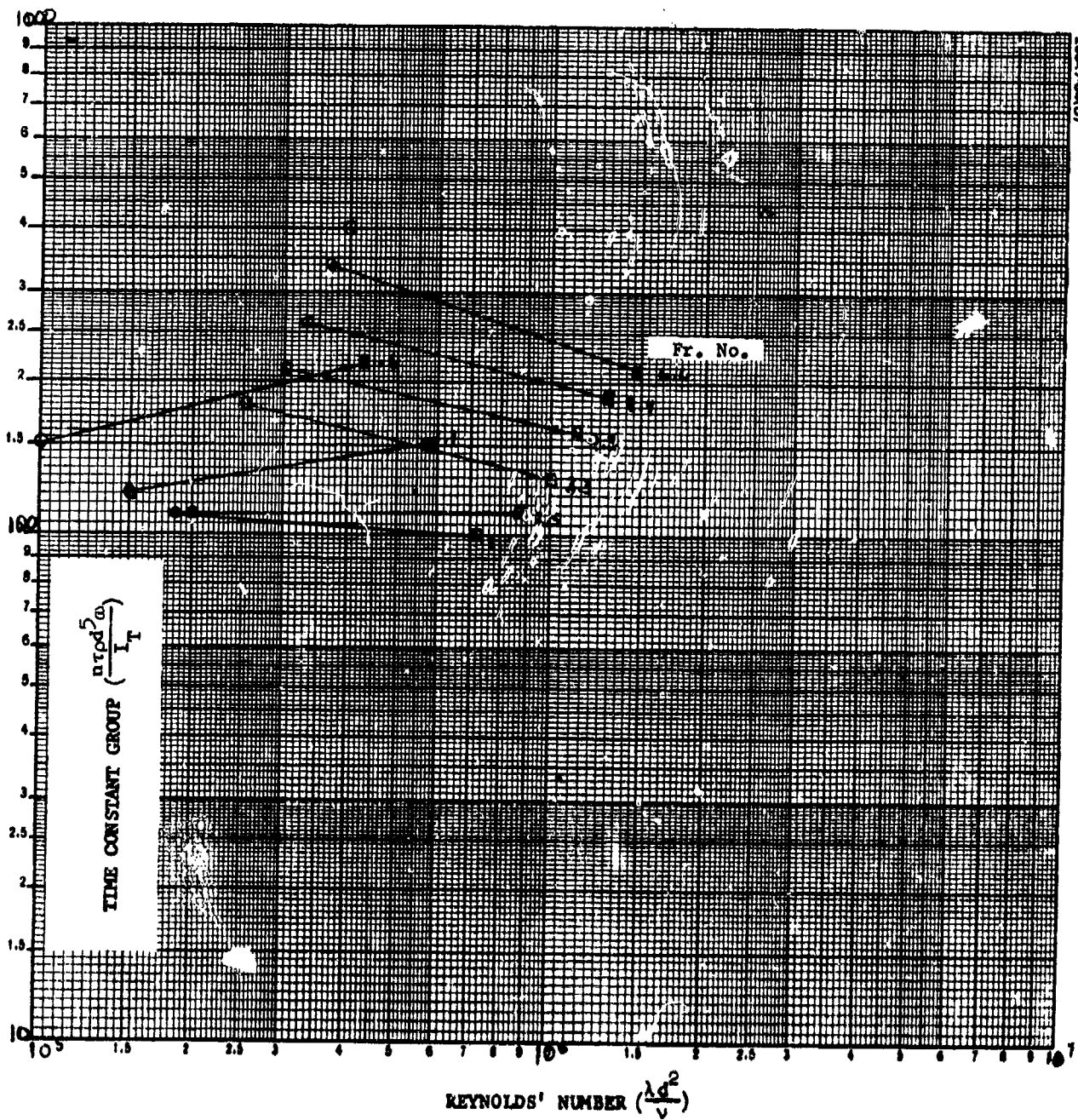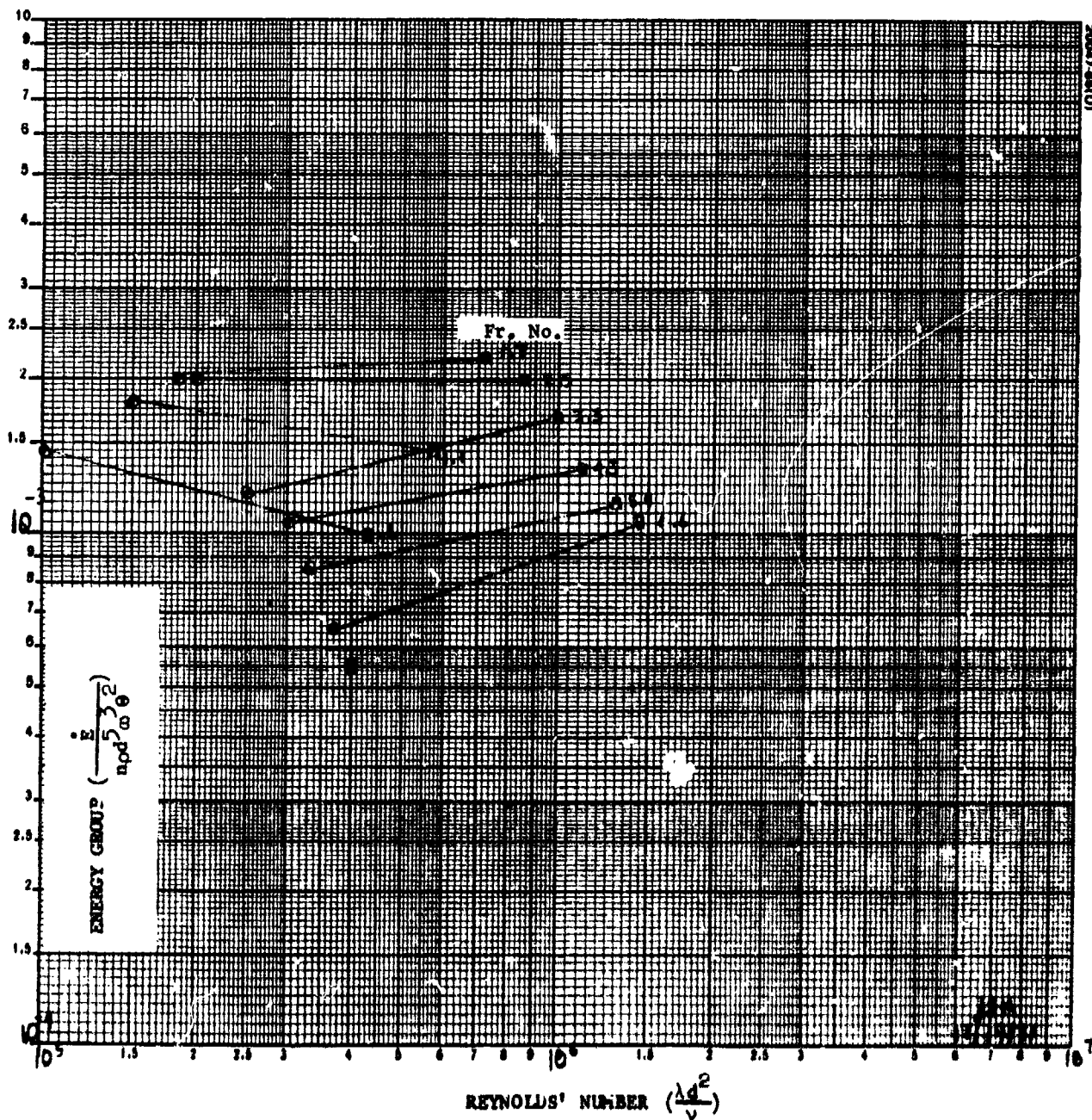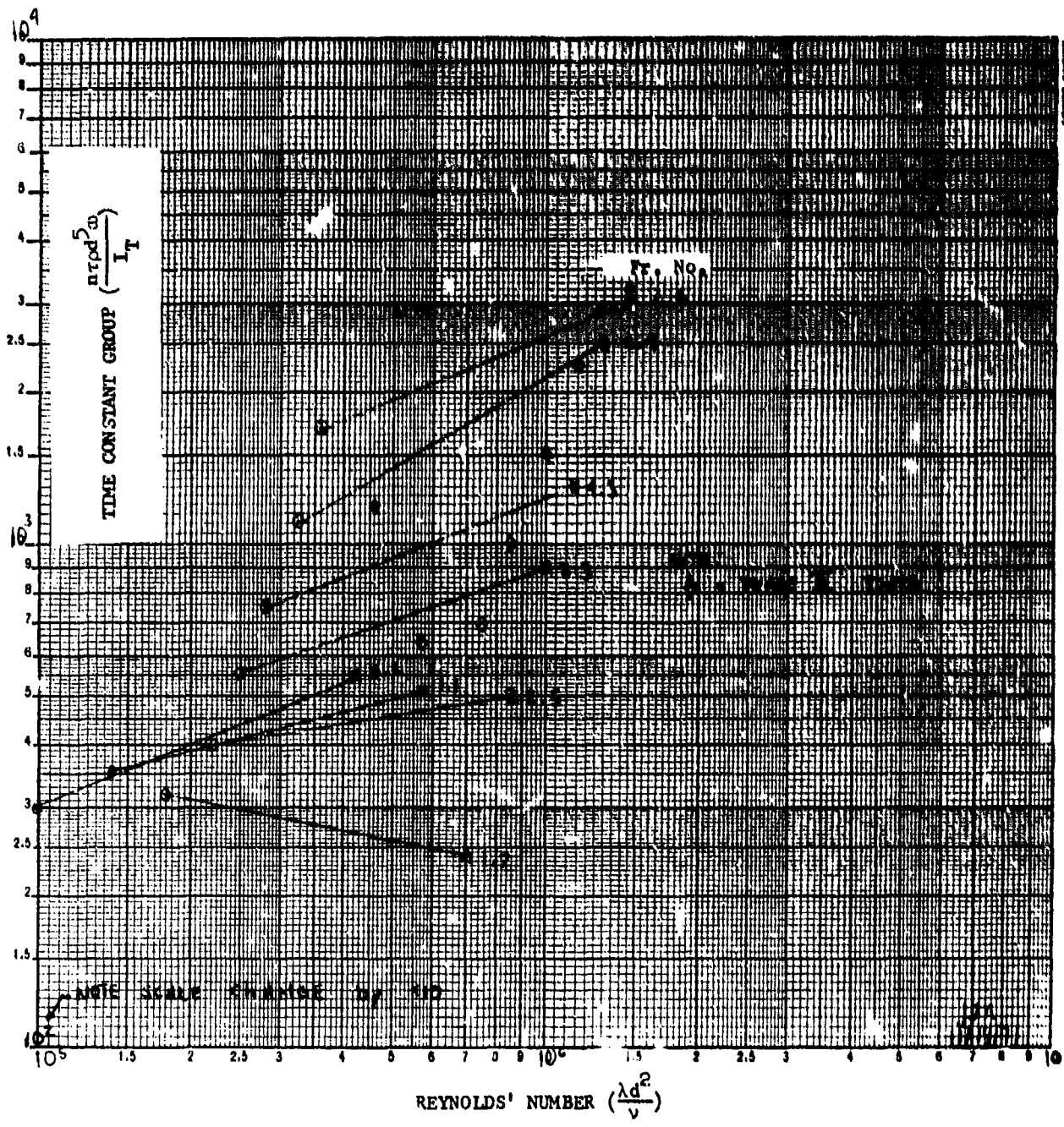100 Percent Fraction Fill ($\sigma = 0.35$)

a) Time Constant Group Versus Reynolds Number

Figure A-3. Phase 1 Conispherical Tank Fuel Sloshing at 66 Percent
Fraction Fill ($\sigma = 0.35$)

b) Energy Group Versus Reynolds Number

Figure A-3 (continued). Phase I Conispherical Tank Fuel Sloshing at 66 Percent Fraction Fill (σ = 0.35)

A-8

a) Time Constant Group Versus Reynolds Number

Figure A-4. Phase I Conispherical Tank Fuel Sloshing at 50 Percent Fraction Fill (σ = 0.35)
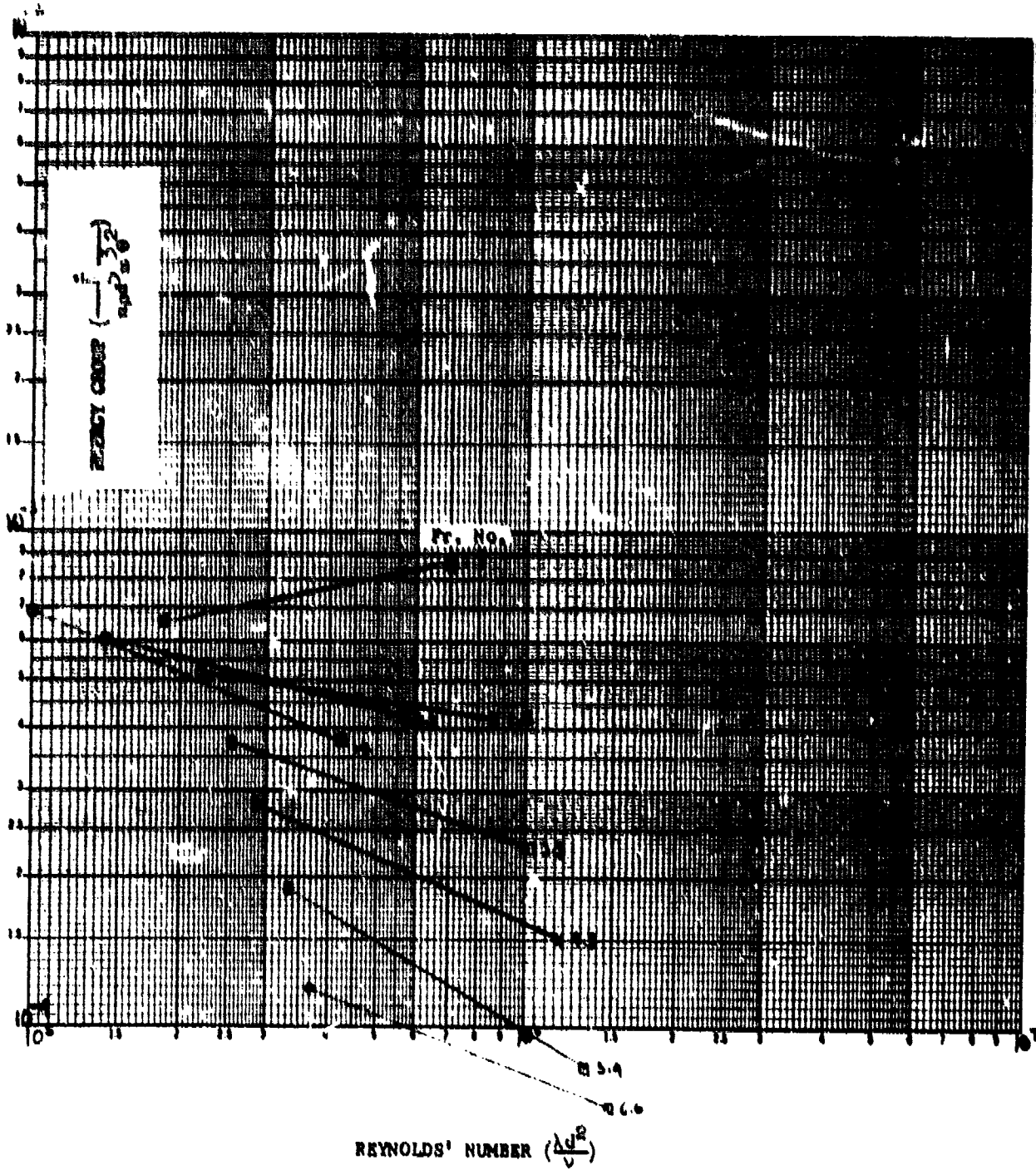
A-9

b) Energy Group Versus Reynolds Number

Figure A-4 (continued). Phase I Conispherical Tank Fuel Sloshing at
50 Percent Fraction Fill ($\sigma = 0.35$)

A-10

a) Time Constant Group Versus Reynolds Number

Figure A-5.   Phase I Conispherical Tank Fuel Sloshing at 30 Percent
Fraction Fill (σ = 0.35)

A-11

b) Energy Group Versus Reynolds Number

Figure A-5 (continued).   Phase I Conispherical Tank Fuel Sloshing at
30 Percent Fraction Fill (σ = 0.35)

a) Time Constant Group Versus Reynolds Number

Figure A-6. Phase I Conispherical Tank Fuel Sloshing at 10 Percent Fraction Fill ($\sigma = 0.35$)

b) Energy Group Versus Reynolds Number

Figure A-6 (continued). Phase I Conispherical Tank Fuel Sloshing at 10 Percent Fraction Fill ($\sigma = 0.35$)

APPENDIX B. ERROR ANALYSIS

The object of this analysis is to determine 1) a be it estimate of the dedamping time constant from the strip chart recording of the nutation angle growth during a specific test and 2) the error associated with this estimate. The analytic techniques employed are based on linear estimation theory as presented in Reference 30. The estimator chosen as optimum is the minimum mean square error estimator. The error, $\underline{e}$, is defined as the difference between the estimate $\hat{\underline{x}}$ and the true value $\underline{x}$. The minimum mean square error estimator minimizes the diagonal elements of the following matrix

$$C_{\underline{e}} = E(\underline{e}\,\underline{e}^T) = E\left| [\hat{\underline{x}} - \underline{x}][\hat{\underline{x}} - \underline{x}]^T \right| \tag{1}$$

In the special case where $\underline{x}$ is a scalar, the optimal estimator minimizes the mean square error, i.e., $E(\hat{x}-x)^2$ is minimized.

It is shown in Reference 30 that the optimal estimate and the error matrix are given by

$$\hat{\underline{x}} = (B^T C_v^{-1} B)^{-1} B^T C_v^{-1} \underline{\theta} \tag{2}$$

$$C_e = (B^T C_v^{-1} B)^{-1} \tag{3}$$

under the following assumptions:

1) The observation vector, $\underline{\theta}$ is linearly related to the true state vector, $\underline{x}$, by

$$\underline{\theta} = B\underline{x} + \underline{v} \tag{4}$$

where B is a matrix, and the vector $\underline{v}$ represents the noise or error in the measurement of $\underline{\theta}$.

2) The correlation between measurement noise and the true state is zero, i.e., $C_{\underline{x}\underline{v}} = E(\underline{x}\underline{v}^T) = 0$.

3) Knowledge of the true state $\underline{x}$ is unknown so that $C_{\underline{x}} = E(\underline{x}\underline{x}^T) \rightarrow \infty$

4) The noise moment matrix $C_{\underline{v}} = E(\underline{v}\underline{v}^T)$ is diagonal, i.e., the measurements are statistically linearly independent and no correlation exists between the observations.

In order to apply this theory, first introduce the theoretical relationship between nutation angle amplitude, A, and dedamping time constant, $\tau = 1/\beta$:

$$A = A_o \exp(\beta t) \qquad (5)$$

where A_o is the amplitude at time equals zero and t is the time of measurement. The problem is to find an optimal estimate of β given a set of measurements A_i at times t_i. Equation 5 is nonlinear and must be put into linear form before applying Equations 2 and 3. The latter form is achieved by taking the logarithm of Equation 5, i.e.

$$\ln(A_i/A_o) = \beta t_i + v_i \qquad (6)$$

where the noise term v_i represents the measurement error. An explicit form for the v_i can be obtained as follows. The measured amplitude is the sum of the true amplitude and some error, i.e., $A_i^t = A_i - \Delta A_i$. Substituting this true amplitude into Equation 5, taking the logarithm using the approximation $\ln(1+\epsilon) \approx \epsilon$, $\epsilon^2 \ll 1$, yields

$$\ln(A_i/A_o) = \beta t_i + \frac{\Delta A_i}{A_i} \qquad (7)$$

At this point, the reasonable assumption is made that the uncertainty in reading any nutation angle amplitude on the strip chart is the same, i.e., $\Delta A_i = \Delta A$. Equation 7 becomes

$$\ln(A_i/A_o) = \beta t_i + \frac{\Delta A}{A_i} \qquad (8)$$

B-2

Equation 8 is now in the proper form to utilize Equations 2 and 3. Simply identify

$$\underline{\theta} = \begin{bmatrix} \ln A_1/A_o \\ \cdot \\ \cdot \\ \cdot \\ \ln A_n/A_o \end{bmatrix}, \quad \mathbf{B} = \begin{bmatrix} t_1 \\ \cdot \\ \cdot \\ \cdot \\ t_n \end{bmatrix}, \quad \underline{x} = \beta, \quad \underline{V} = \begin{bmatrix} \Delta A/A_1 \\ \cdot \\ \cdot \\ \cdot \\ \Delta A/A_n \end{bmatrix}$$

with

$$C_{\underline{V}}^{-1} = \begin{bmatrix} \left[A_1/\Delta A^2\right] & & & & 0 \\ & \cdot & & & \\ & & \cdot & & \\ & & & \cdot & \\ & & & & \cdot \\ 0 & & & & \left[A_n/\Delta A^2\right] \end{bmatrix}$$

Applying Equation 3,

$$C_e = \frac{(\Delta A)^2}{\displaystyle\sum_{i=1}^{n} (A_i t_i)^2} \tag{9}$$

Equation 2 is then used to determine the optimal estimate:

$$\hat{\beta} = \frac{\displaystyle\sum_{i=1}^{n} t_i A_i^2 \ln\left(A_i/A_o\right)}{\displaystyle\sum_{i=1}^{n} (A_i t_i)^2} \tag{10}$$

B-2

The rms error in the estimate is given by

$$\sqrt{E(e^2)} = \frac{\Delta A}{\sqrt{\sum_{i=1}^{n} (A_i t_i)^2}} \tag{11}$$

Since $\beta \approx 1/\tau$ and $d\beta = (-1/\tau^2)d\tau$, the optimal estimate of the time constant and the rms percent error are, respectively,

$$\tau = \frac{\sum_{i=1}^{n} (A_i t_i)^2}{\sum_{i=1}^{n} t_i A_i^2 \, \ell n (A_i/A_o)}$$

$$|d\tau| = \frac{\tau |\Delta A|}{\sqrt{\sum_{i=1}^{n} (A_i t_i)^2}} \tag{12}$$

Note that Equations 12 reduce to the familiar form for $n = 1$. An example is now presented to illustrate how Equations 12 are employed to interpret a typical set of data. Figure B-1 depicts the peak-to-peak amplitude of the Physitech tracker versus the number of nutation cycles during a test on the conisphere with $\sigma = 0.335$, FF= 75 percent, $\omega_g = 207$ rpm, and water as the test fluid. The raw test data are shown in Figure B-2. This test is of particular interest since it represents a data point used to estimate the Intelsat IV initial synchronous orbit time constant. Note also that the dual time constant behavior discussed in Section 5 is also evident, with the transition region in the vicinity of 2 degrees nutation. The first time constant is evaluated for 0.8 degree $\leq \theta \leq 1.9$ degrees, i.e., for the first 175 cycles or 152 seconds. The estimate obtained by drawing a straight line on the figure is 182 seconds. The second time constant is evaluated for 1.9 degrees $\leq \theta \leq 4.8$ degrees, i.e., for the next 125 cycles or 109 seconds. The estimate obtained by drawing a straight line on the figure is 119 seconds. The data and calculations used to obtain the optimal estimates for these two time constants are now summarized.

B-4

CASE 1: 0.8 degree $\leq \theta \leq 1.9$ degrees

$$A_o = 6.5 \text{ mm}$$

$$\Delta A = \pm 1.0 \text{ mm}$$

i	t_i, seconds	A_i mm
1	21.8	7
2	43.5	8
3	65.3	9
4	87.0	10
5	108.8	11
6	130.5	13
7	152.3	15

$$\sum_{i=1}^{n=7} (A_i t_i)^2 = 10.78 \times 10^6 \text{ sec}^2 \text{ mm}^2$$

$$\sum_{i=1}^{n=7} t_i A_i^2 \ln(A_i/A_o) = 5.69 \times 10^4 \text{ sec mm}^2$$

$$\Longrightarrow \tau = 189 \text{ seconds}$$

$$\left| \frac{d\tau}{\tau} \right| = 5.8 \text{ percent}$$

CASE 2: 1.9 degrees $\leq \theta \leq 4.8$ degrees

$$A_o = 15 \text{ mm}$$

$$\Delta A = \pm 1.0 \text{ mm}$$

i	t_i, seconds	A_i, mm
1	21.8	18
2	43.5	21.5
3	65.3	26
4	87.0	31.5
5	108.8	38

$$\sum_{i=1}^{n=5} (A_i t_i)^2 = 28.63 \times 10^6 \text{ sec}^2 \text{ mm}^2$$

$$\sum_{i=1}^{n=5} (t_i A_i^2) \ln(A_i/A_o) = 24.24 \times 10^4 \text{ sec mm}^2$$

$$\Longrightarrow \tau = 118 \text{ seconds}$$

$$\left| \frac{d\tau}{\tau} \right| = 2.2 \text{ percent}$$

The graphical estimates of the time constants are within the error
band of the optimal estimates, providing confidence in the former technique.
The rms error associated with the optimal estimate obviously changes with
different sets of data. However, the error was less than 10 percent for
the vast majority of the data. The conclusion to be drawn from this is that
the data reduction method is rather good. Any dispersion in the dimension-
less curves extrapolated from the test data ought then to be interpreted as
real and associated with some other effect.
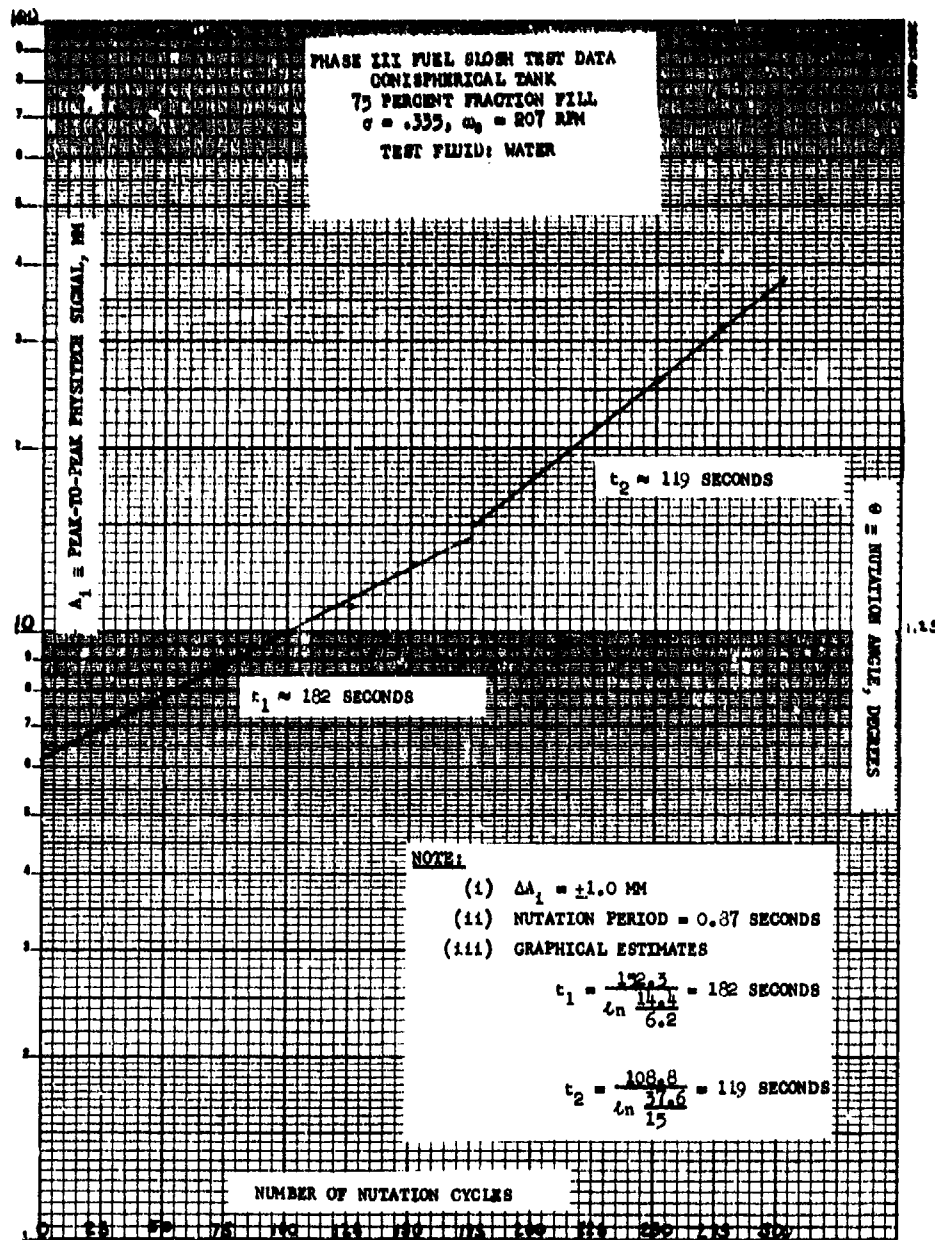
Figure B-1. Amplitude of Physitech Tracker Versus Number of
Nutation Cycles

$T_S = .285$ SEC (SPIN PERIOD)

9-15-30
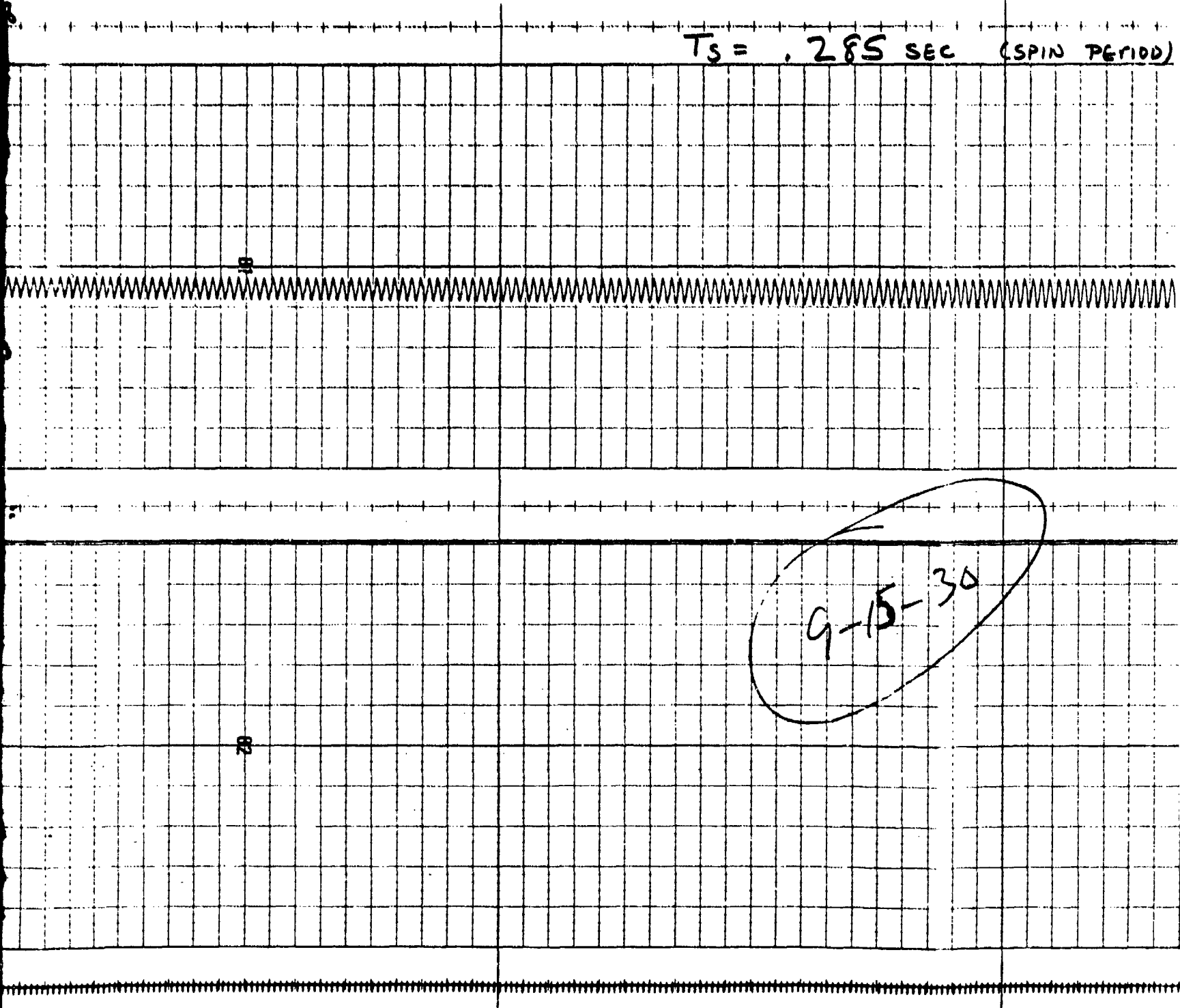
Figure B-2. Physitech Record of Phase III Fuel Sloshing

SEC   (SPIN PERIOD)

PHASE III

CLEVITE CORPORATION / BRUSH INSTRUMENTS DIVISION   CLEVELAND, OHIO   PRINTE

287
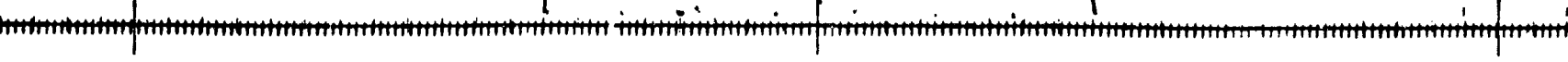
PHASE III FUEL SLOSH TEST DATA — PHYSITECH RECORDING   9/15/71

CONISPHERICAL TANK
75% fraction fill
H₂O — TEST FLUID
WS = 2.10 RPM
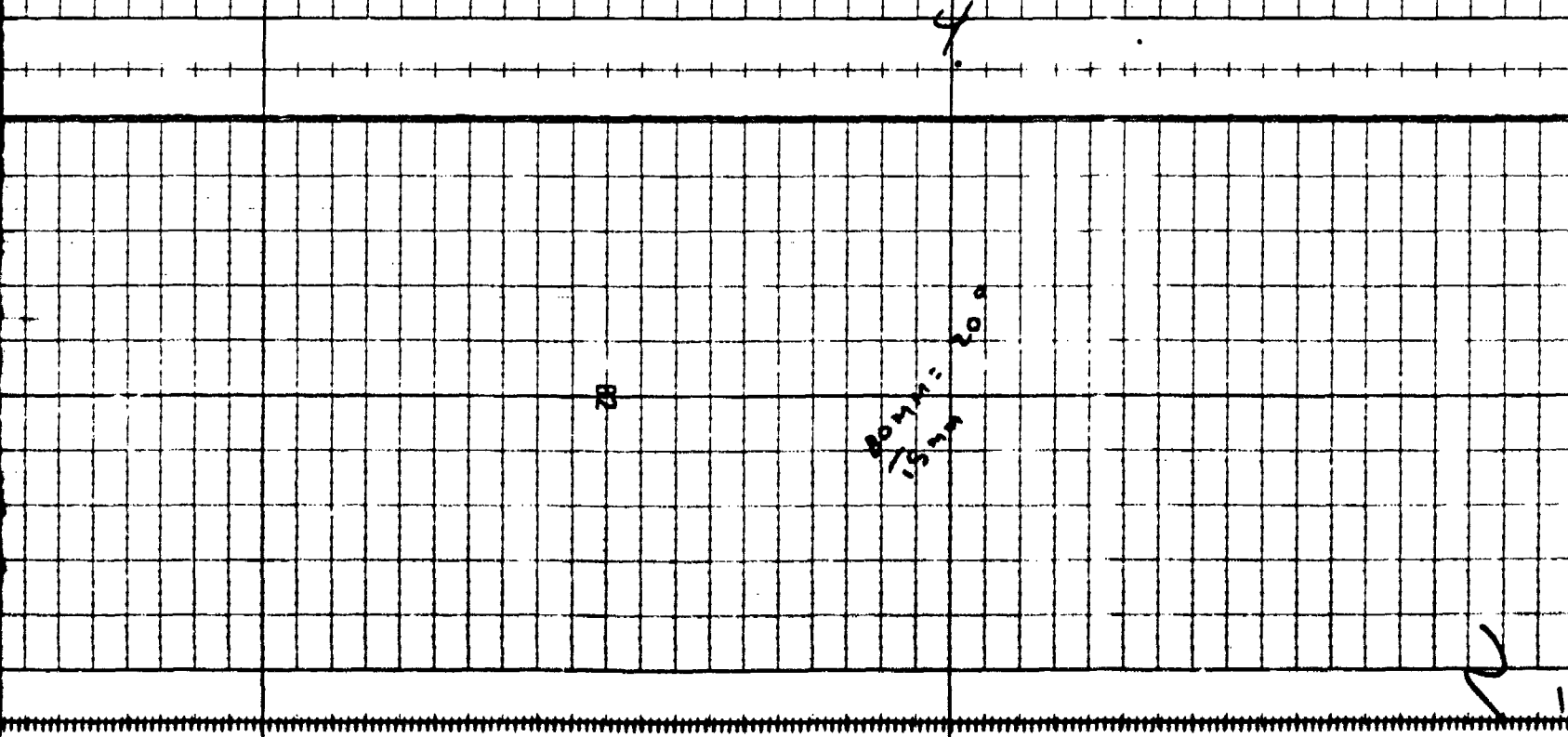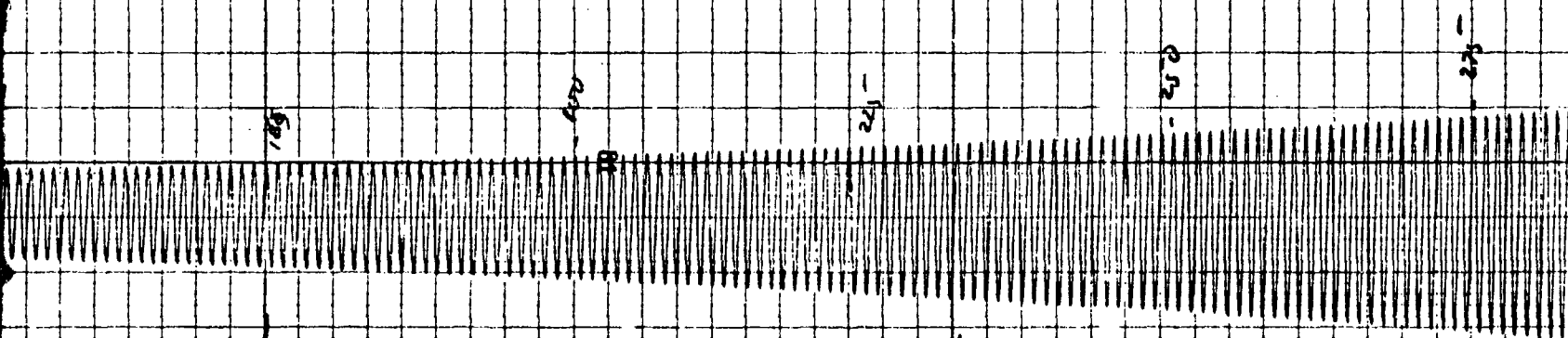
OHIO.   PRINTED IN U.S.A   TIME ($\frac{2mm}{SEC}$

287   .292 sec

VG   9/15/71

.292 sec
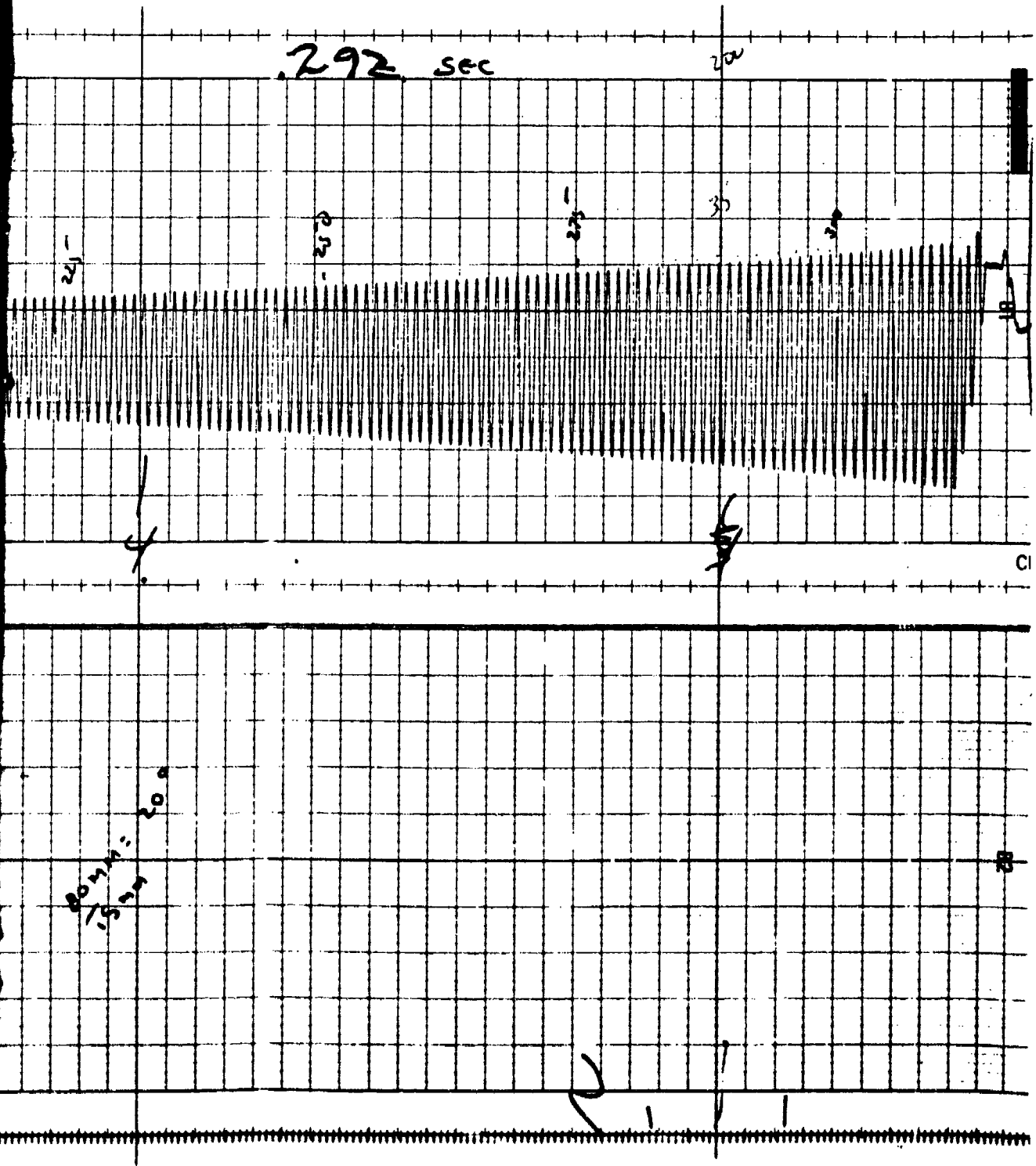
APPENDIX C. ANCILLARY FUEL SLOSH DATA

The purpose of this appendix is to make available additional data and calculations which may serve either as a reference material or as information for future analyses. The curves are mostly self explanatory and will not be discussed to any great extent. The following summarizes the curves presented here:

| Figure	Description
C-1	Presents the Froude number versus test spin for the Phase I and II test vehicle.
C-2	Gives the angle between the fluid-free surface and the vehicle spin axis as a function of spin speed. (An angle of 90 degrees would correspond to an infinite spin speed and a 0 g test condition.)
C-3	Gives a close estimate of the fluid weight contained in the test tanks for the flight and Phase I test and the Phase II tanks as a function of percent fraction fill.
C-4	For a nonspinning con spherical tank in a 1 g field this graph gives the natural frequency of the first fundamental sloshing mode as a function of mass fraction. The test data were compiled by the Comsat Laboratories (Reference 18).
C-5	Gives the radial location of the propellant-free surface and mass centroid as a function of mass fraction for the Intelsat IV flight configuration.
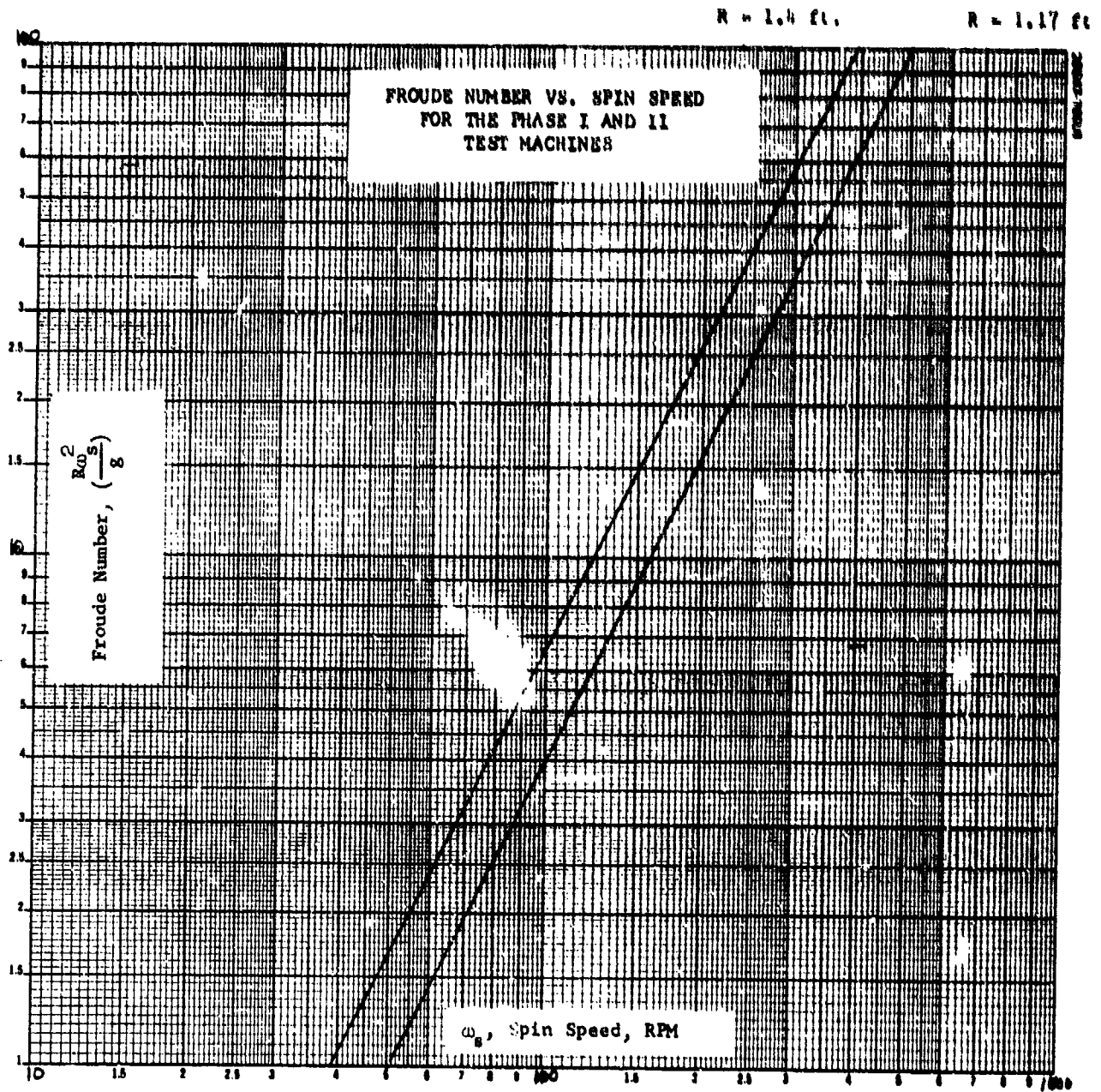
Figure C-1. Froude Number Versus Spin Speed for Phase I and II
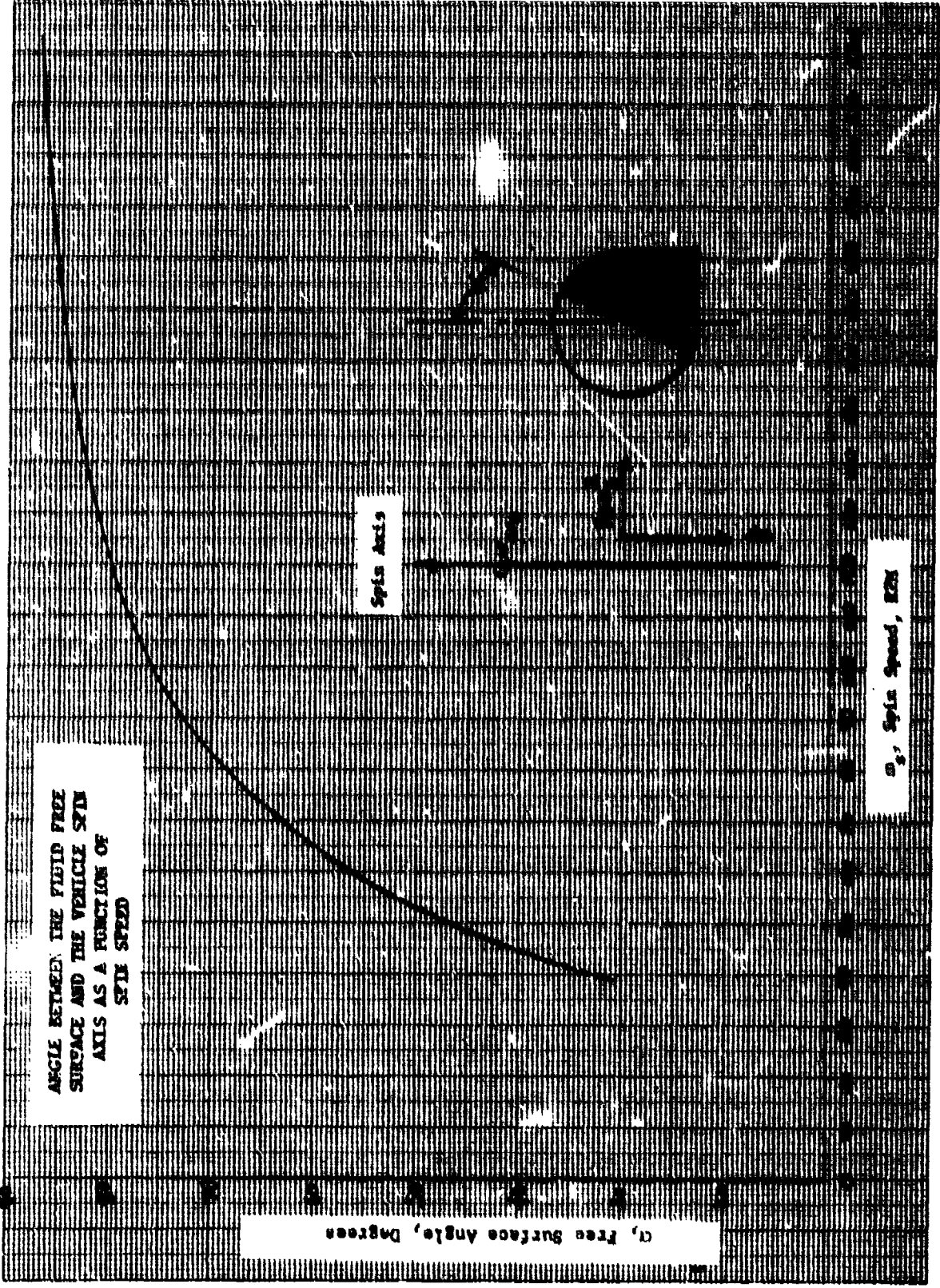Test Vehicles

Figure C-2. Angle Between Fluid-Free Surface and Vehicle Spin Axis as Function of Spin Speed
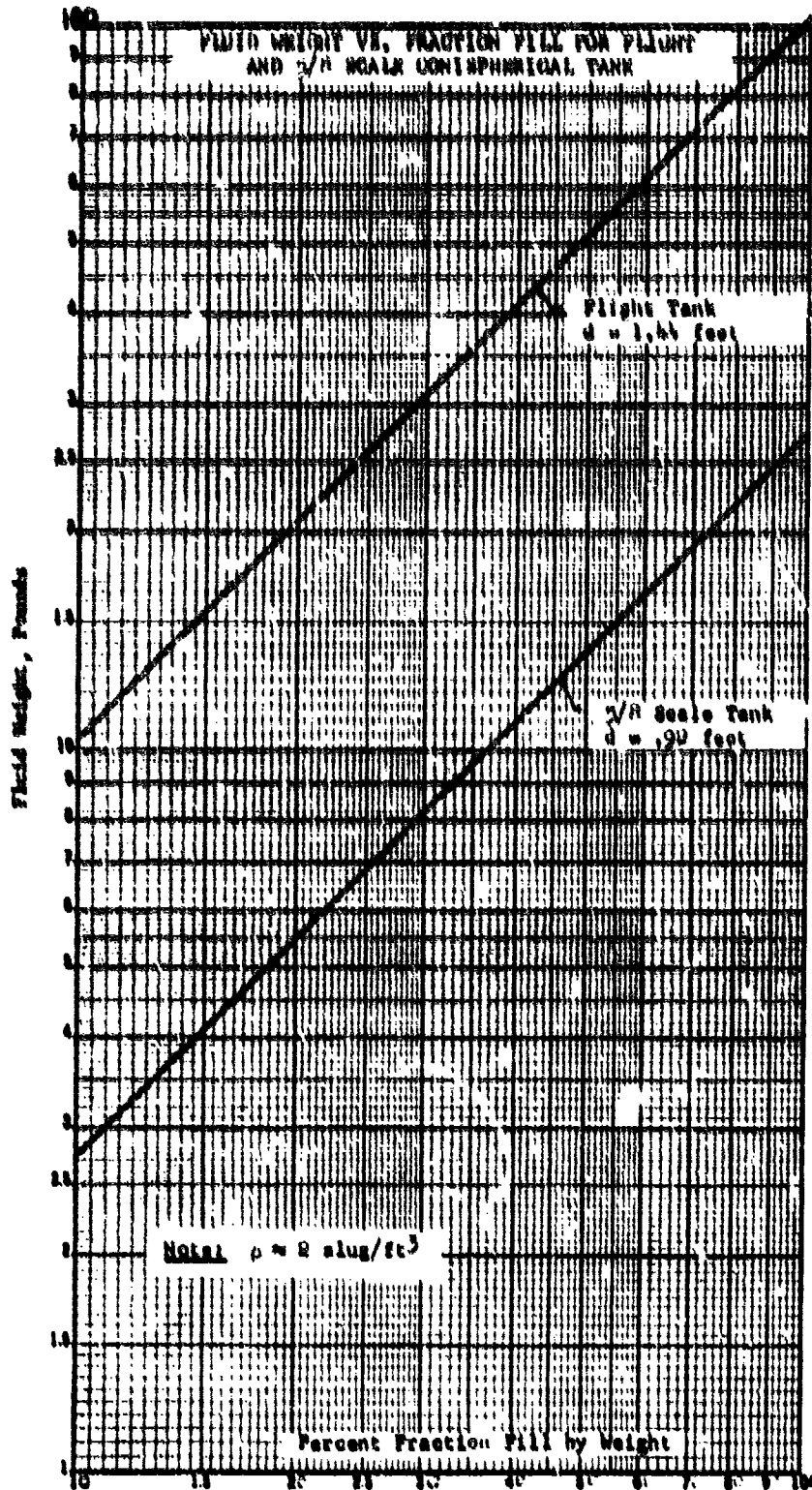
Figure C-3. Fluid Weight Versus Fraction Fill for Flight and 5/8 Scale
Conispherical Tanks

C-4

Figure C-4. Nonspinning Natural Frequency Versus Percent Fraction Fill of H_2O in Intelsat IV Fuel Tank
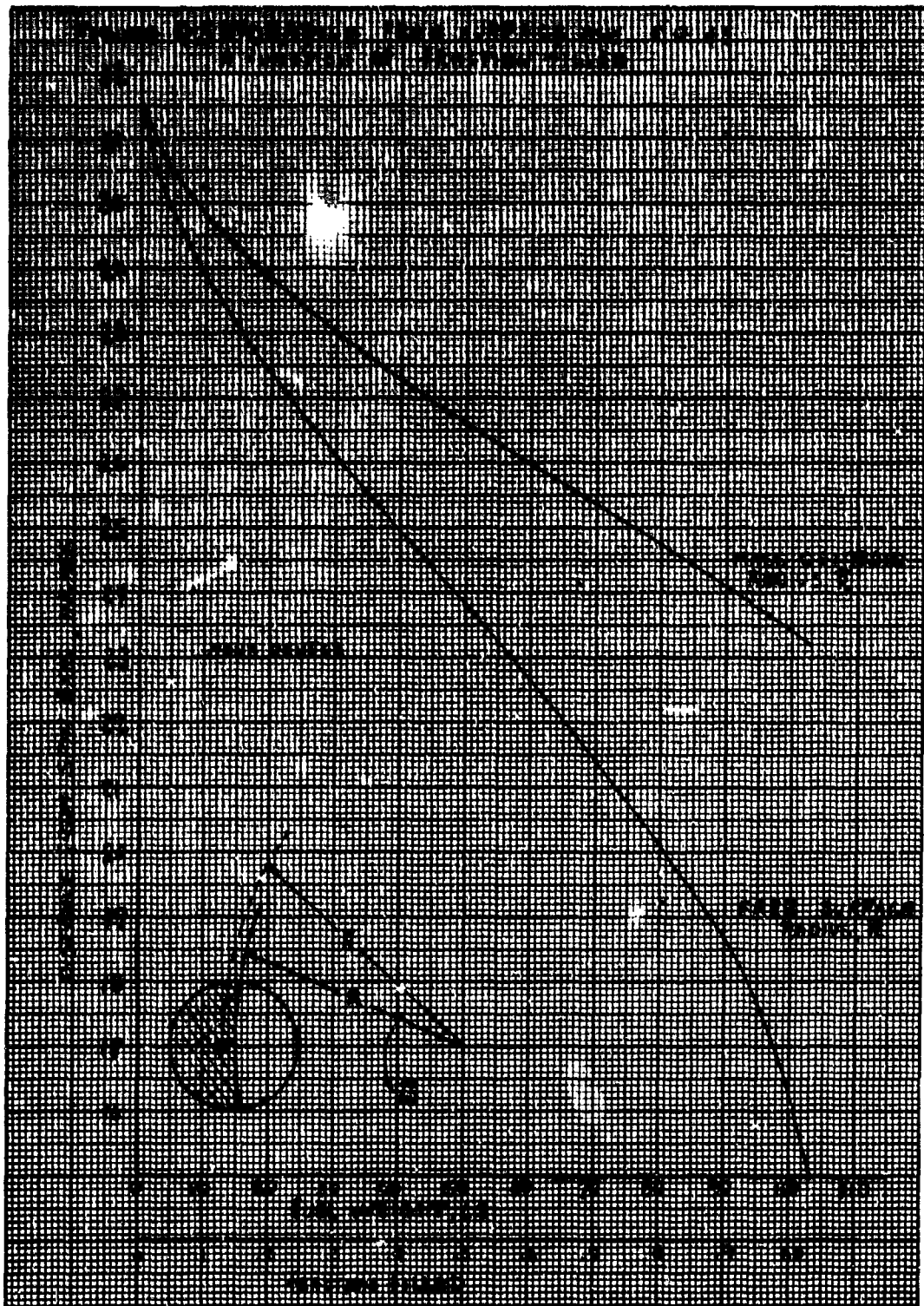
Figure C-5. Hydrazine-Free Surface and Mass Centroid as Function of Fraction Fill

APPENDIX D. SUMMARY OF GRAVITY EFFECTS
ON FUEL SLOSH TEST VEHICLE

As noted in the discussion of the test results, it is obvious that gravity is influential not only to the fluid dynamics but also to the vehicle dynamics. Insufficient knowledge exists at this time to explain the effect of gravity on the fuel motion. For the time being, the test technique is to operate at sufficient Froude numbers to where gravity is negligible. With regards to the gravity effects on the vehicle dynamics, the problem is more deterministic.

When in operation, the kinematic motion of the test vehicle is analogous to a precessing nutation top. Because of the internal fluid motion and attendant energy dissipation, the vehicle is neither rigid nor characterized by a stationary cg. When nutating, the static gravity field becomes modulated with an amplitude proportional to the nutation and at the rotor nutation frequency. Therefore, as will be seen by the three-axis acceleration equations, gravity acts to excite the transverse axis — transverse to the axis excited by nutation alone. In the case of $\sigma = 0.1$, it appears that this transverse excitation by gravity is the dominate forcing input to the fluid motion. That is why the dissipation is so sensitive to the Froude number.

The following discussion briefly reviews the known effects of gravity on the test vehicle.

GRAVITY PRECESSION

The characteristic frequencies of the test vehicle equations of motion are the following (Reference 13):

$$\text{Precession frequency} = \dot{\Omega} = \frac{\lambda_o}{2} - \left(\frac{\lambda_o^2}{4} + \frac{mg\ell}{I_T}\right)^{1/2}$$

$$\text{Nutation frequency} = \lambda_i = \frac{\lambda_o}{2} + \left(\frac{\lambda_o^2}{4} + \frac{mg\ell}{I_T}\right)^{1/2}$$

Since the precession frequency is typically an order of magnitude below the inertial nutation frequency, λ_o, the above frequencies can be approximated as

$$\Omega \doteq \frac{mg\ell}{\lambda_o I_T} = \frac{mg\ell}{I_s \omega_s}$$

$$\lambda_i = \lambda_o = \frac{I_s}{I_T} \omega_s$$

Here Ω is the classical precession frequency of a top. The frequency is proportional to the weight and the moment arm, ℓ, and inversely proportional to the system angular momentum, $I_s \omega_s$. Typical numbers for Ω during Phase II and III testing resulted in precession periods on the order of 2000 seconds (≈ 0.18 deg/sec). With a vehicle mass of 1300 pounds, a spin inertia of 22 slug-ft^2, and a spin rate of 200 rpm, the resulting cg offset from the ball center (ℓ) is 0.015 inch. When operating in the $\sigma = 0.35$ configuration, typical precession periods are about 800 seconds; the resulting offset, ℓ, is comparable to the value given above.

Figure D-1 clearly shows the gravity precession superposed on the diverging nutation sinusoid. The data were taken during the early part of the Phase I program. Subsequent to this, test balancing procedures were improved and the amplitude of the precession was significantly reduced.
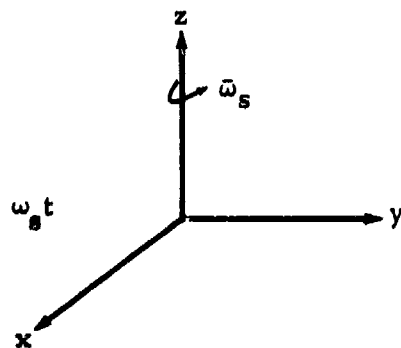
GRAVITY EXCITATION

When the vehicle is precessing and nutating in the static 1 g field, the acceleration field acting on the fluid is considerably modified from the space environment. Using the coordinate system shown in the figure below the following 3-axis accelerations can be derived:

$$a_x = -\theta\left[g + z\sigma^2 \omega_s^2\right] \sin \lambda t - g\alpha \sin \omega_s t$$

$$a_y = +r\omega_s^2 - \theta\left[g + z\sigma^2 \omega_s^2\right] \cos \lambda t - g\alpha \cos \omega_s t$$

$$a_z = -\theta\sigma (2 - \sigma)r\omega_s^2 \cos \lambda t - g$$

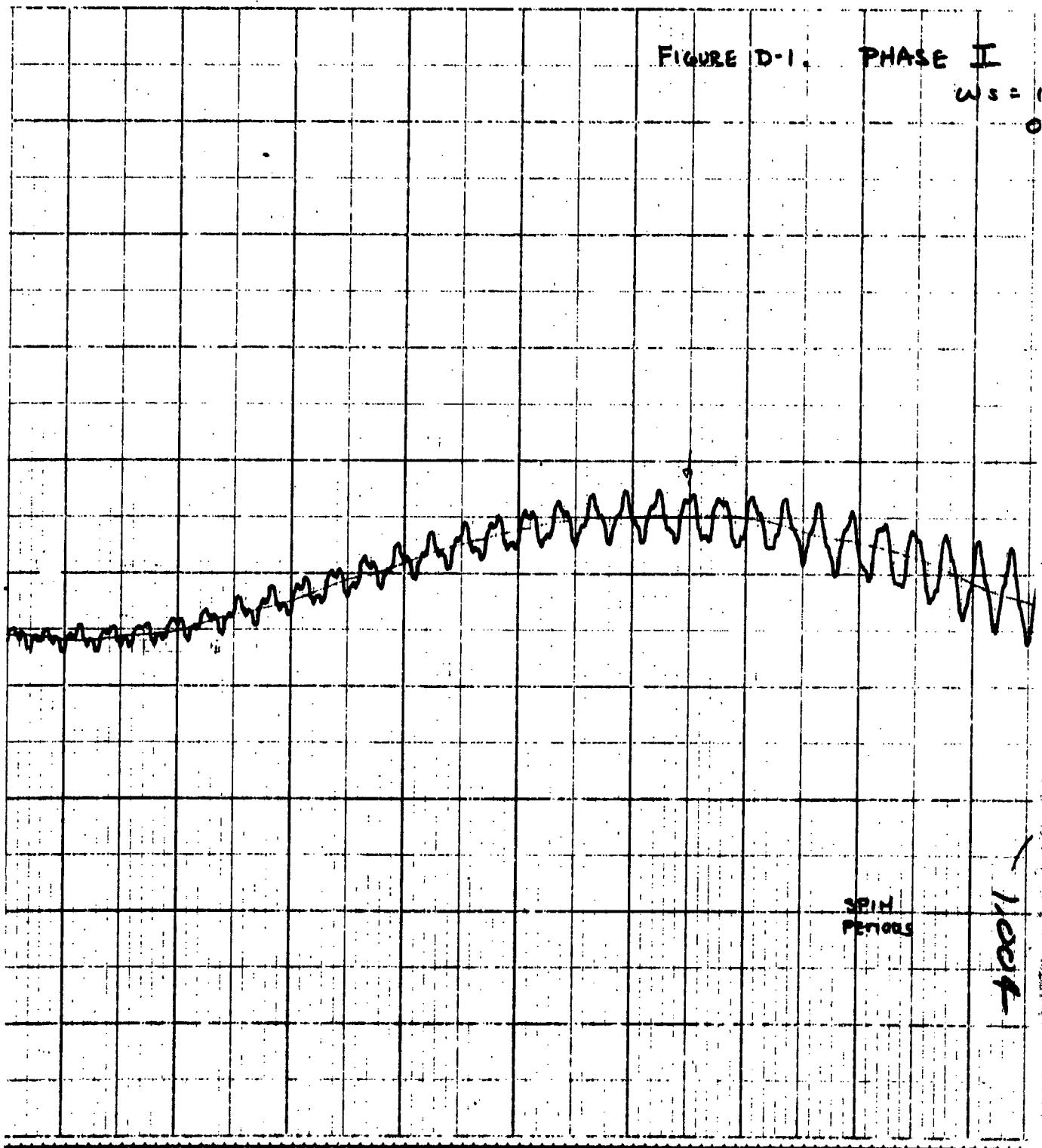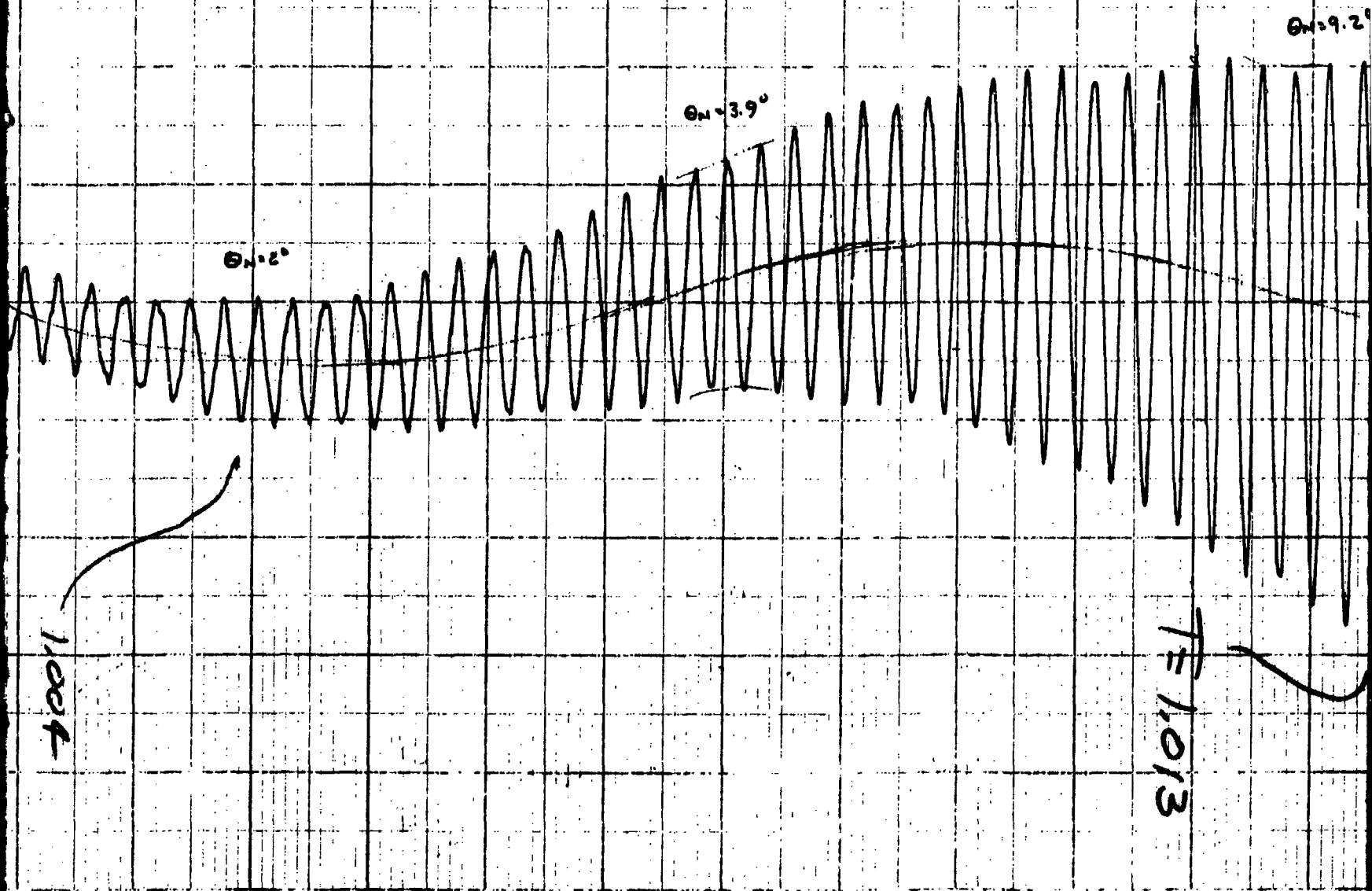where α is the deviation between the local vertical and the angular momentum vector.
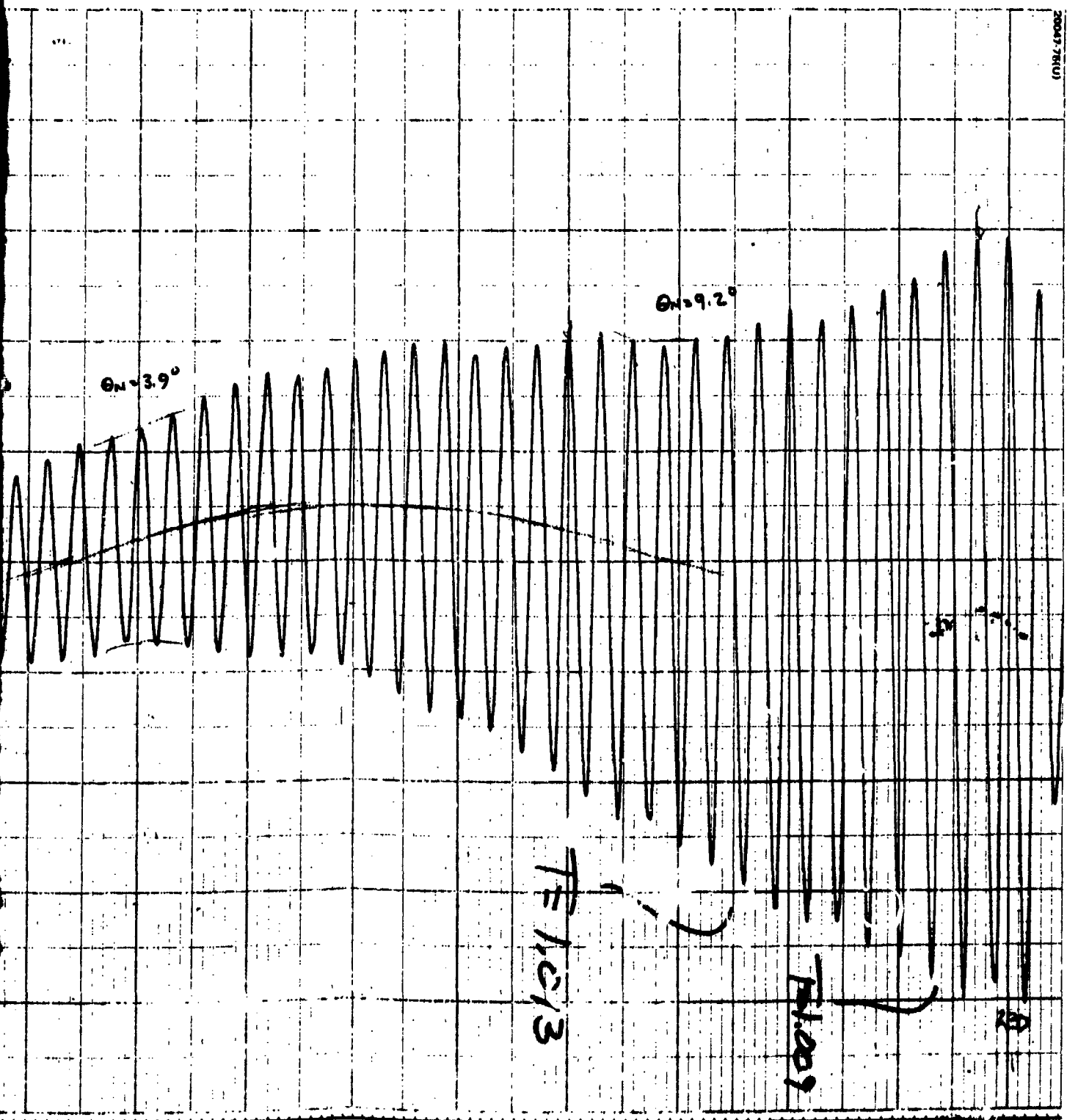
Figure D-1. Gravity Precession Superposed on Diverging Nutation
Sinusoid

II   σ = .380   80% fraction fill

νs = 60 RPM   ; TEST FLUID, H₂O

OPTICAL TRACKER.

$\Theta_N \approx 2°$

$\Theta_N \approx 3.9°$

$\Theta_N \approx 9.2°$

1.004

$\overline{F} = 1.013$

$\Theta_N = 3.9°$

$\Theta_N = 9.2°$

In space, the primary fluid excitation produced by nutation is the axial, a_z, component which is equal to $\theta\sigma(2 - \sigma)r\omega_s^2 \cos \lambda t$. The quadrature component is typically small relative to this term, specifically $\sigma^2 z/\sigma(2 - \sigma)r$. When gravity is present, the total acceleration field is substantially different in the transverse axis. In fact, the above equations indicate that the transverse excitation is nearly an order of magnitude larger in the laboratory than in space. The fluid motion then undergoes a circular or planar forced excitation as opposed to nearly linear excitation in space.

The transverse acceleration components proportional to α occur at spin speed and therefore cannot affect nutational growth. Their effect would be to produce a secular despin torque on the vehicle, thus slowing it down during the run.

The intent of the testing in Phase II and III was to run the vehicle at high enough spin speeds so that the gravity accelerations were small relative to the centrifugal accelerations, $r\omega_s^2$. In Phase I, convergence to a 0 g condition was just reached at the operating limit of the vehicle — typically 100 rpm. However, it was not recognized until Phase III that indeed testing above 120 rpm satisfied the desired 0 g approximation. The test data suggest that the spin speed of 0 g convergence varies of inertia ratio. In the case of $\sigma = 0.1$, as mentioned in Section 5.5, it appears that the critical spin speed, ω_s^*, was not reached.

REFERENCES

1. D.D. Williams, "Estimated of Energy Dissipation and Nutation Damping Due to Fuel Sloshing in a Spherical Tank," Hughes IDC 2280.03/202, 1 June 1965.

2. H. Lamb, Hydrodynamics, Dover Publications, 6th Edition, 1932.

3. A.J. Stofan and A.L. Armstead, Analytical and Experimental Investigation of Forces and Frequencies Resulting from Liquid Sloshing in a Spherical Tank, NASA TN-D-1281, July 1962.

4. H. Normal Abramson, et al., "Liquid Sloshing in Spherical Tanks," AIAA Journal, Vol. 1, No. 2, February 1963.

5. I.E. Summer and A.J. Stofan, An Experimental Investigation of the Viscous Damping of Liquid Sloshing in Spherical Tanks, NASA TN-D-1991, December 1963.

6. A.J. Iorillo, Analyses Related to the Hughes Gyrostat System, Hughes Aircraft Company Report SSD 70538B, December 1967.

7. C.R. Johnson, "TACSAT I Nutation Dynamics," AIAA Paper 70-455, AIAA Third Communication Satellite System Converence, 6-8 April 1970.

8. J.O. Salvatore and W.W. Porter, ATS-V Heat Pipe Tests and Dimensional Analysis, Hughes Aircraft Company Report SCG 10319R, June 1970.

9. W.W. Porter, "Fuel Slosh Damping Test with ATS Tanks and Test Fixture," Hughes IDC 223/2466, 12 May 1970.

10. R.H. Edwards, "Fuel Damping of Intelsat IV," Hughes IDC 2245.2/8, 9 May 1969.

11. J.T. Neer, "Intelsat IV Fuel Slosh Dissipation Rates and Time Constants," Hughes IDC HS312-2286-3-F161, 13 February 1970.

12. J.R. Neer, "Meeting Notes from the Visit with Dr. H.N. Abramson of SWRI," 12 March 1970.

13. R. H. Bernard, "Spinning Fuel Slosh Test Error Analysis," Hughes IDC 2223/3405, 1 May 1970.

14. E. R. Martin, "Progress Report — Spinning Fuel Slosh Test," Comsat Memo TCLS/1130, 26 March 1970.

15. J. T. Neer, "Summary of Comsat Lab Spinning Fuel Slosh Test," Hughes IDC, 14 April 1970.

16. J. T. Neer, "Notes on Comsat Spinning Fuel Slosh Video Tapes, Hughes Aircraft Company IDC, 1 May 1970.

17. Comsat Memo, "Status Report — Spinning Fuel Slosh Test," TCLS/1255, 25 August 1970.

18. J. T. Neer, "Sloshing Frequencies in Intelsat IC Cone-sphere Tanks as a Function of Fraction Fill," IDC HS312-2286-3-F77, 10 August 1970.

19. L. Grasshoff, "Summary of Digital Simulation of Intelsat IV Fuel Slosh Tests Using the Williams' Model of Fuel Slosh Effects," November 1970.

20. J. A. Harrison, "Direct Measurement of On-Orbit Energy Dissipation in a Spinning Satellite by Means of a Ground Based Test," Hughes IDC 4091.2/015, 4 January 1971.

21. J. A. Harrison, "Direct Measurement of On-Orbit Energy Dissipation of a Spinning Satellite by Means of a Ground-Based Test — Part Two," Hughes IDC 4091.2/035, 23 February 1971.

22. W. J. Russell, The Relationship of Ground Test Results to the Effects of Fuel Sloshing on the Nutational Stability of a Dual Spin Spacecraft," Aerospace Report TOR-0059(6143)-30, 5 March 1971.

23. H. O. Curtis and J. V. Harrington, Predictions of Margins for Nutational Stability for Intelsat IV, Technical Report 70-9, Harrington, Davenport and Curtis, Inc., Bedford, Massachusetts, 28 December 1970.

24. H. O. Curtis and J. V. Harrington, Further Considerations of Margins for Nutational Stability of Intelsat IV, Technical Report 70-10, Harrington, Davenport and Curtis, Inc., Bedford, Massachusetts, 31 December 1970.

25. W. W. Porter, "Fuel Slosh Test Procedures (for HS318) and Related Topics," Hughes IDC 413.10/3, 6 January 1971.

26. G. R. Telle, "Predicted Fuel Slosh Test Results," Hughes IDC 4113.00/5, 11 January 1971.

27. D.B. Krimgold, H.V. Nuttall and W.W. Porter, "Fuel Slost Test Results," Hughes IDC 4113.00/26, 16 March 1971.

28. E.R. Martin, "Fuel Slosh and Dynamic Stability of Intelsat IV," AIAA Paper 71-959, presented at AIAA Guidance, Control and Flight Mechanics Conference, Hofstra University, Hemstead, New York, 16 August 1971.

29. J.T. Neer, "Intelsat IV Synchronous Orbit Dedamping Time Constant — Effects on F-2, Comparison with Fuel Slosh Tests, and Implications on Future Missions," Hughes IDC HS 312-4328-3-6558, CAT2, 24 August 1971.

30. P.B. Liebelt, Introduction to Optimal Estimation, Addison-Wesley, 1967.